Thin Functional Conducting Polymer Films
---- Preparation, Properties and Applications

Dissertation

zur Erlangung des Grades

" Doktor der Naturwissenschaften"

am Fachbereich Chemie und Pharmazie

der Johannes Gutenberg-Universität Mainz

Shengjun Tian

geb. in Henan, V. R. China

Mainz, 2005

Dekan: Prof. Dr. R. Zentel

1. Berichterstatter: Prof. Dr. W. Knoll
2. Berichterstatter: Prof. Dr. R. Zentel

Tag der mündlichen Prüfung: 8 April, 2005

Die vorliegende Arbeit wurde unter Betreuung von Herrn Prof. Dr. W. Knoll im Zeitraum zwischen April 2002 bis Februar 2005 am Max-Planck-Institut für Polymerforschung, Mainz, Deuschland angefertigt.

This work was done under the supervision of Prof. Dr. W. Knoll in Max-Planck-Institute for Polymer Research, Mainz, Germany from April 2002 to February 2005.

……To my wife and my son

CONTENTS

Chapter 1

General Introduction

1.1 Background of the present research work

Tremendous advances have been made during the past two decades in the understanding of the chemical, electrochemical, structural, electrical and optical phenomena of inherently conducting polymers, such as polypyrrole (PPy), polythiophene (PT), polyaniline (PANI), polyphenylene (PPh) and their derivatives.[1-3] The great interest in these polymers arises from their relative ease of synthesis by chemical or electrochemical oxidative polymerisation of the monomers and from their considerable importance as candidates for new materials that would lead to the next generation of electronic and optical devices and as promising transducers for chemo- or bio- sensors.[1-4] The fact that the 2000 Nobel Prize in Chemistry went to Alan J. Heeger, Alan G. MacDiarmid and Hideki Shirakawa *"for the discovery and development of conductive polymers" (Nobel Citation)* also reflects both research and practical importance of conducting polymers and their applications in modern science and daily life.[5]

As one of the most important conducting polymers, PANI is probably the oldest known synthetic organic polymer.[6] However, the detailed study on its structures and properties only began in the 1980s.[7,8] Now it is generally accepted that PANI is a mixed oxidation state polymer composed of reduced benzenoid units and oxidized quinoid units (Fig.1-1(A)), with the average oxidation state given by (1-y).[9] PANI can exist in several oxidation states ranging from the completely reduced *leucoemeraldine base (LEB)* state (Fig.1-1(B)), where 1-y = 0, to the completely oxidized *pernigraniline base (PNB)* state, where 1-y = 1. The half-oxidised (1-y = 0.5) *emeraldine base (EB)* state is composed of an alternating sequence of two benzenoid units and one quinoid unit. Each of the above mentioned three forms of PANI is an insulator, although they possess other interesting physical and chemical properties. However, the insulating EB form can be non-redox doped with protonic acids (HA) to yield the *emeraldine salt (ES)* form (also shown in Fig.1-1(B)), which shows a dc conductivity in the metallic regime (ca. 1~5 S/cm).[10] The conducting ES form can
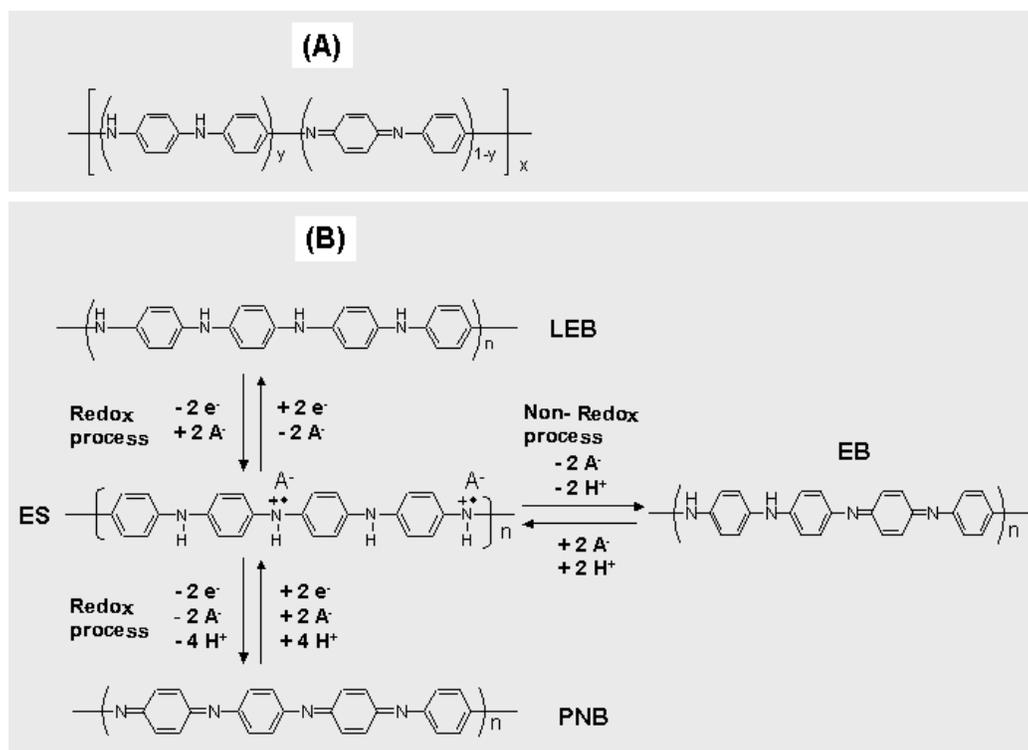
Fig.1-1 *(A) The general chemical structure of PANI that shows the average oxidation state (1-y). (B) The chemical structures of the three normally found oxidation states of PANI (i.e. fully-reduced LEB, half-oxidised EB and fully-oxidised PNB) and the transitions from them to the corresponding salt form (ES) either through a redox doping process or a non-redox doping process.*

also be obtained through a redox-doping process in acidic conditions from its corresponding reduced LEB form or oxidised PNB form by either a chemical or an electrochemical step (c.f. Fig.1-1(B)). Nevertheless, the non-redox doping process is different from the redox doping in that it does not involve the addition or removal of electrons from the polymer backbone. Instead, the imine nitrogen atoms of the polymer are protonated to give a polaronic form where both spin and charge are delocalised along the entire polymer backbone. Both the redox doping process and the non-redox doping process are reversible, the conductive ES form can be converted back to its corresponding insulating base forms if the conditions change, either physically (for non-redox doping) or (electro-) chemically (for redox-doping).

In recent years, conducting polymers have emerged as one of the most promising transducers for chemsensors and biosensors owing to their unique electrical, electrochemical and optical properties that can be used to convert chemical

information or biointeractions into electrical or optical signals, which can easily be detected by modern techniques.[3,11-15] Different approaches to the application of conducting polymers in chemo- or bio-sensing applications have been extensively studied, such as the applicability of PPy or PT in alcohol sensor,[16] gas sensor,[17] enzyme sensors,[18] or for the detecting of antibodies[19], DNA,[20] and even whole living cells.[21]

However, for PANI, although wide applications in gas sensors,[22] ion sensors,[4c] optical pH sensors [23] and other chemisensing schemes[24] have been reported, its direct application for biosensing purposes is rather limited.[25,26] The main reason for this is the fact that the redox activity of PANI can only be maintained in acidic conditions, normally at pH<4.[7,27] We also measured the electroactivity of PANI films both in acid conditions and in neutral pH conditions, as shown in Figure 1-2. Clearly, PANI shows nice redox activity in 0.5 M H_2SO_4 solution. However, if the same film was measured in pH 7 PBS buffer, only a weak broad oxidative peak appeared in the first potential cycling, and even this peak disappeared during the second scan. This loss of redox activity of PANI in neutral pH conditions greatly restricts its applications in bioassays, which normally require a neutral pH environment.
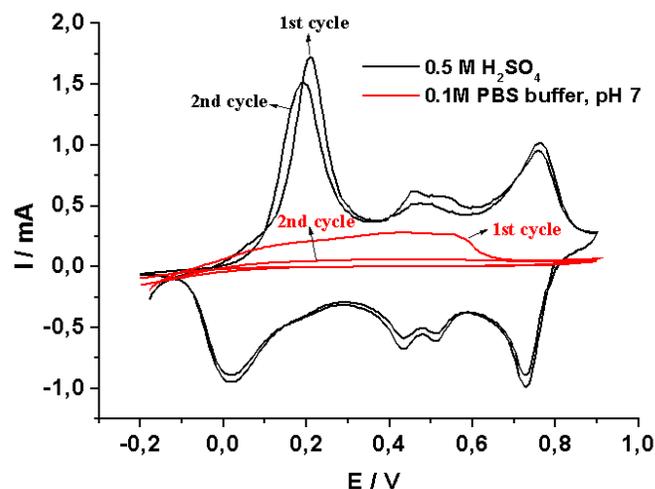
Fig.1-2 *Cyclic voltammograms of PANI measured in acidic and neutral pH solutions for two consecutive scans at a scan rate of 20 mV/s.*

In order to overcome this drawback, many successful efforts have been reported over the past decade. One approach is to introduce acidic groups (e.g. -COOH, -SO_3H, ect.) into the PANI chain and to form a so-called "self-doped" PANI, which

can maintain its electroactivity in neutral or even basic conditions.[27c,28] In this case , the inserted ionogenic groups change the micro-environment of the nitrogen atoms in the PANI chain, thus shifting the local pH.

Another normally used method is to dope PANI with negatively charged polyelectrolytes (such as poly(acrylic acid), poly(vinyl sulfonate), poly(styrene sulfonate), sulfonated polyaniline, etc.) by electrocopolymerization method.[27b,29] All these PANI films showed good redox activity in neutral solutions. This was attributed to the effective doping (protonation) of PANI by the trapped polyelectrolytes in a broad pH range. Moreover, some of above PANI films have been successfully utilized to immobilize enzymes for constructing biosensors.[30]

1.2 Aim of the present research work

The main aim of the present work is to dope PANI with different dopants in order to shift its redox activity to a neutral pH environment and to explore their biosensing applications. However, we use another simple method, i. e. the layer-by-layer (LBL) self-assembly method, to prepare PANI composites other than by the above reported electrocopolymerization method. The LBL self-assembly method developed by Decher et al [31,32] has several advantages as compared to the above mentioned techniques: (a) it is extremely simple; (b) it can be applied to almost any materials as long as they have the opposite charges; (c) it can yield a highly organized structure with excellent control over the positioning of individual layers and the thickness at the nanometer scale.

In addition, the dopants we used were not only limited to the traditionally used negatively charged linear polyelectrolytes. We also tried, for the first time, other novel functionalised materials such as modified gold nanoparticles or modified carbon nanotubes, by the LBL method. Results showed that PANI multilayer films doped by gold nanoparticles or carbon nanotubes exhibit better electroactivity in neutral conditions and better electrocatalytic ability toward the oxidation of β-nicotinamide adenine dinucleotide (NADH), as compared to those doped by negatively charged polyelectrolytes. Actually, the method we used here also offered another simple yet novel approach to incorporate gold nanoparticles or canbon nanotubes into (conducting) polymers which is another hot research topic nowadays.[33,34] Besides, due

to the unique electrical, optical, and optoelectrical properties of PANI and gold nanoparticles or carbon nanotubes, the obtained PANI multilayer films should also find potential applications in other fields such as microelectronics, or for electrochromic and photovoltaic devices.

DNA hybridisation detection based on conducting polymers (such as PPy, PT, ect.) has been reported before.[20] However, for PANI, no such efforts have been reported. Because the PANI/modified gold nanoparticle multilayer film we prepared is electroactive at neutral pH and allows the easy binding of amino-terminated DNA to its surface, the detection of DNA hybridisation based on this PANI system was explored for the first time. The detection event was monitored either by direct electrochemical methods, by an enzyme-amplified electrochemical approach, or by surface plasmon enhanced fluorescence spectroscopy (SPFS). All the methods can effectively differentiate non-complementary DNA from the complementary one, even at the single-base mismatch level.

Finally, patterned PANI composites (gratings or inverse opals) were also prepared by several different patterning techniques, and their potential sensing applications also explored.

It should be noted that, before all the above mentioned studies of PANI composites in neutral conditions, the electropolymerization and doping/dedoping properties of polyaniline films in acidic conditions were investigated first in detail. The dielectric constants of the polyaniline thin film at several doping levels (i.e. different oxidation states) were quantitatively determined. These studies laid a good foundation for our subsequent studies of the properties of PANI composite films in neutral conditions and their applications.

1.3 References

1. T. A. Skotheim, R. L. Elsenbaumer, J. R. Reynolds, Eds. *Handbook of Conducting Polymers*, 2nd ed.; Marcel Dekker: New York, **1998**.
2. G. G. Wallace, G. M. Spinks, P. R. Teasdale, *Conductive Electroactive Polymers: Intelligent Materials Systems*; Technomic: Lancaster, **1997**.

3. J. F. Rubinson, H. B. Mark, Jr, *Conductive Polymers and Polymer Electrolytes: From Biology to Photovoltaics*; ACS, Washington D C, **2002**.

4. a) A. G. MacDiarmid, *Synth. Met.* **1997**, *84*, 27. b) R. D. McCullough, *Adv. Mater.* **1998**, *10*, 93. c) J. Bobacka, A. Ivaska, A. Lewenstam, *Electroanalysis*, **2003**, *15*, 366. d) G. G. Wallace, M. Smyth, H. Zhao, *Trends in Anal. Chem.* **1999**, *18*, 245.

5. http://nobelprize.org/chemistry/laureates/2000.

6. H. Letheby, *J. Chem. Soc.*, **1862**, *15*, 161.

7. A. F. Diaz, J. A. Logan, *J. Electroanal. Chem.* **1980**, *111*, 111

8. A. G. MacDiarmid, A. J. Epstein, *Faraday Discuss Chem. Soc.* **1989**, *88*, 317 and references therein.

9. a) W.-S. Huang, B. D. Humphrey, A. G. MacDiarmid, *J Chem. Soc., Faraday Trans. 1*, **1986**, *82*, 2385. b) J. Y. Shimano, A. G. MacDiarmid, *Synth. Met.* **2001**, *123*, 251.

10. a) J. C. Chiang, A. G. MacDiarmid, *Synth. Met.* **1986**, *13*, 193. b) A. G. MacDiarmid, J. C. Chiang, A. F. Richter, A. J. Epstein, *Synth. Met.* **1987**, *18*, 285.

11. G. Bidan, *Sens. Actuators B* **1992**, *6*, 45.

12. P. N. Bartlett, P. R. Birkin, *Synth. Met.* **1993**, *61*, 15.

13. S. B. Adeloju, G. G. Wallace, *Analyst* **1996**, *121*, 699.

14. W. Göpel, K.-D. Schierbaum, in *Handbook of Organic Conductive Molecules and Polymers, Vol. 4. Conductive Polymers: Transport, Photophysics and Applications* (Ed: H.S. Nalwa), Wiley, Chichester **1997**, pp. 621-659.

15. D. T. McQuade, A. E. Pullen, T. M. Swager, *Chem. Rev.* **2000**, *100*, 2537.

16. M. Josowicz, J. Janata, *Anal. Chem.* **1986**, *58*, 514.

17. J. J. Miasik, A. Hooper, B. C. Tofield, *J. Chem. Soc., Faraday Trans.* **1986**, *82*, 1117

18. a) N. F. Foulds, C. R. Lowe, *J. Chem. Soc., Faraday Trans.* **1986**, *82*, 1259. b) M. Umaña, J. Waller, *Anal. Chem.* **1986**, *58*, 2979.

19. a) I. Taniguchi, T. Fujiyasu, S. Tomimura, H. Eguchi, K. Yasukouchi, I. Tsuji, M. Unoki, *Anal. Sci* , **1986**, *2*, 587. b) L. A. Samuelson, D. L. Kaplan, J. O. Lim, M. Kamath, K. A. Marx, S. K. Tripathy, *Thin Solid Films* **1994**, *242*, 50. c) D. Barnett, O. A. Sadik, M. J. John, G. G. Wallace, *Analyst* **1994**, *119*, 1997.

20. a) H. Korri-Youssoufi, F. Garnier, P. Srivastava, P. Godillot, A. Yassar, *J. Am. Chem. Soc.* **1997**, *119*, 7388. b) J. Wang, M. Jiang, A. Fortes, B. Mukherjee, *Anal. Chim. Acta.* **1999**, *402*, 7. c) T.-Y. Lee, Y.-B. Shim, *Anal. Chem.* **2001**, *73*, 5629. d) J. Cha, J. I. Han, Y. Choi, D. S. Yoon, K. W. Oh, G. Lim, *Biosen. Bioelectron.* **2003**, *18*, 1241. e) L. A. Thompson, J. Kowalik, M. Josowicz, J. Janata *J. Am. Chem. Soc.* **2003**, *125*, 324.

21. A. J. Hodgson, M. J. John, T. Campbell, A. Georgevich, S. Woodhouse, G. G. Wallace, *Proc. SPIE Smart Mater. Technol. Biomimetics* **1996**, *2716*, 164.

22. a) a recent review by D. Nicolas-Debarnot, F. Poncin-Epaillard, *Anal. Chim. Acta* **2003**, *475*, 1. b) S. Virji, J. Huang, R. B. Kaner, B. H. Weiller, *Nano Lett.* **2004**, *4*, 491.

23. a) E. Pringsheim, E. Terpetschnig, O. S. Wolfbeis, *Anal. Chim. Acta* **1997**, *357*, 247. b) E. Pringsheim, D. Zimin, O. S. Wolfbeis, *Adv. Mater.* **2001**, *13*, 819. c) U.-W. Grummt, A. Pron, M. Zagorska, S. Lefrant, *Anal. Chim. Acta* **1997**, *357*, 253.

24. J. Huang, S. Virji, B. H. Weiller, R. B. Kaner, *J. Am. Chem. Soc.* **2003**, *125,* 314.

25. a) P. N. Bartlett, R. G. Whitaker, *Biosensors*, **1987**, *3*, 359. b) H. Shinohara, T. Chiba, M. Aizawa, *Sensors Actuators* **1988**, *13*, 79. c) J. C. Cooper, E. A. H. Hall, *Biosensors*, **1992**, *7*, 473. d) S. Mu, H. Xue, B. Qian, *J. Electroanal. Chem.* **1991**, *304*, 7. e) S. Mu, J. Kan, J. Zhou, *J. Electroanal. Chem.* **1992**, *334*, 121.

26. E. S. Forzani, H. Zhang, L. A. Nagahara, I. Amlani, R. Tsui, N. Tao, *Nano Lett.* **2004**, *4*, 1785.

27. a) T. Ohsaka, Y. Ohnuki, N. Oyama, K. Katagiri, K. Kamisako, *J. Electroanal. Chem.* **1984**, *161*, 399. b) G. E. Asturias, G. W. Jang, A. G. MacDiarmid, K. Doblhofer, C. Zhong, *Ber. Bunsen-Ges. Phys. Chem.* **1991**, *95*, 1381. c) J. Yue, A. J. Epstein, A. G. MacDiarmid, *Mol. Cryst. Liq. Cryst.* **1990**, *189*, 255.

28. A. A. Karyakin, A. K. Strakhova and A. K. Yatsimirsky, *J. Electroanal. Chem.*, **1994**, *371*, 259.

29. a) P. N. Bartlett, P. R. Birkin, E. N. K. Wallace, *J. Chem. Soc., Faraday Trans.* **1997**, *93*, 1951. b) P. N. Bartlett, E. Simon, *Phys. Chem. Chem. Phys.*

2000, *2*, 2599. c) P. N. Bartlett, E. N. K. Wallace, *J. Electroanal. Chem.* **2000**, *486*, 23.

30. a) E. Simon, C. M. Halliwell, C. S. Toh, A. E. G. Cass, P. N. Bartlett, *Bioelectrochemistry*, **2002**, *55*, 13. b) O. A. Raitman, E. Katz, A. F. Bückmann, I. Willner, *J. Am. Chem. Soc.* **2002**, *124*, 6487.

31. a) G. Decher, J. D. Hong, J. Schmitt, *Thin Solid Films* **1992**, *210-211*, 831. b) G. Decher, *Science* **1997**, *277*, 1232.

32. a) M. Ferreira, J. H. Cheung, M. F. Rubner, *Thin Solid Films* **1994**, *244*, 806. b) J. H. Cheung, A. F. Fou, M. F. Rubner, *Thin Solid Films* **1994**, *244*, 985.

33. J. M. Lehn, *Supramolecular Chemistry – Concepts and Perpectives*, VCH, Weinheim, **1995**.

34. R. Gangopadhyay, A. De, *Chem. Mater.* **2000**, *12*, 608, and references therein.

Chapter 2
Experimental Section

2.1 Materials

The preparation and processing of the main materials used in the present study are described in the following.

2.1.1 Polyaniline (PANI)

PANI was prepared by two different methods: electrochemical polymerisation and oxidative chemical polymerisation.

Electrochemical polymerisation. 0.02 M aniline in 0.5 M H_2SO_4 solution was polymerised by potential cycling between -0.2 and 0.9 V at a scan rate of 20 mV/s. The solution was thoroughly degassed in advance by pure N_2. After polymerisation, the PANI film was thoroughly rinsed with 0.5 M H_2SO_4. This method is mainly used in Chapter 3.

Oxidative chemical polymerisation. The chemical method for the preparation of PANI followed the procedures reported before.[1] Briefly, 250 ml 0.25 M ammonium persulfate $((NH_4)_2S_2O_8)$ aqueous solution was added drop by drop to 150 ml 0.5 M aniline dissolved in 1 M HCl solution, both solutions being pre-cooled to 0 ^{o}C. The reaction was allowed to proceed for about 2h under stirring in an ice bath. Then the precipitate which had formed was removed by filtration, washed repeatedly with 1M HCl and dried under vacuum for about 48h. The material thus obtained is in its salt form (ES): polyemeraldine hydrochloride (PANI-HCl), and is green colored.

The above obtained PANI-HCl salt form was converted into the polyemeraldine base (EB) form by treating it with a 0.1M ammonium hydroxide (NH_4OH) solution for about 24h while stirring. The obtained powder was then dried under vacuum for 48h. In order to remove the lower-molecular-weight species, the obtained EB was further extracted with CH_3CN until the extract was colourless.

The prepared PANI in the EB form was made water-soluble according to the procedure used by Rubner et al.[2] PANI was first dissolved in dimethylacetamide

(DMAc) at a concentration of 20mg/ml by sonicating it overnight, then the obtained solution was filtered through a 0.5µm filter. Finally, the dipping solution was prepared by diluting the above solution 10 times using pH 3.1 HCl solution. Next, the pH of the solution was quickly lowered to around 2.6. Just before the LBL self-assembly process, the solution was further filtered through a 0.2µm filter.

Polymerisation mechanism. No matter whether PANI is synthesized electrochemically or chemically, it is generally assumed that there is a close similarity in their polymerisation mechanism.[1,3] In both case, the polymerisation process proceeds via the following mechanism:

The first step is the formation of the radical cation by an electron transfer from the 2s energy level of the aniline nitrogen atom, as shown in Figure 2-1. The formed aniline radical cation has several resonant forms, in which (c) is the more reactive one due to its important substituant inductive effect and its absence of steric hindrance.
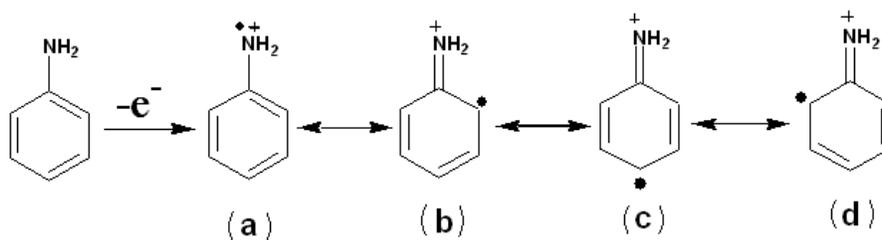
Fig.2-1 *The formation of the aniline radical cation and its different resonant structures.*

The next step corresponds to the dimer formation by the so-called "head to tail" reaction between the radical cation and its resonant forms (most probably form (c)) in acidic medium. Then the dimer is oxidized to form a new radical cation dimer, as shown in Figure 2-2.

Next, the formed radical cation can react either with the radical cation monomer or with the radical cation dimer to form, respectively, a trimer or a tetramer. If this continues, similar to the above steps, the PANI polymer is finally formed (Fig.2-3).

2.1.2 Sulfonated Polyaniline (SPANI)

The above prepared PANI EB can be transformed to sulfonated polyaniline (SPANI) using the reported method by Epstein.[4] In a typical preparation experiment,

0.25 g PANI EB was dissolved in 20 ml of fuming sulphuric acid with constant stirring for about 2h. The solution was then slowly added at a rate of 2 ml/min to 100
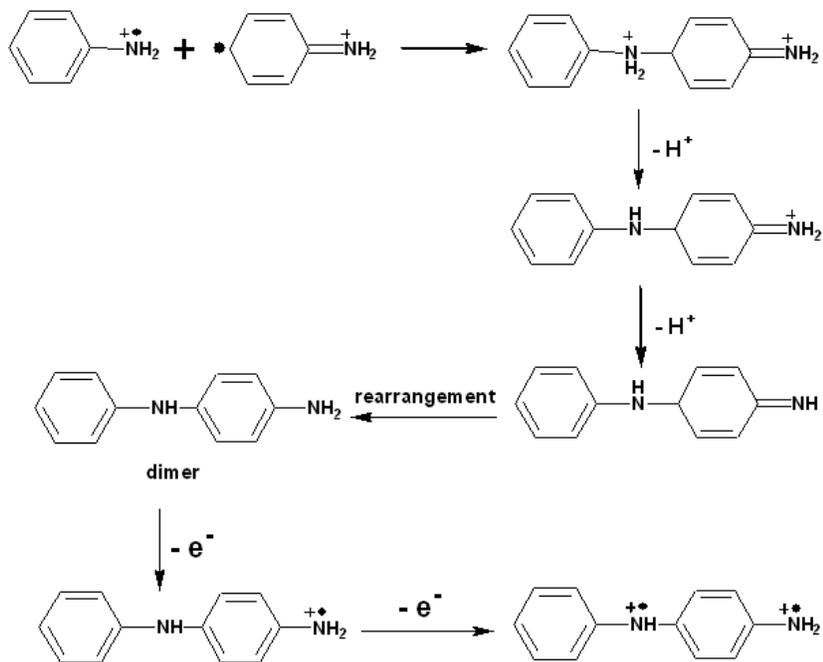
Fig.2-2 *Formation of the dimer and its corresponding radical cation.*
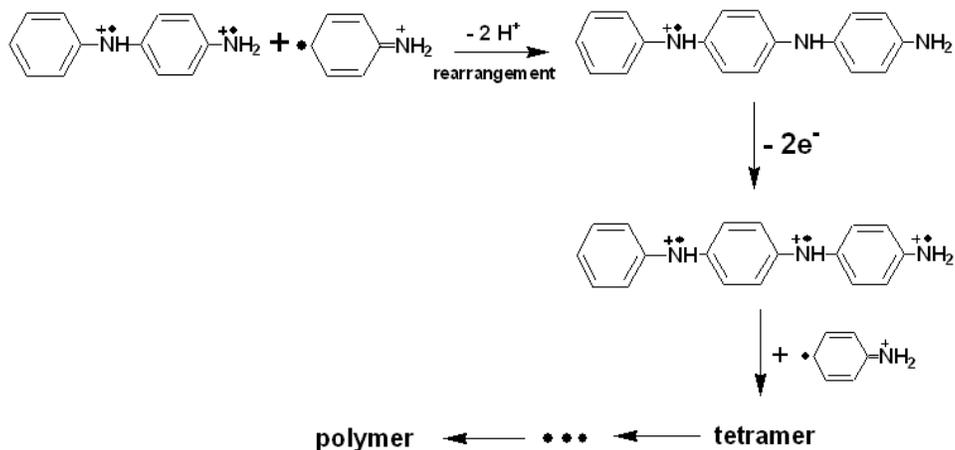
Fig.2-3 *One possible way of PANI polymer formation.*
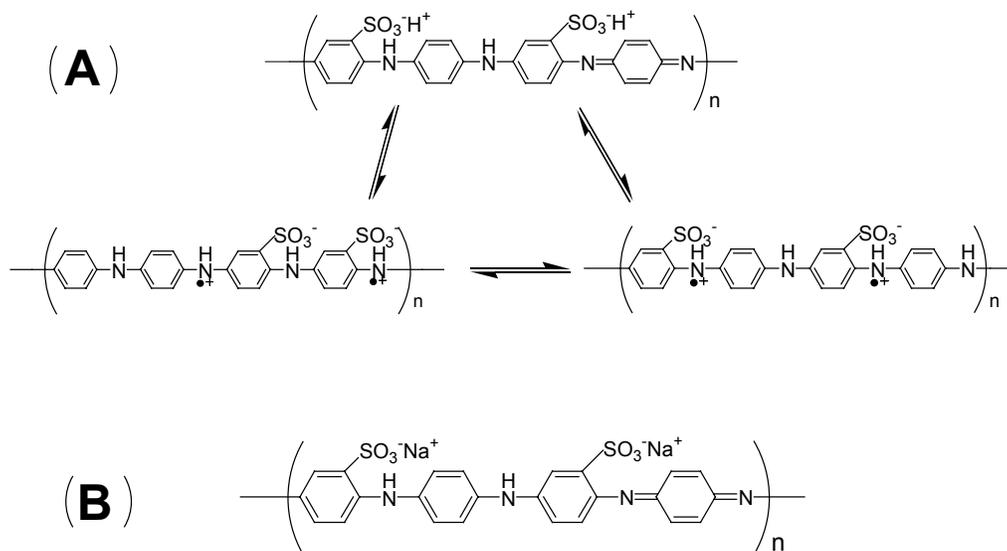
Fig.2-4 *(A) The coexisting structures of prepared SPANI; (B) The salt form of SPANI when treated with 0.1M NaOH.*

ml of methanol to precipitate most of the product. During this process, the temperature was held between $10 \sim 20$ °C by an ice bath. Precipitation was completed by the addition of 50 ml of acetone. The green precipitate was filtered and washed thoroughly with methanol, and then dried under dynamic vacuum for 24h. The obtained product (SPANI) has the structures as shown in Figure 2-4 (A).

The prepared SPANI was readily soluble in 0.1M NaOH solution. In this case, it exists in the nonprotonated sodium salt form (c.f. Fig.2-4 (B)). The pH of the solution was adjusted to near pH = 3 just before the LBL self-assembly process.

2.1.3 Mercaptosuccinic-acid-capped Gold Nanoparticles (MSAG$_{NP}$)

Gold nanoparticles modified with mercaptosuccinic acid (MSAG$_{NP}$) were synthesized with several different sizes. The preparation methods of MSAG$_{NP}$ are a little different for different sizes. For the smaller ones (diameter < 5nm), the synthesis and the modification were accomplished in one step, while for the bigger ones (diameter > 5nm), the Au nanoparticles were first synthesized, and then modified with mercaptosuccinic acid (MSA). The size of the prepared MSAG$_{NP}$ was checked by transmission electron microscope (TEM) and UV-Vis spectroscopy. The prepared MSAG$_{NP}$ are water-soluble and can be readily used for the LBL self-assembly. Just

before use, $MSAG_{NP}$ powder was re-dispersed in Milli-Q water at a concentration of 0.03mg/ml.

2.1.3.1 $MSAG_{NP}$ with diameter < 5nm

$MSAG_{NP}$ (diameter < 5 nm) was prepared following Kimura's method.[5] In this method, the synthesis of the Au nanoparticles and their modification with MSA were done in only one step (see Fig.2-5). The size of the obtained $MSAG_{NP}$ can be easily controlled by the molar ratio of $HAuCl_4$ and MSA. In our case, we use an equal molar ratio. In brief, in a 500ml 3-neck round bottom flask, 1.25mmol $HAuCl_4 \cdot 3H_2O$ in 5ml Milli-Q water and 1.25mmol MSA in 245ml methanol were mixed and vigorously stirred for 30min at room temperature. A freshly prepared 12.5mmol $NaBH_4$ in 25ml water solution was added drop by drop at a rate of 60~80 drops per minute, and finished in ca. 5 min. After further stirring for one hour, the precipitate was collected and washed by a repeated centrifugation-ultrasonic dispersion process in mixed methanol/H_2O, and finally dried in vacuum. The main product was collected as 220mg powder. The average particle size was around 2.0 ± 0.4 nm (details see Chapter 4).
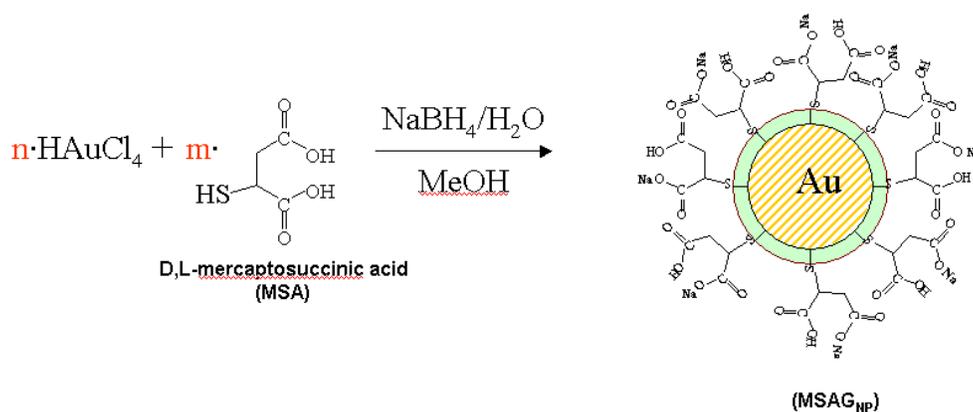
Fig.2-5 *Schematic of the preparation of $MSAG_{NP}$ with a diameter < 5 nm.*

2.1.3.2 $MSAG_{NP}$ with diameter > 5nm

For $MSAG_{NP}$ with diameter > 5 nm, the synthesis of the Au nanoparticles and their modification with MSA were carried out in two separate steps.

(a) Synthesis of Au nanoparticles

Au nanoparticles were synthesized by citrate reduction of gold chloride as reported before (c.f. Fig.2-6(A)).[6] Two batches of Au nanoparticles with a diameter around 10nm and 15nm, respectively, were prepared.
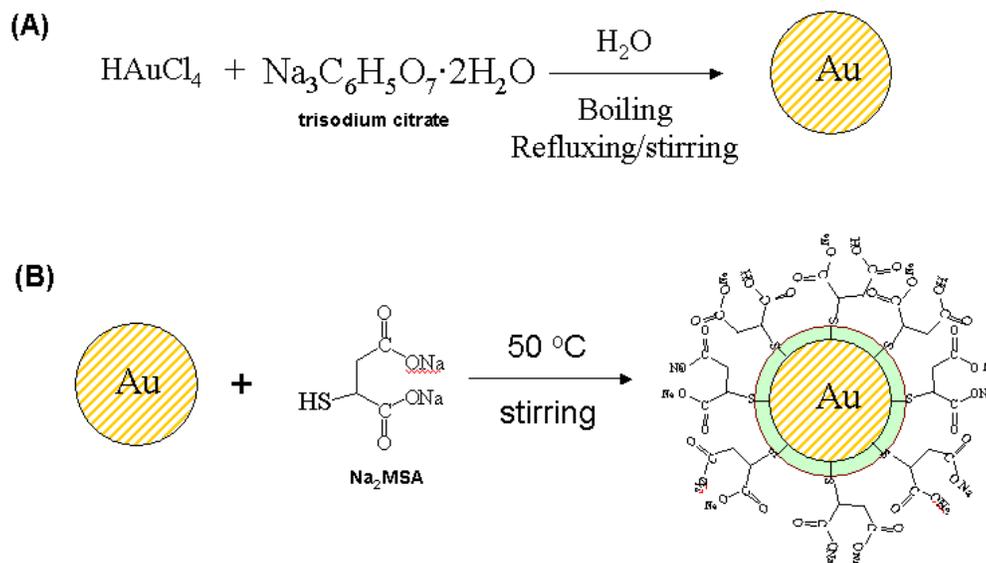
Fig.2-6 *Schematic of the preparation of MSAG$_{NP}$ with a diameter > 5 nm. (A) synthesis of the Au colloids; (B) modification of the Au colloids with MSA.*

Preparation of Au nanoparticles with a diameter of 10 nm. In a clean 250 ml two-neck round-bottom flask, 106 ml 0.064% (w/v) trisodium citrate aqueous solution was brought to boiling under reflux and stirring and then 1 ml 0.955% (w/v) HAuCl$_4$ aqueous solution was injected quickly. After the color change finished in around 2 min, the mixture was kept boiling and stirred for another 15min. Then the heating source was removed, but the solution was kept stirred until it cooled to the room temperature. The colloidal suspension prepared this way had a mean particle size of around 9.9 ± 0.8 nm.

Preparation of Au nanoparticles with a diameter of 15 nm. For preparation of Au nanoparticles with this size, the order of adding sodium citrate and HAuCl$_4$ is reversed. Firstly, 150 ml 0.01% (w/v) HAuCl$_4$ aqueous was heated to a boiling state in a 250 ml two-neck round-bottom flask under reflux and stirred conditions, and then 10 ml 1% (w/v) trisodium citrate aqueous solution was quickly injected. The reaction was left to continue for about 25 min under boiling and stirred state. Then the heating

source was removed, but the solution was kept stirred until it cooled to the room temperature. The colloidal suspension prepared this way had a mean particle size of around 15.2 ± 1.4 nm.

(b) Modification of Au nanoparticles with MSA

Surface modification of the Au nanoparticles with MSA was carried out using the reported procedures (c.f. Fig.2-6(B)).[7] That is, a certain volume of the above-described Au colloids were mixed with an aqueous solution containing a large excess of MSA (typically, 100 ml Au colloid with 15 ml 0.01 M Na$_2$MSA) and stirred at 50 $^{\circ}$C for about 8-12h. After reaction, the modified samples were dialysed with Milli-Q water several times. Then the product was centrifuged and finally dried under vacuum.

2.1.4 Polyaminobenzene Sulfonic Acid-Modified Single-Walled Carbon Nanotubes (PABS-SWNTs)

Polyaminobenzene sulfonic acid-modified single-walled carbon nanotubes (PABS-SWNTs, OD×L: 1.1nm×0.5-100μm) were obtained from Sigma. The modification procedure of the carbon nanotubes with PABS can be found in the literature (c.f Fig.2-7).[8] Firstly, the SWNTs were treated with nitric acid to open the end caps and to leave them terminated with carboxylic acid groups (-COOH). Then SWNTs-COOH
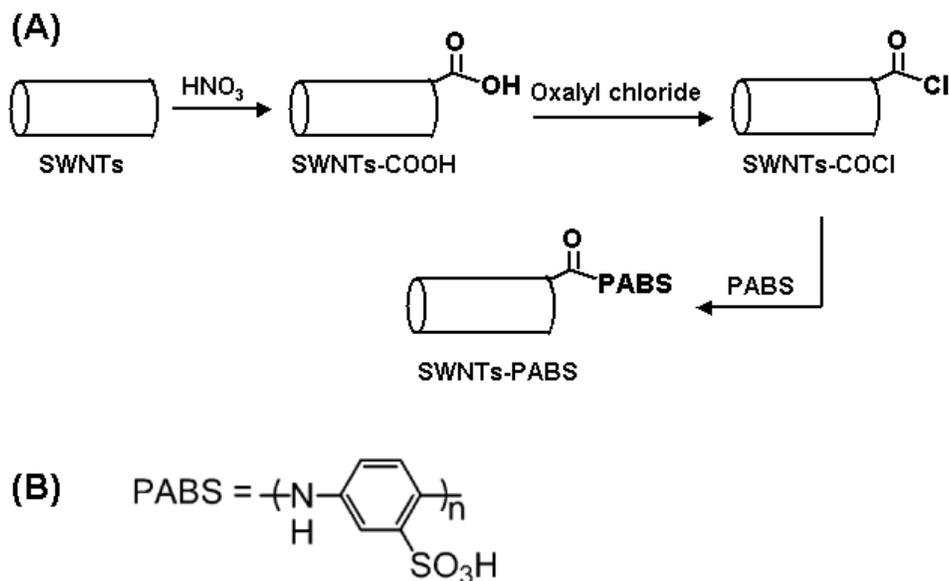
Fig.2-7 (A) Schematic of chemical functionalization of SWNTs with PABS. (B) Chemical structure of PABS.

were transformed into acyl chloride form (SWNTs-COCl) as an intermediate product for further chemical functionalization by reacting them (in DMF) with oxalyl chloride at 0 $^\circ$C under nitrogen atmosphere. Finally, SWNTs-COCl was further functionalised with PABS at 100 $^\circ$C for 5 days to get PABS-SWNTs. The surface charge density of the obtained PABS-SWNTs was reported to be in the range of 0.2~0.5 atomic %.[8,9]

When carrying out the LBL self-assembly process, PABS-SWNTs were dissolved directly in Milli-Q water by sonication for 30s at a concentration of 0.25mg/ml.

2.1.5 ß-Nicotinamide Adenine Dinucleotide (NAD$^+$, reduced form NADH)

NADH (disodium salt hydrate, purity > 98%) was obtained from Sigma.

NADH and NAD$^+$ are important coenzymes that act as electron and proton shuttle in metabolic reactions, esp. in tissue respiration. Their structures are shown in Figure 2-8. Attention should be directed to the coloured carbon nitrogen ring structure: there are an extra H and two electrons (not visible, but important) in the ring structure of NADH.
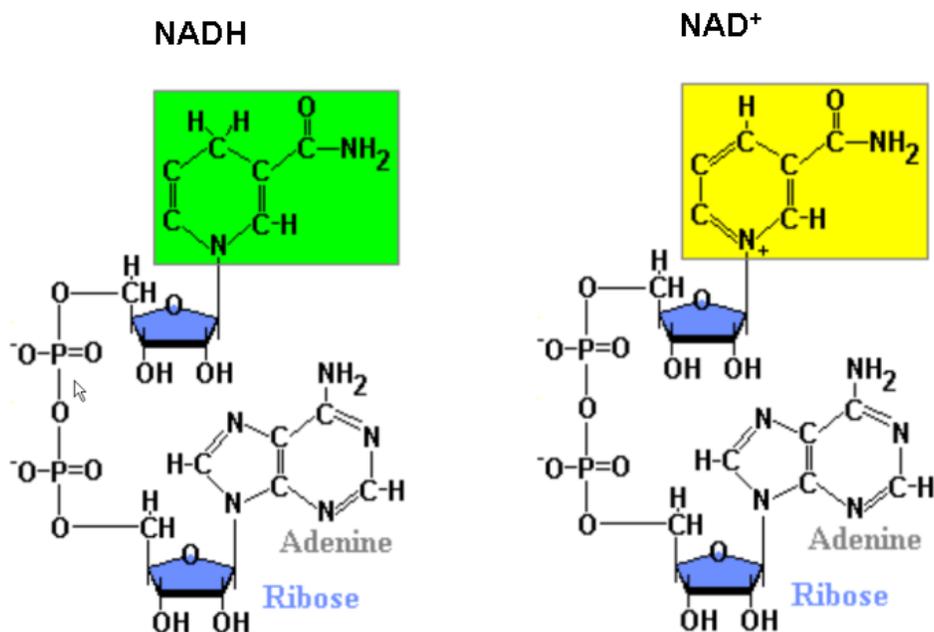
Fig.2-8 *The structures of NADH and NAD$^+$.*

NADH / NAD$^+$ take part in a number of dehydrogenase enzymatic reactions, and play a key role in developing amperometric enzyme sensors or biofuel cells that use

dehydrogenase dependent enzymes. However, the direct oxidation of NADH at bare electrodes in a neutral environment normally requires high overpotentials up to 1.0V.[10] Consequently, different redox mediators have been used to reduce the overpotential for NADH oxidation. Among them, PANI doped with polyanions by the electropolymerisation has been shown to be a good candidate.[11] Here in our study we demonstrated that the PANI composites prepared via the LBL method could also electrocatalyze the oxidation of NADH at a lower potential in a neutral pH condition, which serves as a first example of the applications of the prepared PANI multilayer films for bioassays.

2.1.6 DNA samples

All the DNA samples used in this study were synthesized and purified either by MWG-Biotech AG (Ebersberg, Germany) or by Eurogentec (Seraing, Belgium), their sequences are listed in Table 2-1.

Table 2-1 The DNA sequences and their nomenclatures

Name	Sequences
NH$_2$-DNA (probe NDA)	NH$_2$-C$_6$H$_{12}$- 5'-TGT ACA TCA CAA CTA-3'
MM0 (complementary DNA)	3'-ACA TGT AGT GTT GAT-5' (-Cy5 or -HRP)
MM15 (non-complementary DNA)	3'-ATC AAC ACT ACA TGT-5' (-Cy5 or -HRP)
MM1 (single-base mismatch)	3'-ACA TGC AGT GTT GAT-5' (-Cy5 or -HRP)
MM2 (two-base mismatch)	3'-ACA CGT ACT GTT GAT-5' (-Cy5 or -HRP)

The amino-terminated probe DNA (NH$_2$-DNA) was attached to the carboxyl group of the prepared PANI multilayer film by formation of an amide bond with the aid of 1-Ethyl-3-(3-dimethylaminopropyl)-carbodiimide (EDC) and N-Hydroxysuccinimide (NHS), as shown in Figure 2-9. First, the carboxyl groups on the outside of the PANI multilayer film was activated by EDC to form an O-urea derivative that is an unstable amine-reactive intermediate. Then the intermediate was further reacted with NHS to produce a more stable reactive intermediate ester which has been shown to give a greater reaction yield.[12] Finally, the amino-terminated probe DNA reacted with the

active ester by covalent coupling via an amide bond formation. Further details to use this substrate to detect target DNA with different sequences by different techniques can be found in Chapter 5.
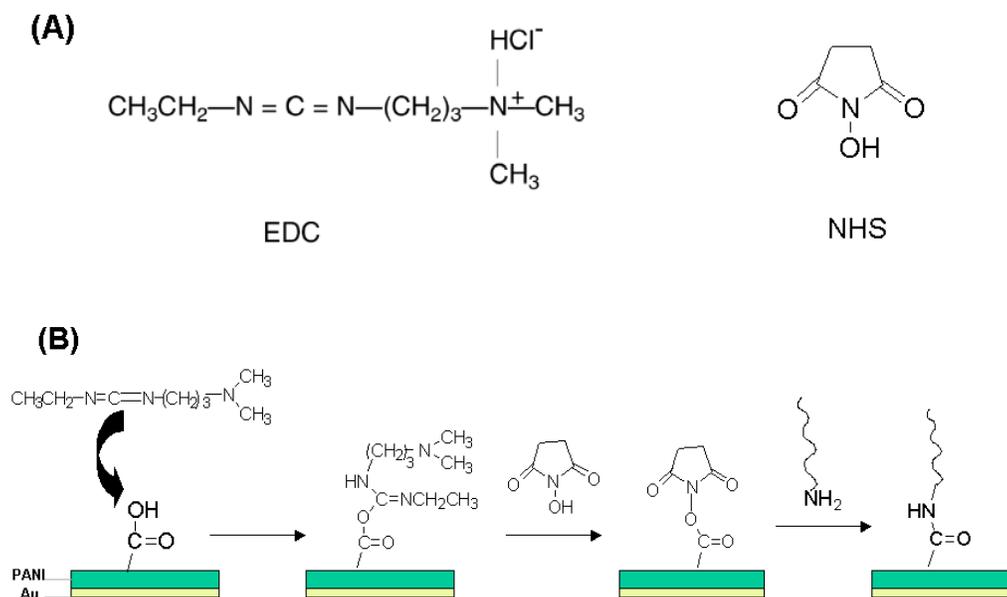
Fig.2-9 *(A) Chemical structures of EDC and NHS. (B) Schematic diagram showing the covalent attachment of an amino-terminated probe DNA to PANI multilayer film terminated with carboxylic acid groups.*

2.1.7 Au Substrate

Au substrates play an important role in the present study. It was used not only to couple the surface plasmons in the SPR measurements, but also as the working electrode in the electrochemical experiments.

Au substrates were prepared by the successive vacuum evaporation ($P<1.0\times10^{-6}$ mbar) of a 2nm Cr layer followed by a 50nm Au layer onto a clean high-index LaSFN9 glass slide (Schott, n=1.85 at 633nm) at a evaporation rate of ~ 0.1nm/s. The prepared Au substrates were used right away or stored under Argon for no more than 10 days.

2.2 Measurement and Instrumentation

The main detection method in the present study is the combination of electrochemistry with surface plasmon based optical techniques (ESPR, c.f. Fig.2-10). Besides, electrochemistry was also combined with the quartz crystal microbalance (EQCM) in order to gain more information of the studied systems. Other techniques used include transmission electron microscopy (TEM), atomic force microscope (AFM), low potential scanning electron microscope (LPSEM), UV-vis spectroscopy, etc.

2.2.1 Electrochemistry-Surface Plasmon Spectroscopy (ESPR)

Since conducting polymers are electroactive materials, their properties depend heavily on the degree of oxidation (p-doping) or reduction (n-doping) of the conjugated polymer backbone.[13] Therefore, electrochemistry plays an important role in the synthesis, characterization and applications of conducting polymers. Besides, due to the low cost, fast response, high sensitivity and easy compatibility with different technologies, electrochemistry is gaining much more popularity than any other techniques in studying conducting polymers.

Surface plasmon optical techniques have been shown to be an effective optical tool for the characterization of interfaces and thin films,[14] as well as for the sensitive detection of kinetic processes, e.g. for monitoring interfacial binding reactions[15] or the swelling or shrinking processes of a conducting polymer.[16]

In recent years, the combination of electrochemistry with surface plasmon spectroscopy (ESPR) has emerged to be a powerful tool for probing extremely small changes of various films at the metal/solution interface.[16,17] In our study, we use ESPR not only to monitor the film deposition in real-time, but also to examine the film conformation and properties in its different oxidation states (i.e. different doping levels). Besides, we demonstrated here that the bioelectrocatalytic processes can also be monitored in situ by ESPR.

Shown in Figure 2-10 (A) are the schematic drawing of the ESPR setup we used and its various extensions, based on the Kretschmann geometry.[18] The laser beam passes first a chopper (for lock-in detection) and two polarizers (for attenuation and polarization, respectively), and then is reflected off the base of the coupling prism

(A)

Photodiode detector
or CCD camera

lens

electrodes

goniometer

lens

attenuator

filter

PMT

laser

shutter   polarizers

chopper

valves   Tygon tubes

teflon
cell

peristaltic
pump

waste   sample

computer

| Shutter controller | Motor-steering | Photon counter | Electrochemical setup | Lock-in amplifier |

(B)

laser
P-pol

θ   θ

Prism

Glass slide

Working electrode(Au)

Outlet

Electrochemical
instrument

Inlet

Counter electrode

Reference electrode

Glass slide   Polymer film   O-ring   Teflon cuvette

***Fig.2-10*** *(A) Schematic drawing of a combined setup of electrochemistry with surface plasmon spectrometer based on the Kretschmann configuration (ESPR). (B) The enlarged part of mounting of the prism and the electrochemical flow cell.*

(LaSFN9, n=1.85 at 633nm). Coupled to the prism is an Au substrate (both for coupling surface plasmons and as the working electrode, c.f. Section 2.1.7), index

matched by an immersion oil (n=1.725) with the prism. The reflected light is focused by a lens onto a photodiode which is connected to the lock-in amplifier. Both the prism/sample and the photodiode are mounted on two co-axial goniometers, respectively, allowing different operation modes such as an angular scan in a θ-2θ reflection geometry or a kinetic mode at a fixed incident angle, but as a function of time.

The enlarged image of the electrochemical flow cell is shown in Figure 2-10 (B). This Teflon cuvette has two holes for reference and counter electrodes for the electrochemical measurements, as well as an inlet and outlet for sample exchange and rinsing. The whole cell is attached to the Au substrate, and sealed by O-rings and a BK7 glass slide. The effective area of the Au substrate exposed to the solution is 0.65cm^2. The electrochemical measurements were performed with an EG&G 263A potentiostat or an AutoLab (Eco Chemie B.V., The Netherlands), with a coiled platinum wire being used as the counter electrode, and an Ag/AgCl(3M NaCl) electrode as the reference electrode. All potentials reported here are with respect to this reference electrode.

For fluorescence measurements, a photomultiplier (PMT) is attached to the SPR setup from the backside of the cell to monitor the photons emitted from the metal/dielectric interface. The emitted light is focused by a lens and passes through an interference filter before it is collected by the PMT, which is connected to a photon-counter unit. The whole module is mounted to the sample goniometer so that it rotates with the sample cell, thus always collecting the emitted light at a constant angle relative to the metal surface. To minimize photo-bleaching effects of the fluorescent dyes, a programmable shutter is also installed to constantly block the laser unless during the data recording. In this case, the SPR setup is transformed into a surface plasmon resonance enhanced fluorescence spectroscopy (SPFS) setup.

2.2.2 Electrochemical Quartz Crystal Microbalance (EQCM)

In some parts of this study, EQCM was also used in order to get more information of the investigated systems or to confirm the results from the ESPR experiments.

QCM is very sensitive for probing small changes (especially mass changes) in thin surface films.[19] This technique relies on the fact that the resonant frequency of a quartz crystal oscillator changes linearly with the amount of *rigidly* attached mass.[20]

In the early 1980s, several groups reported the combination of electrochemistry with QCM (EQCM) by using one of the oscillator electrodes also as the working electrode of an electrochemical cell (c.f. Fig.2-11).[21] In this way, the mass changes and various other processes (such as viscoelasticity change) involving thin films on electrode surface could be monitored in real-time. Since then, EQCM has matured into a powerful tool that has found broad applications in studies of adsorption, electrodeposition, corrosion, oxide formation and reactivity, chemo- and bio- sensors, polymer and material sciences, ect., as have been reviewed by several groups.[22]

The schematic diagram of the EQCM setup we used is shown in Figure 2-11,
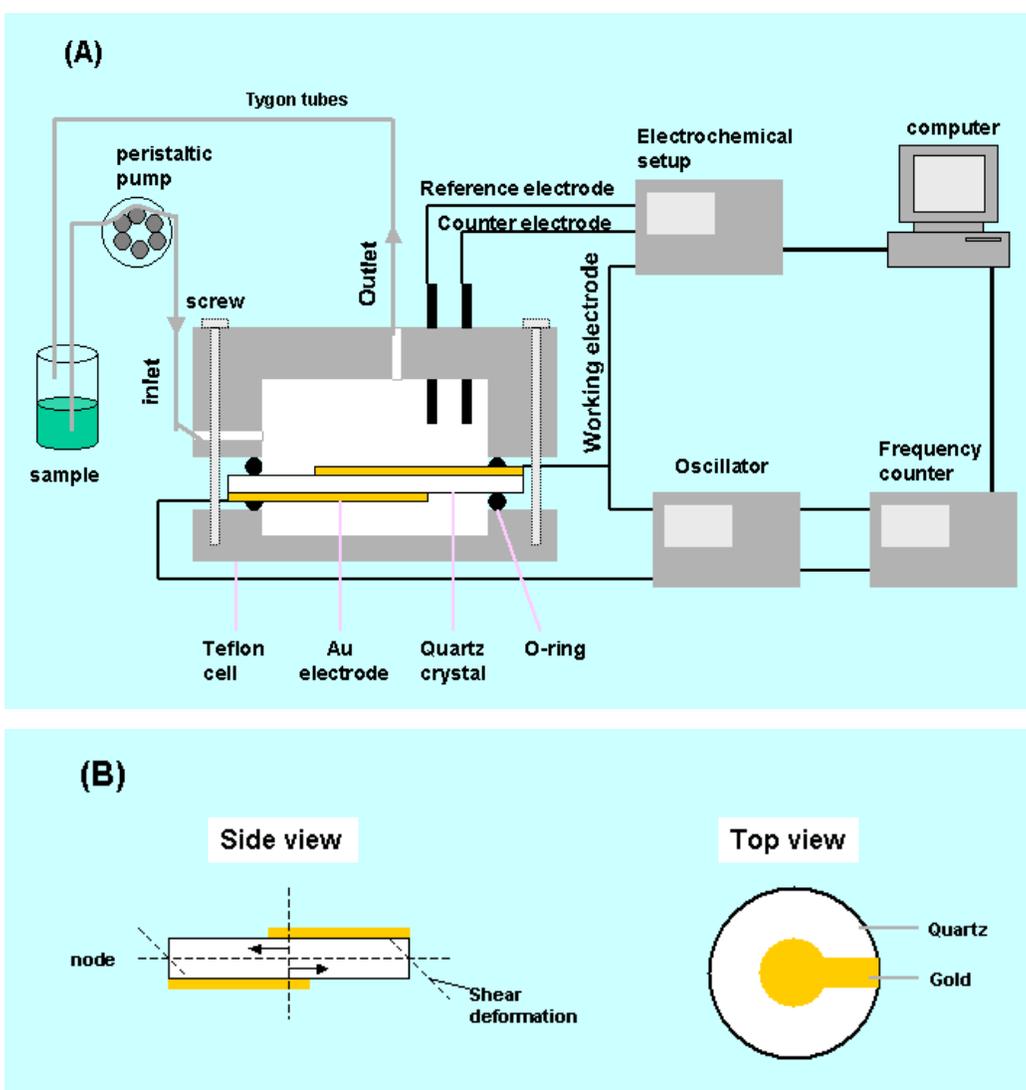

Fig. 2-11 *(A) Schematic diagram of the EQCM setup used in this study. (B) Schematic side and top views of a quartz crystal disk with deposited Au electrodes. Also shown in the side view is the acoustic wave and the deformation (shear) of the crystal under application of an electric field across the crystal (c.f. reference 23).*

similar to that reported previously.[22b,23] The quartz crystal (c.f. Fig.2-11B) is clamped in a Teflon flow cell sealed by appropriate O-rings to expose only one of the Au electrodes to the solution. This Au electrode is also the working electrode for electrochemistry and is thus part of both the electrochemical instrument and the oscillator circuits. The crystal is driven by a broadband oscillator circuit that tracks the resonant frequency change of the crystal caused by the electrochemically-induced changes on the electrode surface. The frequency is measured with a frequency counter. Both the oscillator/frequency counter and the electrochemical instrument are directly interfaced to a computer. The computer not only generates the electrochemical excitation waveforms, but also measures the current passing through the EQCM working electrode as well as the frequency of oscillation of the quartz disk.

The quartz crystals employed in this work were obtained from Maxtek Inc. (USA), which were of the "AT-cut" type, with a fundamental resonance frequency of 5 MHz. In EQCM measurements, the electrode surface area was determined to be 1.33 cm^2. The crystals were plasma cleaned before every experiment.

2.2.3 Other Techniques

Transmission electron microscopy (TEM, LEO EM912, operated at 120kV) was used to characterize the prepared Au nanoparticles. The specimen was prepared by first dispersing the particles in an aqueous ethanol solution, placing a few drops of particle solution onto the amorphous carbon-coated copper microgrids and then let it dry for the measurements. Image J software was used to analyse the obtained images to get the size distribution of the Au nanoparticles.

Atomic force microscope (AFM, Dimension 3100 or Mutimode) was used to examine the quality of the prepared PANI gratings operated in a tapping mode. A silicon cantilever was used, which has a spring constant of 42 N/s and a resonant frequency of 300 kHz.

A *Low potential scanning electron microscope* (LPSEM, LEO 1530 Gemini, operated at 1 kV) was used to check the obtained PANI inverse opals.

UV-vis spectroscopy was carried out on a Lambda UV/VIS/NIR spectrophotometer (Perkin-Elmer) to characterize the prepared Au nanoparticles.

2.3 Preparation of PANI Multilayer Films

Most of the studied PANI composite films were prepared on Au substrate using the layer-by-layer (LBL) method, as pioneered by G. Decher et al.[24] The preparation procedure is sketched in Figure 2-12.
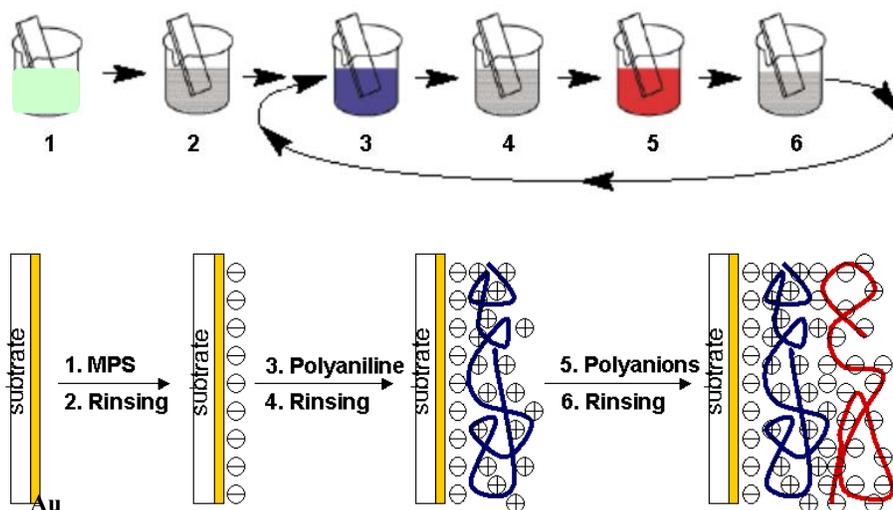
Fig. 2-12 *Schematic drawing of the process for preparing the PANI multilayer films via the LBL method.[24b] In our case, all the above process were carried out in a flow cell.*

First, the freshly prepared Au substrate was functionalised with a layer of 3-mercapto-1-propanesulfonic acid (MPS) by immersing it into a 1mM MPS ethanol solution for 2h, then rinsing first with ethanol, followed by rinsing with Milli-Q water, and then dried under a stream of nitrogen (steps 1 and 2). The functionalised Au substrates were negatively charged, and then immersed alternately in the solutions of PANI and the corresponding poly(anion)s for 15min each, with rinsing steps in between (steps 3-6). Repeating steps 3-6 allows one to get a multilayer film with a desired thickness. It should be noted that, in our case, all the above processes were carried out in a flow cell (c.f. Fig.2-10 and Fig.2-11) in order to monitor the film self-assembly process in real-time.

2.4 References

1. a) A. G. MacDiarmid, J. C. Chiang, A. F. Richter, N. L. D. Somasiri, a. J. Epstein, In *Conducting Polymers*; L. Alcacer, Ed.; D. Reidel Publishing Co: Dordrecht, The Netherlands, **1987**; p105. b) A. A. Syed, M. K. Dinesan, *Talanta* **1991**, *38*, 815.

2. a) E. P. Koval'chuk, S. Wittingham, O. M. Skolozdra, P. Y. Zavalij, I. Y. Zavaliy, O. V. Reshetnyak, M. Seledets, *Mater. Chem. Phys.* **2001**, *69*, 154. b) D. Nicolas-Debarnot, F. Poncin-Epaillard, *Anal. Chim. Acta* **2003**, *475*, 1.

3. Cheung, J. H.; Stockton, W. B.; Rubner, M. F. *Macromolecules* **1997**, *30*, 2712.

4. J. Yue, A. J. Epstein, *J. Am. Chem. Soc.* **1990**, *112*, 2800.

5. S. Chen, K. Kimura, *Langmuir* **1999**, *15*, 1075.

6. G. Frens, *Nature Phys. Sci.* **1973**, *241*, 20.

7. T. Zhu, K. Vasilev, M. Kreiter, S. Mittler, W. Knoll, *Langmuir*, **2003**, *19*, 9518.

8. H. Hu, Y. Ni, V. Montana, R. C. Haddon, V. Parpura, *Nano Lett.* **2004**, *4*, 507.

9. a) S. C. Tsang, Y. K. Chen, P. J. F. Harris, M. L. H. Green, *Nature* **1994**, *372*, 159. b) B. C. Satishkumar, A. M. J. Govindaraj, G. N. Subbanna, C. N. R. Rao, *J. Phys. B* **1996**, *29*, 4925.

10. a) P. N. Bartlett, P. R. Birkin, E. N. K. Wallace, *J. Chem. Soc., Faraday Trans.* **1997**, *93*, 1951. b) P. N. Bartlett, E. Simon, *Phys. Chem. Chem. Phys.* **2000**, *2*, 2599. c) P. N. Bartlett, E. N. K. Wallace, *J. Electroanal. Chem.* **2000**, *486*, 23.

11. a) J. Moiroux, P. J. J. Elving, *Anal. Chem.* **1978**, *50*, 1056. b) H. Jaegfeldt, *J. Electroanal. Chem.* **1980**, *110*, 295.

12. J.V. Staros, R.W. Wright, D.M. Swingle, *Anal. Biochem.* **1986**, *156*, 220.

13. a) W.-S. Huang, B. D. Humphrey, A. G. MacDiarmid, *J Chem. Soc., Faraday Trans. 1*, **1986**, *82*, 2385. b) D. Orata, D. A. Buttry, *J. Am. Chem. Soc.* **1987**, *109*, 3574. c) J. Bobacka, A. Ivaska, A. Lewenstam, *Electroanalysis*, **2003**, *15*, 366.

14. W. Knoll, *Annu. Rev. Phys. Chem.* **1998**, *49*, 569.

15. a) V. H. Perez-Luna, M. J. O'Brien, K. A. Oppermann, P. D. Hampton, G. P. Lopez, L. A. Klumb, P. S. Stayton, *J. Am. Chem. Soc.* **1999**, *121*, 6469. b) T. Liebermann, W. Knoll, *Colloids Surf. A* **2000**, *171*, 115. c) T. Liebermann, W. Knoll, P. Sluka, R. Herrmann, *Colloids Surf. A* **2000**, *169*, 337. d) D. Kambhampati , P. E. Nielsen, W. Knoll, *Biosen. & Bioelectron.* **2001**, *16*, 1109.

16. V. Chegel, O. Raitman, E. Katz, R. Gabai, I. Willner, *Chem. Commun.* **2001**, 883.

17. a) D. K. Kambhampati, W. Knoll, *Curr. Opin. Colloid Interface Sci.* **1999**, *4*, 273. b) S. Boussaad, J. Pean, N. J. Tao, *Anal. Chem.* **2000**, *72*, 222. c) X. F. Kang, Y. D. Jin, G. J. Cheng, S. J. Dong, *Langmuir* **2002**, *18*, 1713. d) A. Baba, M.-K. Park, R. C. Advincula, W. Knoll, *Langumir* **2002**, *18*, 4648.

18. E. Kretschmann, H. Raether, *Z. Naturforsch. Teil A* **1968**, *23*, 2135.

19. *Applications of Piezoelectric Crystal Microbalances-Methods and Phenomena* C. Lu, A. W. Czanderna, Eds.; Elsevier: New York, **1984**, *Vol.7*.

20. G. Sauerbrey, *Z. Phys.* **1959**, *155*, 206.

21. a) T. Nomura, M. Iijima, *Anal. Chim. Acta* **1981**, *131*, 97. b) S. Bruckenstein, M. Shay, *Electrochim. Acta* **1985**, *30*, 1295. c) O. Melroy, K. K. Kanazawa, J. G. Gordon, D. A. Buttry, *Langmuir* **1987**, *2*, 697. d) S. Bourkane, C. Gabrielli, M. Keddam, *Electrochim. Acta* **1989**, *34*, 1081.

22. a) M. D. Ward, D. A. Buttry, *Science*, **1990**, *249*, 1000. b) D. A. Buttry, M. D. Ward, *Chem. Rev.* **1992**, *92*, 1355. c) A. Janshoff, H.-J. Galla, C. Steinem, *Angew. Chem. Int. Ed.* **2000**, *39*, 4004. d) K. A. Marx, *Biomacromolecules*, **2003**, *4*, 1099. e) A special issue in *Electrochimica Acta* **2000**, vol 45, issues 22-23, edited by A. R. Hillman.

23. A. J. Bard, L. R. Faulkner, *Electrochemical Methods-Fundamentals and Applications*, 2nd Edition **2001**, pp 725-728.

24. a) G. Decher, J. D. Hong, J. Schmitt, *Thin Solid Films* **1992**, *210-211*, 831. b) G. Decher, *Science* **1997**, *277*, 1232. c) M. Ferreira, J. H. Cheung, M. F. Rubner, *Thin Solid Films* **1994**, *244*, 806.

Chapter 3

Electropolymerization and Doping / Dedoping Properties of Polyaniline Thin Films in Acidic Conditions

3.1 Introduction

As mentioned before, Polyaniline (PANI) has been studied extensively since the 1980s[1]. The interest in this material and its derivatives is mainly due to their interesting electrical and optical properties together with their chemical tunability, ease of derivatization, processability into fibers and films, and its stability. During the past two decades, the chemical and physical properties of polyaniline have been studied extensively under different conditions, and tremendous advances in the chemistry, electrochemistry, physics, theory, and processing of polyaniline have been achieved.[2] Although it is generally regarded that PANI has three main stable oxidation states, i.e. the fully reduced *leucoemeraldine base (LEB)* form, the half-oxidized *emeraldine base (EB)* form, the fully oxidized *pernigraniline base (PNB)* form. Each of the above insulating base forms can be transformed into the corresponding *emeraldine salt (ES)* form either by redox doping or non-redox doping (c.f. Chapter 1). However, the reported properties (either optical or electrical) of PANI are not always the same. Just as it is well known, that "there are as many different types of polyaniline as there are people who make it!"[3] So in this first part of this work, the properties of PANI in acidic conditions were investigated, in order to lay a good foundation for the subsequent studies of the properties of PANI composites in neutral conditions and their potential applications.

The electropolymerization and doping/dedoping properties of PANI ultrathin films on Au electrode surfaces in acidic conditions were investigated by a combination of in situ electrochemical techniques, i.e., electrochemical surface plasmon spectroscopy (ESPR) and the electrochemical quartz crystal microbalance (EQCM). In the ESPR measurements, we employed two wavelengths, i.e., λ=632.8 and λ=1152 nm in order to distinguish independently the electrochromic behavior. In addition, we used spectroelectrochemical transmittance measurements in order to probe further the

optical properties of the polymer films as a function of the applied potential. The real and imaginary parts of the dielectric constants of the PANI thin films at several doping levels was determined quantitatively by taking into consideration the thickness values obtained from the EQCM measurement.

3.2 Electropolymerisation of Aniline

Electrochemical polymerization of aniline on the gold surface was achieved by applying potential cycling between −0.2 and 0.9 V at a scan rate of 20 mV/s (c.f Chapter 2, Section 2.1.1). The cyclic voltammograms (CV) obtained during the electropolymerization are shown in Figure 3-1 (A) up to the seventh cycle. Similar conditions in aqueous H_2SO_4 in the potential range described, has been used by many groups.[4] As reported previously, the first redox process (ca. 0.22 V in the positive scan and 0.05 V in the negative scan) corresponds to the electron transfer from/to the electrodeposited PANI film. In order to compensate the charge of the PANI film, anion transport from/to the electrolyte solution, i.e., anion doping and dedoping, should occur.[5] This phenomenon is responsible for the dramatic change in the conductivity of the PANI film. The electrodeposition of PANI on the Au electrode proceeds via a radical cation mechanism (c.f Chapter 2, Section 2.1.1). The second redox process (ca. 0.5 and 0.45 V, for the oxidation and reduction, respectively) probably corresponds to side reactions such as decomposition of the polymer. The
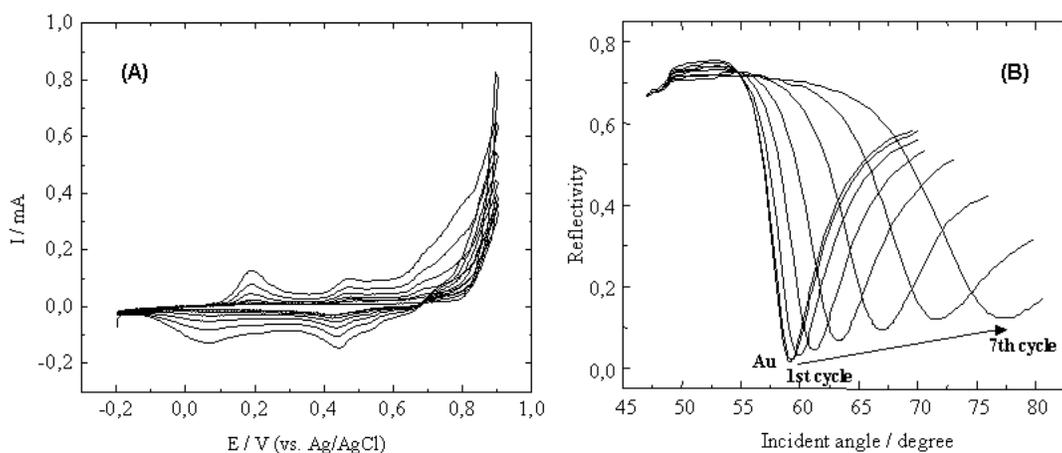
Fig. 3-1. *(A) Cyclic voltammograms of the electropolymerization of aniline (0.02 M) in H_2SO_4 (0.5 M) solution and (B) angular SPR reflectivity curves measured after each potential cycle.*

28

large currents observed at the positive end of the CV are due to the superposition of two distinct processes: one is the electron transfer from the PANI film corresponding to the oxidation of the PANI film and the other is the electron transfer from the aniline monomer to the electrode corresponding to the oxidation of the aniline monomer to produce a precursor for the PANI film.[6] A series of angular SPR curves taken after each potential cycle are shown in Figure 3-1 (B). These scans were measured in the solution at open circuit potential (OCP ≈ 0.15 V). Shifts of the minimum resonance angles in the SPR curves were observed, indicating that PANI was deposited onto the gold film electrode during each potential cycle. Besides, as can also be seen, the deposited PANI in each following cycle increased almost exponentially.

The in situ formation of the PANI film on the gold electrode surface was monitored simultaneously by the measurement of the charge transferred, by QCM and by SPR. Figure 3-2 shows the complex frequency change during electropolymerization by
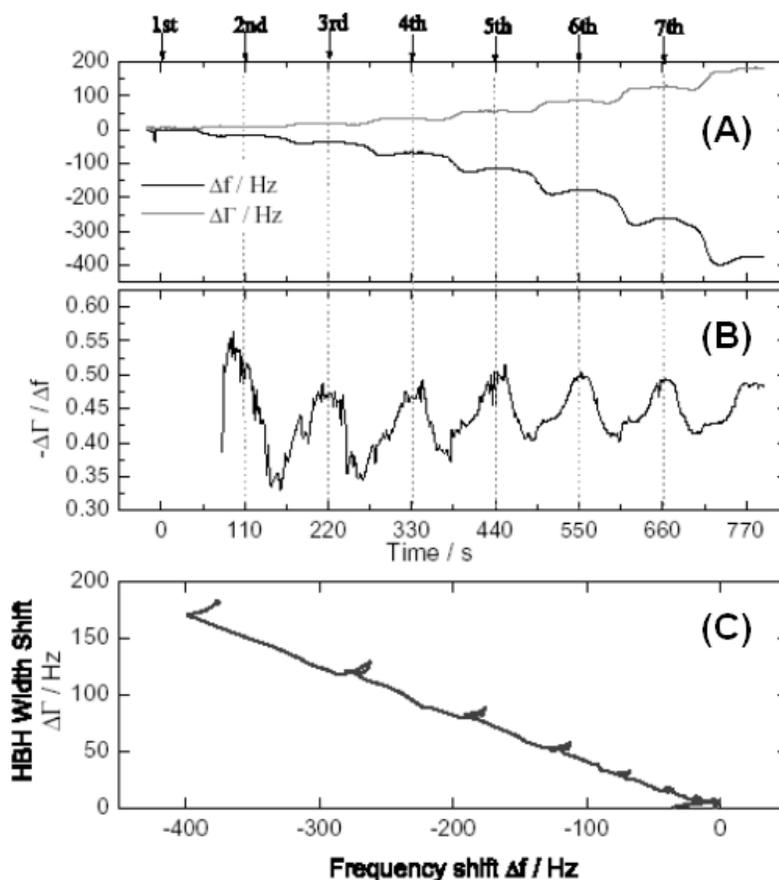
Fig. 3-2 *In situ monitoring of complex frequency change (A), ΔΓ/Δf plot (B) as a function of time, and ΔΓ–Δf plot (C) during electropolymerization of aniline by potential cycling between −0.2 and 0.9 V at a scan rate of 20 mV/s.*

cycling the potential between −0.2 and 0.9 V at a scan rate of 20 mV/s. Each arrow shows the starting point of each potential cycling, i.e., −0.2 V. In the QCM measurements, the Sauerbrey equation[7] in its approximation form was used for the analysis of the frequency shifts, stating that the frequency shift is mostly caused by deposition of mass on the crystal surface. Thus one obtains:

$$\frac{\Delta f}{f} \approx -\frac{\Delta m}{m_q} = -\Delta m \frac{2 f_0}{Z_q} \tag{1}$$

with Δf the frequency shift, f the frequency, f_0 the fundamental frequency, Δm the change in area mass density for the film, $m_q = Z_q / (2 f_0)$ the area mass density of the quartz plate, and $Z_q = 8.8 \times 10^6$ kg m^{-2} s^{-1} the acoustic impedance of the AT-cut quartz crystal. The Sauerbrey approximation does not account for viscous losses or viscoelastic effects. In air, such viscoelastic effects scale as the cube of the film thickness and can be neglected. In liquids this is not the case. Because the liquid exerts a lateral stress onto the moving upper surface of the film, there are viscoelastic effects which scale *linearly* with the mass. This leads to a modified Sauerbrey equation,[8] which is

$$
\begin{aligned}
\frac{\Delta f + \mathrm{i}\Delta\Gamma}{f} &\approx -\frac{\Delta m}{m_q}\left\{ 1 - \left(\frac{Z_q^2}{Z_f^2} - 1 \right) \frac{2\pi \mathrm{i} f \rho_l \eta_l}{Z_q^2} \right\} \\
&\approx -\frac{\Delta m}{m_q}\left\{ 1 - \frac{2\pi \mathrm{i} f \rho_l \eta_l}{Z_f^2} \right\} \\
&= -\frac{\Delta m}{m_q}\left\{ 1 - J_f \frac{2\pi \mathrm{i} f \rho_l \eta_l}{\rho_f} \right\}
\end{aligned}
\tag{2}
$$

where ρ_l is the density of the liquid, η_l is the viscosity of the liquid, Z_f is the acoustic impedance of the film, ρ_f is the density of the film, and $J_f = J_f' - \mathrm{i} J_f''$ is the complex compliance of the film. In the second line the relation $Z_q \gg Z_f$ (film is softer than quartz plate) has been used. Note that the above expression is only the first term of a Taylor expansion in the film mass Δm. More complicated equations apply for films with a thickness comparable to the wavelength of sound.[9] For the analysis of conventional QCM data, the above equation is of limited use because it does not allow for a separation of mass effects and viscoelastic effects (the second term in the curly brackets). One defines a "Sauerbrey mass" which is the true mass times the

unknown correction factor in curly brackets. If, on the other hand, the bandwidth (HBHW) is available, it can be interpreted in the frame of this equation. The ratio of $\Delta\Gamma$ and $-\Delta f$ should be independent of mass. This is indeed the case for our data, as shown in Figure 3-2 (C). The quantity $-\Delta\Gamma/\Delta f$ corresponds to the ratio of the imaginary and the real part of the curly bracket, namely

$$\frac{-\Delta\Gamma}{\Delta f} \approx \frac{J'_\mathrm{f}}{\rho_\mathrm{f}/(2\pi f \rho_\mathrm{l}\eta_\mathrm{l}) - J''_\mathrm{f}} \tag{3}$$

The above equation allows for some further conclusions. Assuming $\rho_\mathrm{f} \approx \rho_\mathrm{l}$ the first term in the denominator is of the order of the viscous compliance of the liquid. Further assuming that the liquid is much softer than the film, $J_\mathrm{f}''<<1/(2\pi f\eta_\mathrm{l})$ (a safe assumption for most polymeric films) one reaches the conclusion

$$\frac{\Delta\Gamma}{\Delta f} \approx J'_\mathrm{f}(2\pi f\eta_\mathrm{l}) \approx J'_\mathrm{f}/[30 \text{ MPa}^{-1}] \tag{4}$$

where $\eta_\mathrm{l} \approx 10^{-3}$ Pa s and $f = 5 \times 10^6$ have been used in the second line. The quantity $-\Delta\Gamma/\Delta f$ therefore provides a measure of the elastic compliance of the films. Note that this interpretation contradicts simple intuition to some degree: while one would naively associate a shift in bandwidth to a dissipation inside a film (given by J''), the detailed derivation shows that it is actually the *elastic* compliance, J', which is measured.

Again, in liquids a *modified* Sauerbrey equation holds, which is different from the dry case in two respects: first, the mass, $\Delta m,$ includes the trapped liquid. Second, there are viscoelastic corrections as given by the curly bracket in Equation (2). As for the frequency shift, nothing can be learned because the elastic correction is inseparable from the effect of the (unknown) mass. One can, however, extract information from the bandwidth. Making some assumptions, the bandwidth can be used to estimate the elastic compliance, J', of the film.

The application of this formalism to our data is illustrated in Figure 3-2. Figure 3-2 (A) shows the raw data. $-\Delta f$ and $\Delta\Gamma$ mostly go in parallel, but not quite. During every positive scan, the ratio $-\Delta\Gamma/\Delta f$ drops slightly (Fig.3-2 (B)). During every negative scan, it increases again. This behavior is largely independent of the thickness (Fig.3-2 (C), the "*D*–*f*-plot", where "*D*" stands for "dissipation"). The above quantitative

discussion suggests that the (average) elastic compliance of the film is in the range of 10 MPa. It drops slightly during a positive scan and recovers during a negative scan. One possibility for this is that the PANI film becomes more porous by de-doping but recovers by doping.

Shown in Figure 3-3 (A) are the mass change as a function of time during the seven electropolymerization cycles and the corresponding SPR minimum angle shifts measured after each potential cycle. Each arrow shows the starting point of each potential cycle, i.e. −0.2 V. In observing the mass change, the increase in each of the cycles mostly corresponds to the oxidation of aniline to form the polyaniline film and the doping of anions into the deposited polyaniline film. The decrease of the curve is mostly due to the dedoping of the anions from the deposited polyaniline film. The trace of the SPR minimum angle shift was similar to the mass change at −0.2 V, i.e., at the end of each potential cycle. This indicates that the optical thickness corresponds to the acoustic mass. Figure 3-3 (B) shows the kinetic measurements for SPR performed at a fixed angle, 58.0°, slightly below the angle of the reflectivity minimum of the blank gold substrate (c.f. Fig.3-1(B)). It is clear that the behavior of the reflectivity shows a large difference from the mass change. In the case of the SPR reflectivity, the curve is very sensitive to the thickness, the real (ε') and the imaginary (ε'') parts of the dielectric constant. The increase in reflectivity below about +0.2 V was seen in the figure whereas no increase was observed in the mass. This clearly indicates that the dielectric constant changes dramatically in this potential range (−0.2 to +0.2 V). Figure 3-3 (C) shows the current efficiency, $\Delta m/\Delta Q$ during the electropolymerization process. From this plot, it was found that the current efficiency increases with time. This property is also seen in the change of the mass as a function of charge transferred as shown in the inset. In EQCM measurements, the area mass density m_f during electropolymerization is related to the charge density passed Q, on the other hand, it also contributes to the generation of solute oligomer.[8b] In the case of electropolymerization for the conducting polymer, the theoretical value of the current efficiency, m_f / Q is calculated from

$$\frac{m_f}{Q} = \frac{(M_M - 2M_H) + x_A M_A}{(2 + x_A)F} \tag{5}$$

where M_M, M_A, and M_H are the molar masses of the monomer, the incorporated anion, and hydrogen. The quantity x_A is the doping level equal to the ratio of the number of moles of inserted anion to that of monomer group in the film. F is the Faraday constant, 96485 C·mol^{-1}. The incorporation of water molecules and neutral salts which can cause apparently higher $\Delta m/\Delta Q$ values, were not included in this model. Assuming $x_A = 0.4$, the theoretical current efficiency $\Delta m / \Delta Q$ is expected to be 0.952 µg /mC. As shown in Figure 3-3(C), the value found experimentally, was at first, much smaller than the theoretical value, and then finally was much larger (the ratio of experimentally determined $\Delta m/\Delta Q_{exp}$ to the theoretical current efficiency $\Delta m/\Delta Q_{theo}$: 48.6 % after seven cycles) than for the initial potential cycles of electropolymerization
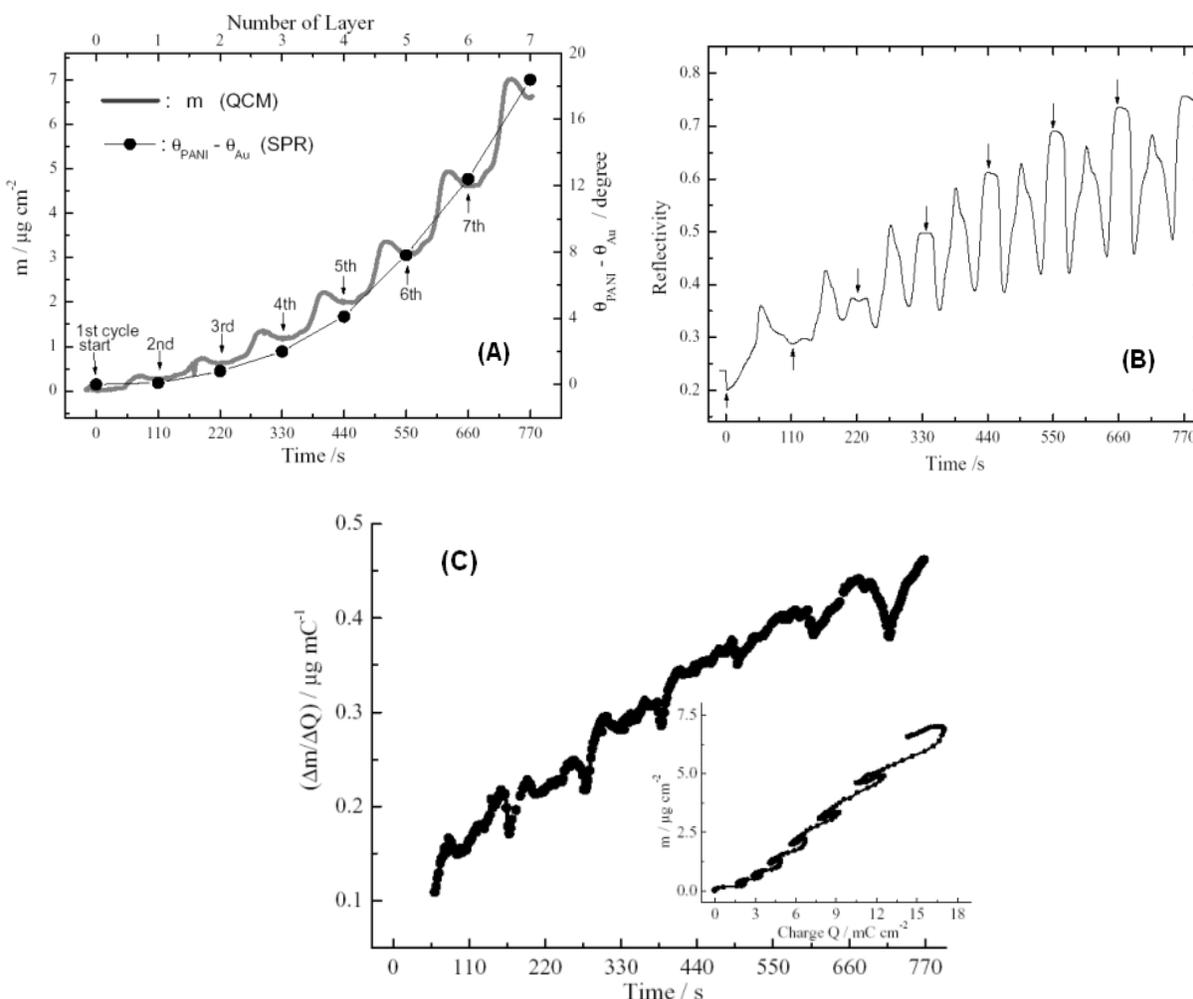
Fig.3-3 *(A) In situ monitoring of mass change during electropolymerization of aniline by potential cycling between −0.2 and 0.9 V at a scan rate of 20 mV/s, and the corresponding SPR minimum angle shifts measured after each potential cycle. (B) The reflectivity as a function of time during the electropolymerization. (C) A current efficiency Δm/ΔQ plot during electropolymerization. Inset is the mass change as a function of the charge amount.*

(17.3 % after 1 cycle). This indicates that a number of side reactions, which do not correspond to a mass increase, e.g., the formation of oligomers, accompany the ultrathin film formation.[10]

3.3 Doping/Dedoping Properties of Deposited PANI Thin Films in Monomer-Free Solution

3.3.1 During Potential Cycling

The cyclic voltammograms of a deposited PANI film in monomer-free solution is shown in Figure 3-4 (A). The cyclic voltammetry was scanned between −0.2 and 0.9 V for five sequential cycles at a scan rate of 20 mV/s in a monomer-free 0.5 M H_2SO_4
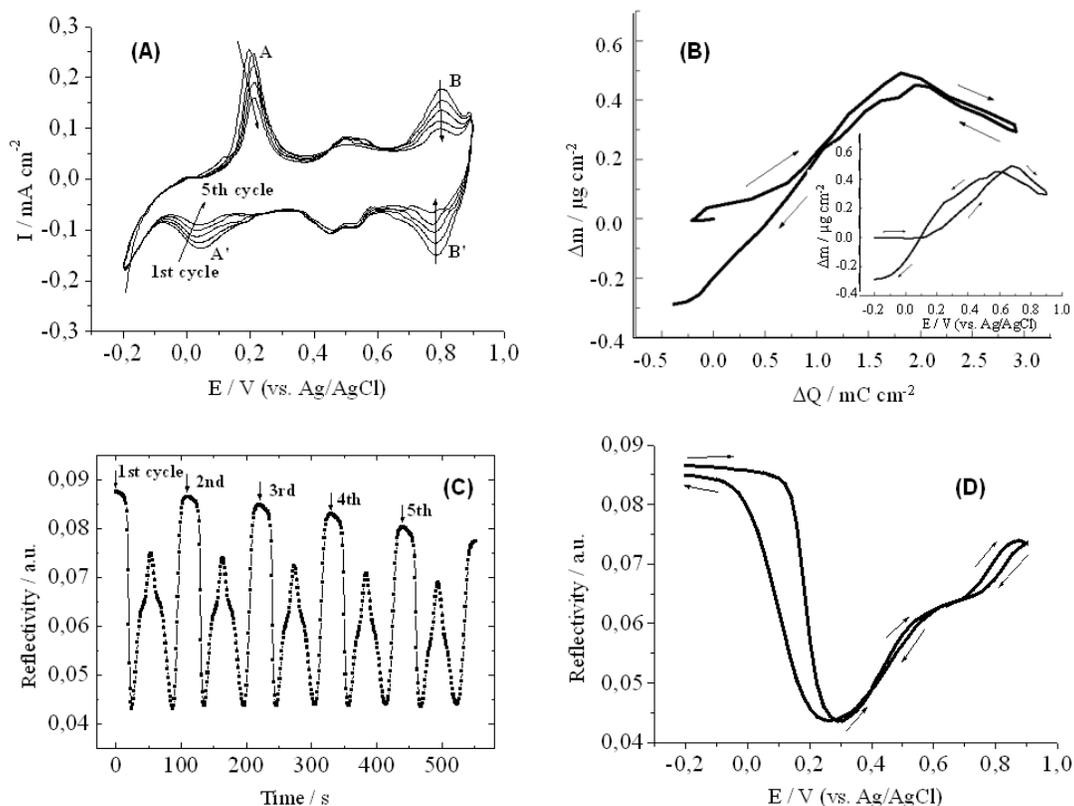
Fig.3-4 *(A) Cyclic voltammograms of deposited PANI film in monomer-free 0.5 M H_2SO_4 solution;(B) Mass response as a function of charge amount (second cycle). Inset is the mass response as a function of potential.(C) SPR reflectivity changes during the potential cycling. (D) Reflectivity change with the potential (second cycle).*

34

solution. As mentioned before, the first redox peak (A, A′) is commonly assumed to correspond to the electron transfer from/to the PANI film. In order to compensate the charge of the PANI film, anion doping/dedoping of the PANI film occurs. This is also seen in the EQCM measurement in which the mass increase at around 0.2 V corresponds to this doping process. During this redox process, the SPR reflectivity also changes sharply, as shown in Figure 3-4 (C) and (D), due to the fast refractive index changes. And the following slow SPR reflectivity changes correspond to the doping/dedoping process. The second redox peak (B, B′) corresponds to a deprotonation and protonation process. Besides the proton/cation exchange, the anion is also expelled from the PANI film during deprotonation,[6a] as reflected by a mass loss over 0.7V shown in Figure 3-4(B).The small peak at around 0.5 V is probably due to a side reaction in the PANI film. From the cyclic voltammograms, we can also see that the PANI film is not stable upon repeated potential scanning in the potential range as shown above. After each potential cycling, the peak currents decreased a little, indicating that some of the deposited PANI degraded or peeled off from the electrode (vide post). This phenomenon was also reflected in the SPR kinetic measurement (Fig.3-4(C)): SPR reflectivity decreased after each potential cycling.

If one correlates the deposited mass with the transferred charge (Fig.3-4(B)), first, the mass increased with the amount of charge transferred and then decreased again. The $\Delta m/\Delta Q$ value in this region is 0.27 µg/mC. This value is smaller than the theoretical $\Delta m/\Delta Q$ value of SO_4^{2-} (0.50 µg/mC). This might be due to the participation of protons for the charge compensation. At around 1.8 mC/cm^{-2} (0.7 V), the mass started to decrease again. The $\Delta m/\Delta Q$ value in this region is 0.18 mC/cm^{-2}. This should be attributed to a combination of protonation, anion de-doping, and degradation.[11] The degradation could be seen clearly in this figure, reflected by a mass loss after the potential cycling. In our QCM experiments, a mass loss of 60% of the deposited PANI film was observed after 10 potential cycles between −0.2 and 0.9 V (c.f. Fig.3-7).

In order to complement the information obtained by the ESPR and the EQCM experiments, transmittance measurements were carried out using two He-Ne lasers (632.8nm and 1152nm) during the potential cycling (cyclic voltammetry), between −0.2 and 0.9 V at a scan rate of 20 mV/s, as shown in Figure 3-5. In this case, the gold film thickness was reduced to 20 nm to allow transmission measurements on the glass substrates. The wavelengths used were intentionally chosen in order to compare with

ESPR results discussed later. From Figure 3-5, it can be seen that the decrease of the transmitted intensity begins at around 0.1 V for both wavelengths, λ=632.8 and λ=1152 nm. It is known from the Fresnel algorithm calculations[12] that the transmitted intensity depends mostly on the imaginary part (ε'') of the dielectric constant of the deposited PANI film. The absorption around λ=632.8 nm is generally attributed to the exciton absorption of the quinoid ring structures.[13] Therefore, the decrease at around 0.1 V shows the oxidation of the PANI film from its *LEB* state to its *EB* state, which contains quinoid ring structures. The absorption in the near infrared (NIR) region is known to be due to free charge carriers in a highly conductive state.[14] At the first oxidation peak, the PANI film changes to the *EB* form from the *LEB* form. This *EB* form is protonated in the acid solution so that it has a high conductivity. At the second oxidation peak, the PANI film is changed to the *PNB* state from the *EB* form and is deprotonated so that it is not highly conductive.
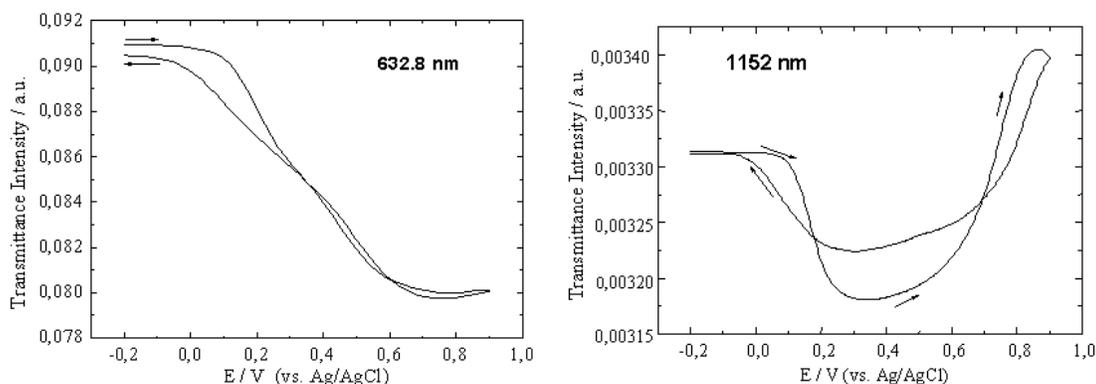
Fig.3-5 *Transmittance intensity response at 632.8 nm and 1152 nm,respectively, during potential cycling in monomer-free 0.5 M H₂SO₄ solution.*

3.3.2 Potentiostatic Measurements

In the previous section, a qualitative analysis of the imaginary part of the dielectric constant could be given for the three states of the PANI film. In order to be quantitative to all parameters of the films, i.e., its thickness, and the real and imaginary part of dielectric constant, we carried out ESPR and EQCM measurements under potentiostatic conditions. Shown in Figure 3-6 are the potentiostatic SPR scans for both λ=632.8 and λ=1152 nm, respectively. All SPR angular scans were started after each potential was applied for 2 min in order to have the same conditions as in
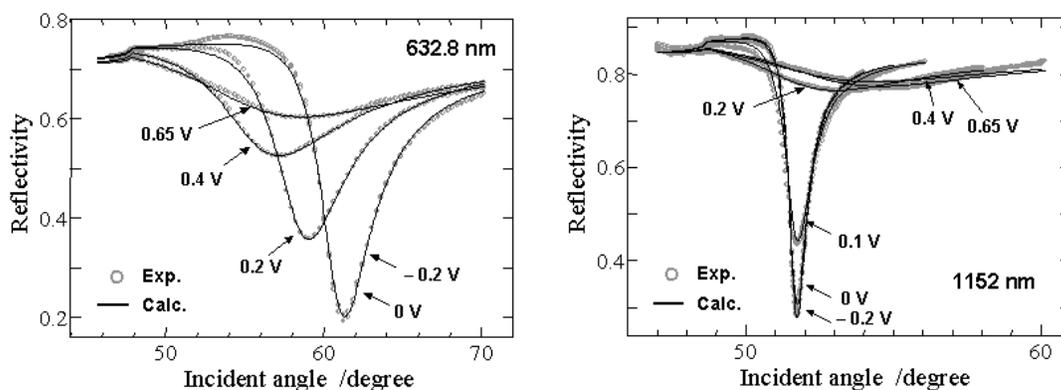
Fig.3-6 *Experimental angular SPR reflectivity curves (dotted) and calculated curves (solid) under different applied potentials at 632.8 and 1152 nm, respectively.*

the QCM measurements. Some very interesting information was obtained from the analysis of these curves. First, it is noticeable that the change in the reflectivity curves at around 0.2 V occurs when the PANI "base" film changes, upon doping, into the corresponding conducting PANI salt. This process is reversible and many cycles can be performed without any noticeable variation (except for any degradation processes). If the film, in the absence of monomers, is kept at 0.9 V, the SPR behavior is again similiar to that of the insulating state and subsequent SPR scans at 0.65, 0.4, −0.2, 0.4, and 0.65 V showed no difference. This indicates that in the absence of the aniline monomer, oxidation at potentials higher than ca. 0.65 V leads to an irreversible degradation of the electrochemical response of the PANI film.

Since it is difficult to obtain independent information on the thickness and the real
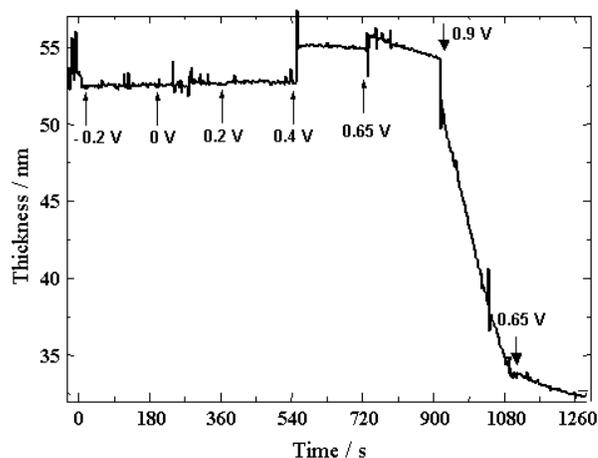
Fig.3-7 *Thickness changes measured by QCM under different applied potentials.*

and imaginary parts of the dielectric constant from mere SPR measurement, we also used the QCM in a potentiostatic mode of the measurement. As explained before, the Sauerbrey equation could be applied to relate frequency shifts to mass changes. Figure 3-7 shows the potentiostatic QCM measurements for several potentials and the corresponding thickness, roughly estimated on the assumption of a mass density of 1.3 g·cm^{-3} [15] for comparison with the ESPR results. For changing the potential, a step potential program was used. In contrast to the SPR reflectivity curves, which show a large change at 0.2 V, the thickness from the QCM measurement was found to be roughly constant between −0.2 and 0.2 V. As can be seen from Figure 3-7, a substantial degradation and loss of material appear at 0.9 V so that one cannot obtain a meaningful film thickness at 0.9 V. The loss of film thickness at 0.9 V was found to be 38 % after 3 min. Fitting the experimental SPR reflectivity results with the thickness values obtained from QCM measurement (except the value of 0.9 V) gives the theoretical reflectivity curves that are also shown in Figure 3-6. The calculation was done by using Fresnel's equations for a Prism/Cr/Au/PANI/electrolyte solution architecture. Details for the fitting procedure can be found elsewhere.[12] Although the SP resonance at λ=1152 nm is very broad at high potentials, excellent fitting curves were obtained in most cases. The fitting parameters obtained are shown in Figure 3-8. Dramatic changes both in the real part and the imaginary part of the dielectric constants were determined at both wavelengths. The trends of changes in the imaginary part at both wavelengths coincide well with the transmittance measurements shown in Figure 3-5. The error bars in Figure 3-8 are based on the density fluctuation of the polymer upon doping/de-doping, that is 1.25–1.35. Based on these calculations, the accuracy for the determination of the complex dielectric constant is estimated to be better than ±0.02 for the real part and ±0.10 for the imaginary part of the dielectric constant in this density range, i.e., ESPR measurements are able to determine the complex dielectric constants of the conducting polymer films in the doped/de-doped state rather independently of the uncertainty in the film density. Thus, the electrochromic phenomena of PANI films can be characterized by this ESPR technique with high sensitivity, which may lead to new designs for SPR-based sensors/biosensors based on the electrochromism of thin conducting polymer films. In the following work, ESPR was also used to monitor the
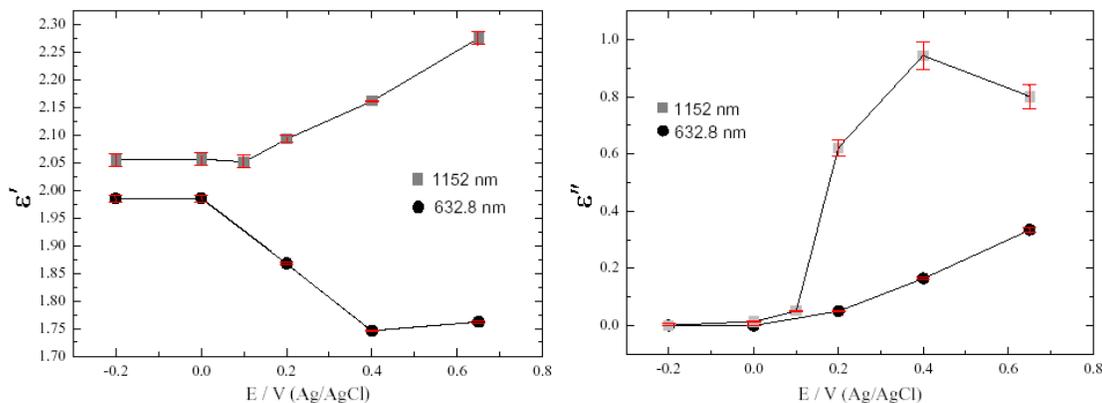
Fig.3-8 *Real part (ε') and imaginary part (ε'') of the dielectric constants of PANI at different potentials (i.e. different oxidation states) at 632.8 nm and 1152 nm, respectively.*

LBL self-assembly process and to study the properties of PANI multilayer films in neutral pH conditions.

3.4 Conclusions

The electropolymerization and doping/dedoping properties of polyaniline films in acidic conditions on a flat gold substrate surface were investigated and well characterized by the combination of ESPR and EQCM. Transmittance and potentiostatic SPR measurements were also carried out with two wavelengths in order to obtain independent information about the electrochromic properties of the thin PANI film. The changes in the electrochemical/optical properties of the thin film upon doping/dedoping produce a dramatic change in the SPR responses, mainly due to a distinct change in the real and imaginary parts of the dielectric constant. Using the combination techniques, the thickness, the real and imaginary parts of the dielectric constants of PANI at different oxidation states were obtained. All these results will provide some basic data for our subsequent study of PANI multilayer films in neutral conditions. Besides, the combination techniques used here were shown to be a powerful in situ approach for the investigation of ultrathin polymer films. So in the following work, these techniques were also used to monitor the LBL self-assembly process of PANI multilayer films and to study their properties and applications in neutral pH conditions.

3.5 References

1. A. G. MacDiarmid, A. J. Epstein, *Faraday Discuss Chem. Soc.* **1989**, *88*, 317 and references therein.

2. A. G. MacDiarmid, *Synth. Met.* **1997**, *84*, 27 and references therein.

3. A. G. MacDiarmid, W. E. Jones, Jr, I. D. Norris, J. Gao, A. T. Johnson, Jr, N. J. Pinto, J. Hone, B. Han, F. K. Ko, H. Okuzaki, M. Llaguno, *Synth. Met.* **2001**, *119*, 27.

4. a) G. Zotti, S. Cattarin, N. Comisso. *J. Electroanal. Chem.* **1988,** *239,* 387. b) L. Duic, Z. Mandic. *J. Electroanal. Chem.* **1992,** *335,* 207. c) K. Prasad, N. Munichandraiah. *Synth. Met.* **2001**, *123,* 459. d) D. Ljerka, M. Zoran, K. Franjo. *J. Polym. Sci.* **1994**, *32*, 105.

5. a) W. S. Huang, B. D. Humphrey, A. G. MacDiarmid. *J. Chem. Soc. Faraday Trans. 1*, **1986**, *82*, 2385. b) S. Mu, C. Chen, J. Wang. *Synth. Met.* **1997**, *88*, 249.

6. a) D. Orata, D. A. Buttry. *J. Am. Chem. Soc.* **1987**, *109*, 3574. b) E.M. Genies, C. J. Tsintavis. *J. Electroanal. Chem.* **1985**, *195*, 109.

7. G. Sauerbrey, *Z. Phys* **1959**, *155*, 206.

8. a) D. Johannsmann, *Macromol. Chem. Phys.* **1999**, *200*, 501. b) A. Bund, G. Schwitzgebel, *Electrochim. Acta* **2000**, *45*, 3703.

9. D. Johannsmann. *J. Appl. Phys.* **2001**, *89*, 6356.

10. R. Nyffenegger, E. Ammann, H. Siegenthaler, O. Haas. *Electrochim. Acta* **1995**, *40*, 1411.

11. a) L. Kwanghee, A. J. Heeger, Y. Cao. *Synth. Met.* **1995**, *72*, 25. b) T. Kobayashi, H. Yoneyama, H. Tamura. *J. Electroanal. Chem.* **1984**, *177*, 293.

12. W. Knoll, *Annu. Rev. Phys. Chem.* **1998**, *49*, 569.

13. a) S. Stafstrom, J. L. Bredas, A. J. Epstein, H. S. Woo, D. B. Tanner, W. S. Huan, A. G. MacDiarmid. *Phys. Rev. Lett.* **1987**, *59,* 1464. b) D. E. Stilwell, S.-M. Park. *J. Electrochem. Soc.* 1989, *136*, 427. c) J. Stejskal, P. Kratochvil, N. Radhakrishnan. *Synth. Met.* **1993**, *61*, 225. d) A. A. Nekrasov, V. F. Ivanov, A.V. Vannikov. *J. Eelctroanal. Chem.* **2000**, *482,* 1.

14. a) Y. Min, Y. Xia, A. G. MacDiarmid, A. *J* Epstein. *Synth. Met.* **1995**, *69***,** 159.

b) I. Kulszewicz-Bajer. *Macromolecules* **1995**, *28***,** 610. c) O. P. Dimitriev, N. V. Lavrik. *Synth. Met.* **1997**, *90*, 1.

15. J. Stejskal, R. G. Gilbert, *Pure Appl. Chem.* **2002**, *74*, 857.

Chapter 4

Polyaniline Composite Films Prepared Via the LBL Method and Their Properties in Neutral Aqueous Solution

4.1 Background

As has mentioned in Chapter 1, polyaniline (PANI) is one of the most studied conductive polymers, due to its many attractive properties (such as ease of synthesis, being cheap, and of relatively stable electrical conductivity, with interesting electrochemical and optical properties) and the resulting potential applications as battery electrodes, as electrochromic or electronic devices, for the immobilization of enzymes, in biosensors, etc.[1-3] However, unmodified PANI films remain electroactive only in acidic solutions (normally pH<3),[4] which to a large extent restricts its applications, especially in bioengineering. Efforts have been directed toward overcoming such limitations. One approach is to introduce acidic groups (e.g. -COOH, -SO₃H, ect.) into the PANI chain and to form a so-called "self-doped" PANI, which can maintain its electroactivity in neutral or even basic conditions.[5] Another way is to dope PANI with negatively charged linearly polyelectrolytes (such as poly(acrylic acid) (PAA), poly(vinyl sulfonate) (PVS), poly(styrene sulfonate) (PSS), sulfonated polyaniline (SPANI), etc.) by forming copolymers using an electropolymerization approach.[6] The copolymers thus obtained have been successfully utilized to immobilise enzymes in neutral solutions.[7]

The layer-by-layer (LBL) self-assembly method developed by Decher et al [8-9] is an extremely simple approach that can yield nanoarchitecture films with excellent control over the positioning of individual layers in a highly organized structure. It has been shown that PANI can form multilayer films by the LBL method with several poly(anions).[9,10] But almost all of these results were obtained in acidic conditions or in air. Until now, no one has investigated in detail whether such PANI multilayer films

can also remain electroactive in neutral solutions just as copolymers do, which is a most important aspect for their use in biosensor formats.

So in this Chapter, the LBL self-assembly method was used to prepare different PANI composite films by doping it with different dopants, and the properties of the obtained PANI multilayer films were examined at a neutral pH, in order to explore their potential biological applications.

The structures of the dopants used in this study are shown in Figure 4.1-1. The dopants not only include the negatively charged linearly polyelectrolytes (i.e. SPANI, PAA, PSS, PVS) that are normally used in the above reported examples, but also include some other novel materials, like mercaptosuccinic-acid-capped gold nanoparticles (MSAG$_{NP}$) or polyaminobenzene sulfonic acid-modified single-walled carbon nanotubes (PABS-SWNTs). Our results showed that all the used dopants could effectively shift the electroactivity of PANI to a neutral pH environment. All the prepared PANI multilayer films showed good redox activity in neutral conditions and
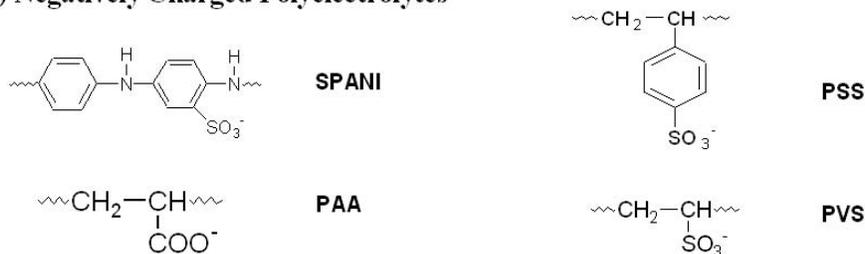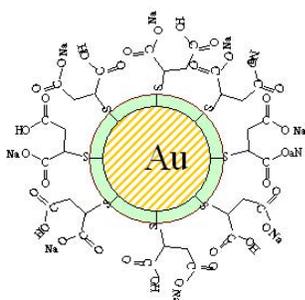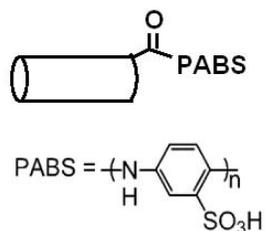
Fig. 4.1-1 *Structures of the dopants used in the present study.*

can electrocatalyze the oxidation of β-nicotinamide adenine dinucleotide (NADH). The electrocatalytic abilities of different PANI system toward the oxidation of NADH were compared, with those of PANI doped by Au nanoparticles or canbon nanotubes being higher than those of PANI doped by linear polyelectrolytes. Some of the prepared PANI multilayer films were also used for the first time to detect DNA hybridization event, as will be discussed in Chapter 5.

4.2   Polyaniline   Doped   by   Linearly   Negatively   Charged   Polyelectrolytes

In this section, self-assembled multilayer films of PANI were prepared using the LBL method with a series of linear poly(anions), i.e., SPANI, PAA, PSS, and PVS. Their electrochemical behavior and their efficiency to electrocatalyze the oxidation of NADH in neutral solutions were investigated in detail by electrochemical techniques combined with surface plasmon resonance spectroscopy (SPR) and the quartz crystal microbalance (QCM). The results showed that all the formed PANI multiplayer films were very stable and reversibly electroactive in neutral solutions. Their catalytic abilities to electrocatalyze the oxidation of NADH were compared under identical conditions. Comparison was also made between the copolymers and the multilayers.

4.2.1 The LBL Self-Assembly Process

Shown in Figure 4.2-1 are the scheme of the LBL self-assembly process (A), in situ SPR (B) and the QCM (C) responses measured during this process. The details about the LBL process can be found in the Experimental part (Chapter 2). From the SPR kinetic measurement (B), a clear trend of the progressive deposition in each cycle is observed, although the signal becomes saturated with the films becoming thicker, due to the fixed angle (56.3°) used in the measurement. Besides, it can also be seen that in each cycle, the deposited amount of PANI is larger than that of SPANI. This can be seen even clearer from the frequency change during deposition/adsorption as measured in situ by QCM (C). The inset shows the frequency change with the number of layers. Here, the monotonous frequency decrease with increasing number of layers indicates the linear deposition of the PANI/SPANI onto the substrate. One can also see that for each bilayer, the frequency change caused by the deposition of PANI is much larger than that of SPANI, indicating a larger amount of deposited PANI than SPANI in each bilayer, as seen in the SPR kinetic measurement (B). This difference is mostly due to the different charge densities of PANI layer and SPANI

layer under the pH conditions used here. Owing to this difference in charge densities, PANI and SPANI adopt different conformations, thus adsorb in different amounts.[11]

To further probe the LBL process, the cyclic voltammograms and the SPR
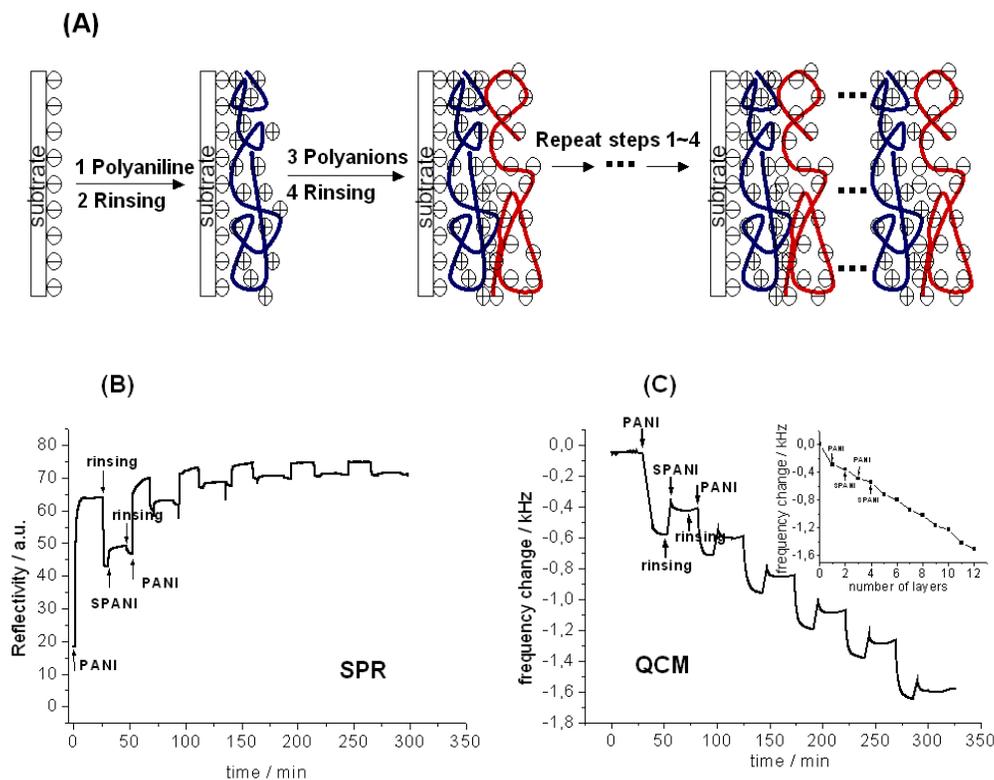
Fig.4.2-1 *Scheme of the LBL self-assembly process (A) and the in situ SPR (B) and QCM (C) responses measured during this LBL process.*

spectra were measured in 0.1M PBS buffer (pH=7.1) after each deposition of one bilayer of PANI/SPANI onto the Au substrates, as shown in Figure 4.2-2. Both the linear increase of the peak currents in the cyclic voltammograms as well as the equal shifts of the SPR minimum angles (except for the first bilayer) with the number of bilayers indicate a progressive deposition with an almost equal amount of polyion deposited in each circle. In Figure 4.2-2 (A), the peak-peak separation increases with the number of bilayers. The main reason is that the ion transfer becomes more difficult with increasing film thickness (*vide infra*). The relatively larger minimum angle shift of the first bilayer compared to those of the following bilayers in Figure 4.2-2 (B) may be due to the different charge densities of the functionalised MPS layer

and the SPANI layers under otherwise identical conditions.
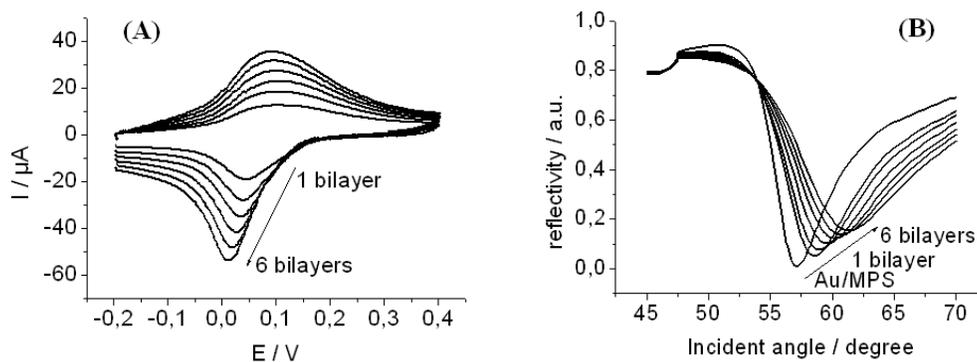
Fig.4.2-2 *Cyclic voltammograms (A) and SPR spectra (B) of different bilayers of PANI/SPANI multilayer films self-assembled on Au electrodes recorded in 0.1M PBS buffer, pH=7.1. Scan rate 50mV/s.*

4.2.2 Electroactivity of PANI Multilayer Films in Neutral Solution

We can see from Figure 4.2-2 (A) that PANI/SPANI multilayer films show very good electroactivity in 0.1M PBS buffer, pH=7.1. A broad redox peak is found for different bilayers of PANI/SPANI, and the redox potential is around 0.05V. This broad redox peak is the superposition of two redox processes usually found for PANI in strong acidic solutions, i.e., a doping/dedoping and a deprotonation/protonation process. This can be confirmed by the electrochemical behaviour of PANI/SPANI multilayer films measured in different pH buffer solutions, as shown in Figure 4.2-3. At low pH values, two separate redox peaks can be clearly seen. The redox peak at the low potential corresponds to the doping/dedoping process, while the one at the higher potential corresponds to the deprotonation/protonation process which is highly pH dependent. With increasing pH, the second redox peak shifts quickly towards low potentials with a rate of about −100mV/pH and finally merges with the first redox peak at pH>6 to show only one broad peak. The sharp and large peaks at pH=1 and pH ≥ 7 upon a positive potential scan up to 0.7V, and the peaks between 0.3V and 0.8V when pH ≥ 7 upon a negative potential scan are due to the oxidation of Au, as confirmed by a control experiment done under the same conditions using bare Au. The redox peak here at pH 7 is a little deformed compared with that in Figure 4.2-2.
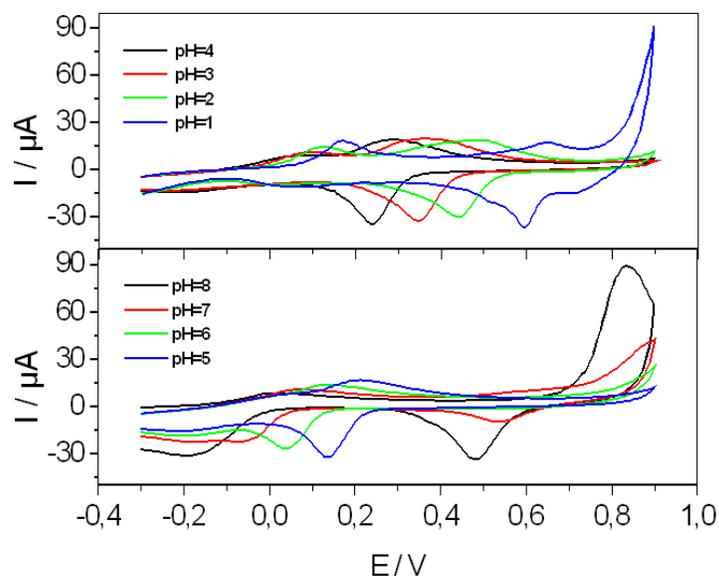
Fig.4.2-3 *Cyclic voltammograms of Au electrode self-assembled with 6 bilayers of PANI/SPANI recorded in buffers with different pH values: pH=1 and 2, HCl solution; pH>3, 0.1M citrate-phosphate buffer. Scan rate: 20mV/s.*

This is due to the cyclic scanning of the film over a wide potential in different pH solutions. The above results are similar to those found for PANI copolymers.[6a,6b]

Figure 4.2-4 shows the cyclic voltammograms of 6 bilayers of PANI/SPANI recorded in 0.1M PBS buffer (pH=7.1) at different scan rates. The inset shows the plot
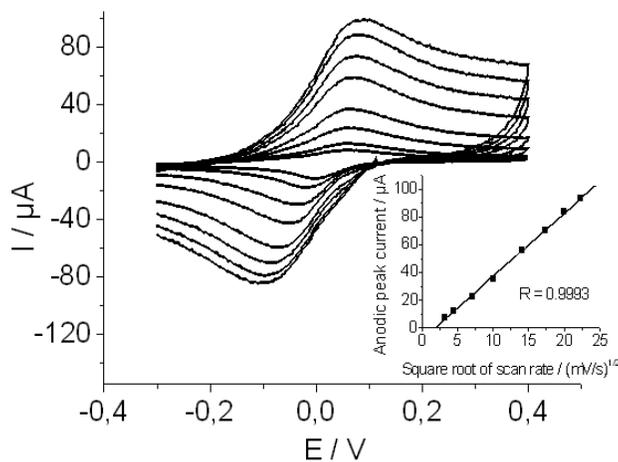
Fig.4.2-4 *Cyclic voltammograms of 6 bilayers of PANI/SPANI modified Au electrodes recorded in 0.1M PBS buffer (pH7.1) at a scan rate of 10, 20, 50, 100, 200, 300, 400, 500mV/s, respectively. Inset shows the relationship between anodic peak currents and the scan rates.*

of the anodic peak current versus the square root of the scan rate. A very good linear relationship is found, indicating a diffusion-controlled redox process. For PANI copolymers this process was reported to be surface-controlled.[6b] The difference may arise from the different structures of PANI/SPANI multilayer films and PANI copolymers. The former is more ordered and compact than the latter.

In order to further investigate the redox behaviour of PANI/SPANI multilayers in neutral solution, we measured both the SPR reflectivity change and the QCM frequency change of a sample of 6 bilayers of PANI/SPANI during 5 cyclic potential scans, as shown in Figure 2.4-5. The SPR reflectivity increases during the anodic potential scan and decreases during the cathodic scan. The corresponding frequency changes can also be observed. These changes are the net results of doping/dedoping
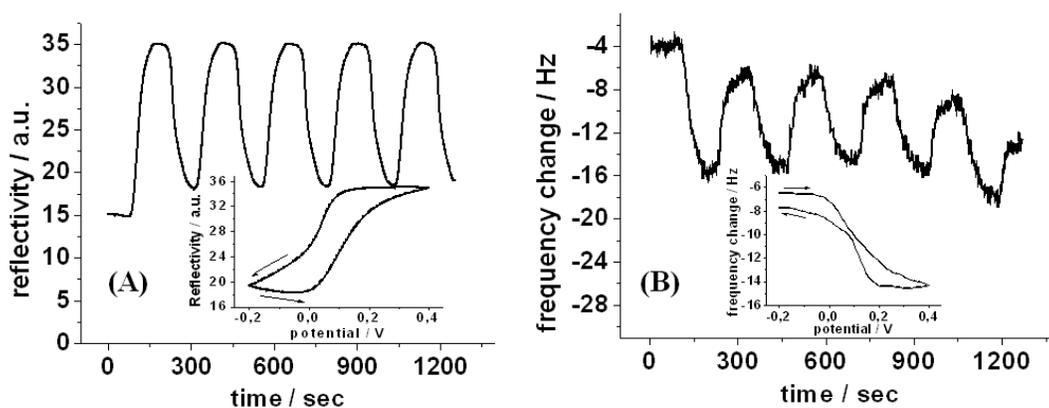
Fig.4.2-5 *Reflectivity change measured at a fixed angle (61.5°) (A) and frequency change (B) of 6 bilayers of PANI/SPANI measured in situ upon the application of 5 circles of potential scanning in 0.1M PBS buffer, pH=7.1. Insets are reflectivity change and frequency change versus potential changes (third cycle), respectively.*

and deprotonation/protonation processes, respectively, along with contributions from the solvent and/or of the anions in the solution. These processes result in the change of the dielectric constant and the density of the film, thus the change of the reflectivity. As for the frequency change, we think the main contribution is from the transport process of solvent and counterions and/or changes in the viscoelasticity of the film accompanying the above processes.[12,13]

4.2.3 Stability and Reversibility of PANI Multilayer Films

For all practical purposes, the stability and the reversibility of the prepared PANI multilayer films in a neutral solution are important aspects to pay attention to. From the SPR reflectivity change and the frequency change displayed in Figure 4.2-5, one could see that PANI/SPANI multilayer films are very stable and reversible upon potential scanning. We also measured the SPR reflectivity changes of a 10 bilayers of PANI/SPANI modified Au electrode upon the application of potential square waves (PSW) with steps of 20s and 4s, respectively, as shown in Figure 4.2-6. Figure 4.2-6
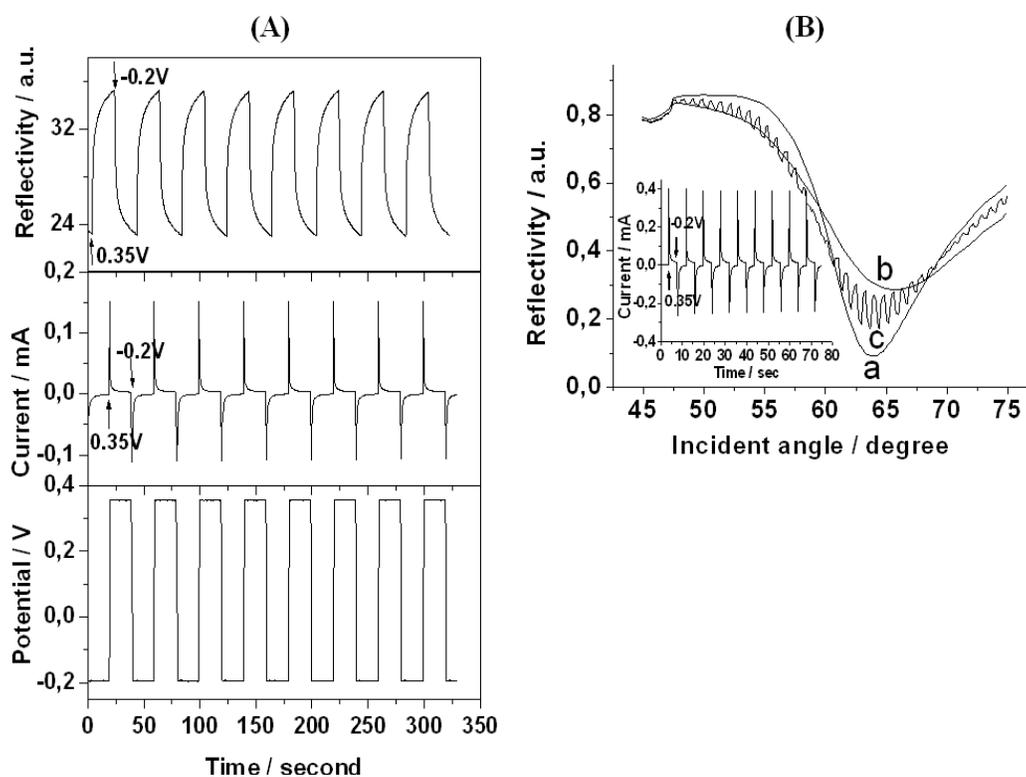
Fig.4.2-6 *(A) SPR reflectivity change of 10 bilayers of PANI/SPANI multilayer films measured at a fixed angle (62°) in 0.1M PBS buffer (pH7.1) upon application of potential square waves with a time step of 20s. (B) SPR spectra of 10 bilayers of PANI/SPANI recorded in 0.1M PBS buffer (pH7.1) while the potential was fixed at –0.2V (a), 0.35V (b) and stepped between them with a time interval of 4s(c) upon the PSW scanning between –0.2V and 0.35V (inset).*

(A) was measured at a fixed angle (62°) while the potential was stepped between –0.2V and 0.35V with a time interval of 20s. The SPR reflectivity increases as the potential is stepped from –0.2V to 0.35V and decreases as the potential is stepped

from 0.35V back to –0.2V. The reflectivity changes are very reproducible, indicating excellent stability and reversibility of the PANI/SPANI multilayer film. Experiments show that even after 500 cycles of PSW, the SPR reflective intensity only degrades by less than 10 percent. The fast increase in the SPR reflectivity intensity is ascribed to the refractive index change of the multilayer film upon the oxidation of PANI/SPANI. The following slower increase is ascribed to the swelling of the oxidised film caused by the hydration of the multilayer film and/or the uptake of some of the counteranions in the solution. These processes are reversed if the potential is stepped back to –0.2V.[7b] Figure 4.2-6 (B) shows the SPR spectra measured at –0.2V (curve a), 0.35V (curve b) and while the potential was stepped between them with a time interval of 4s (curve c), respectively. It is clear that even within 4s time intervals, the PANI/SPANI multilayer film still shows very good reversibility between its reduced and its oxidized states. Such excellent stability and reproducibility of the PANI multilayer films lay a strong foundation for their practical use.

4.2.4 Electrocatalytic Activity of PANI Multilayer Films for the Oxidation of NADH

Recently, it has been reported that PANI copolymers can electrocatalyze the oxidation of NADH in neutral solution.[6,7b] Since the PANI/SPANI multilayer films prepared in this work can also maintain very good electroactivity at pH 7.1, so it also should be possible to electrocatalyze the oxidation of NADH. Figure 4.2-7 (A) shows the cyclic voltammograms of a 6 bilayer PANI/SPANI multilayer film measured in 0.1M PBS buffer (pH7.1) in the absence and presence of different amounts of NADH. As can be seen, upon the addition of NADH, the anodic peak current increases, while the cathodic peak current decreases significantly, indicating clearly the catalytic capability of PANI/SPANI multilayer films for the oxidation of NADH. As can also be seen, the anodic catalytic peak currents increase gradually with the increase of the concentration of NADH (Fig.4.2-7(A), inset).

This catalytic behavior of PANI/SPANI multilayer film can also be characterized by in situ electrochemical-SPR (ESPR) measurements. Figure 4.2-7 (B) shows the SPR spectra of 6 bilayers of PANI/SPANI measured in 0.1M PBS buffer (pH7.1) in the presence of different concentrations of NADH with the potential held at –0.2V and 0.35V, respectively. If the potential is at –0.2V, the film is in its reduced state. Upon the addition of NADH, both the critical angle and the minimum angle shift towards higher values. The higher the concentration of NADH, the larger the shift. These changes are caused by the change of the refractive index of the solution as a
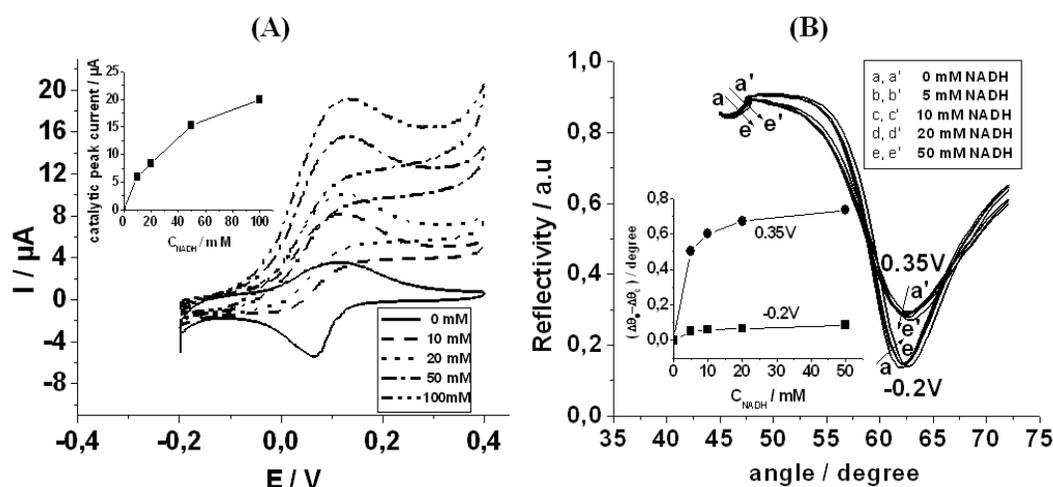
Fig.4.2-7 *(A) Cyclic voltammograms of 6 bilayers of PANI/SPANI measured in 0.1M PBS buffer(pH=7.1) containing different concentrations of NADH. Scan rate 5mV/s. Inset shows the anodic catalytic peak current change with the concentration of NADH. (B) SPR spectra of 6 bilayers of PANI/SPNI measured at a fixed potential of –0.2V and 0.35V in 0.1M PBS buffer (pH7.1) with different concentrations of NADH, respectively. Inset shows the minimum resonance angle shifts after taking into account of the critical angle changes due to the addition of NADH.*

result of adding NADH. But if a potential of 0.35V is applied at which the film is in its oxidized state, a different behavior is found upon the addition of NADH: the critical angle still shifts to higher values, but the minimum angle shifts to lower values. This is the net result of the refractive index change of the solution and the refractive index change of the multilayer film caused by the reduction of the multilayer film by its electrocatalyzed oxidation of NADH. This can be seen more clearly from the inset

in Figure 4.2-7 (B), which shows the corrected minimum resonance angle shift
($\Delta\theta_0$-$\Delta\theta_c$) after taking into account of the critical angle shift caused by the addition of
NADH. At –0.2V, the corrected minimum angle shift changes very little while adding
NADH, but at 0.35V, the corrected minimum angle shift increases gradually with the
increase of the amount of NADH.

SPR kinetic measurement can also be applied to detect the catalytic phenomena
directly. Figure 4.2-8 showed the SPR reflectivity changes of 6 bilayers of
PANI/SPANI measured at a fixed angle (61.5^o) upon cyclic potential scan measured in
0.1M PBS buffer (pH7.1) with 50mM NADH, scan rate 5mV/s. The inset is the
reflectivity change with the potential (third cycle). If we compare this figure with
Figure 4.2-5 (A) in which there was no NADH, a shoulder appears in the presence of
NADH. It is much clearer to see from the insets of both figures. Without NADH, SPR
reflectivity during the negative scan is larger than that during the positive scan when
the potential is higher than 0.2V. This is due to the swelling of the oxidised multilayer
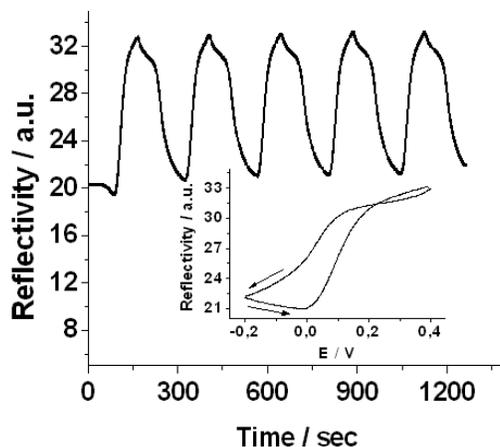
Fig.4.2-8 *SPR reflectivity changes of 6 bilayers of PANI/SPANI measured at a fixed angle*
(61.5^o) upon cyclic potential scan measured in 0.1M PBS buffer (pH7.1) with 50mM
NADH. Scan rate 5mV/s. Inset is the reflectivity change with the potential (third cycle).

film. But in the presence of NADH, the reflectivity during the negative scan is lower
than that of the positive scan in the same potential range. The reason is that in this
potential range the multilayer film catalyses the oxidation of NADH, and thus the film

itself is partly reduced.

In a typical catalytic reaction, the increase of the amount of catalyst will certainly enhance the catalytic response. In the present experiment, one can control the amount of catalysts in the multilayer film by controlling the number of layers in order to get a high catalytic response. Figure 4.2-9 shows the cyclic voltammograms of different bilayers of PANI/SPANI on Au electrodes recorded in 0.1M PBS buffer (pH7.1) with and without 10mM NADH. The inset shows the dependence of the anodic catalytic peak current on the number of bilayers. As can be seen clearly, for thin films, the current increases linearly with the increase of the number of bilayers, because there
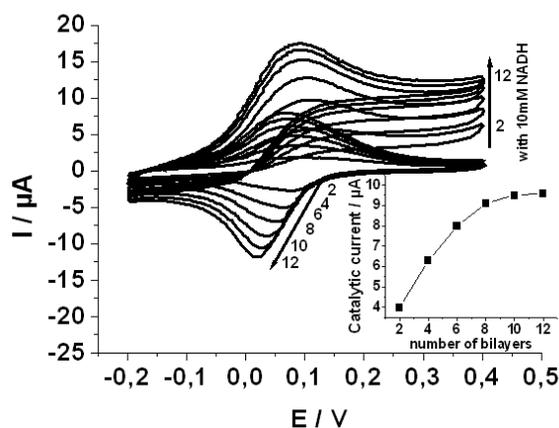
Fig.4.2-9 *Cyclic voltammograms of different bilayers of PANI/SPANI recorded in 0.1M PBS buffer(pH7.1) in the absence and presence of 10mM NADH. Scan rate 5mV/s. Inset shows the relationship between the anodic catalytic peak current and the number of bilayers of PANI/SPANI.*

are more catalytic reaction sites available in the film. But if the film reaches a certain thickness (>8 bilayers), the current no longer changes linearly with the number of bilayers but tends to level off. It is reasonable that for thicker films, the diffusion process becomes more difficult, and NADH can't penetrate through the whole film and is consumed mainly near the outer part of the film.

4.2.5 Other PANI Multilayer Films

Besides PANI/SPANI multilayer films, a series of other PANI multilayer assemblies, i.e., PANI/PAA, PANI/PVS and PANI/PSS, respectively, were also prepared. Their assembly processes and their electro- and catalytic abilities toward the oxidation of NADH were also investigated in detail under the same conditions as those used for PANI/SPANI. The results showed that all the PANI multilayer films are very stable and show excellent electroactivities in neutral solution. However, for the same number of bilayers, their optical thickness (as indicated by the resonance angular shift), electroactivity and their efficiency to electrocatalyze NADH oxidation are quite different under identical conditions, as summarized in Figure 4.2-10 (A) ~ (C). Clearly, the electroactivity of the different PANI system is in rough accordance
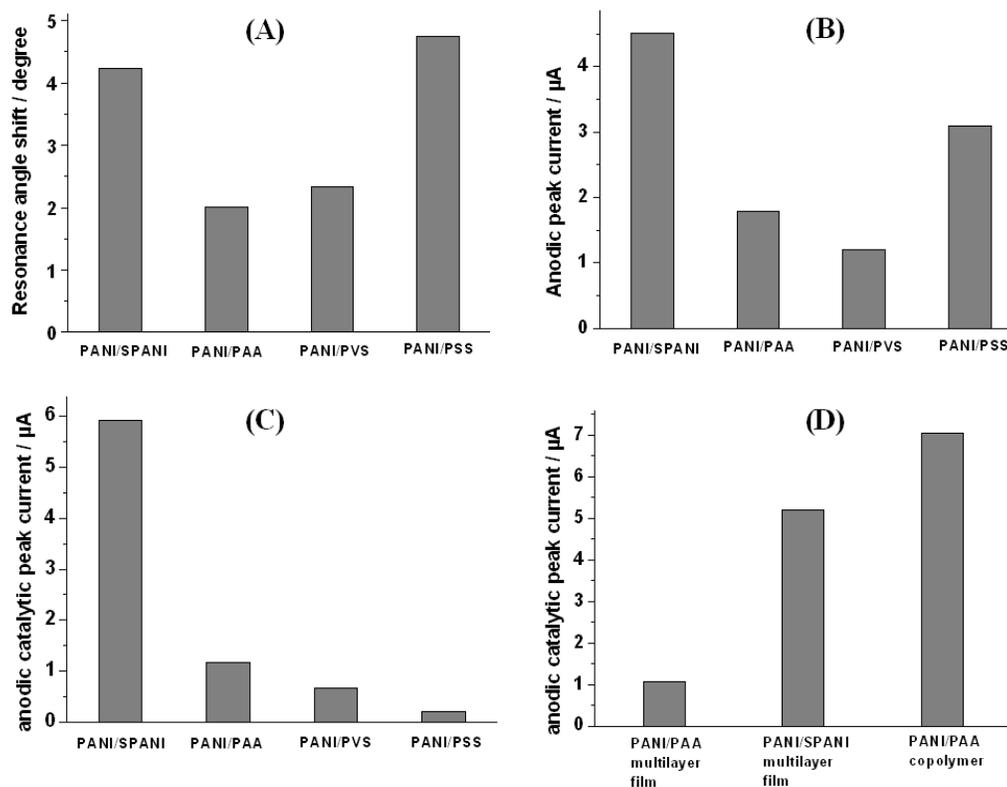
Fig.4.2-10 (A) Resonance angular shift of 6 bilayers of different PANI system measured in 0.1M PBS buffer, pH7.1. (B) Electroactivity of 6 bilayers of different PANI system measured in 0.1M PBS buffer, pH7.1. (C) Anodic catalytic peak currents of 6 bilayers of different PANI systems measured in 0.1M PBS buffer (pH7.1) in the presence of 10mM NADH. (D) Anodic catalytic peak currents of PANI films with the same optical thickness prepared by electropolymerization method and by LBL method, respectively, measured in 0.1M PBS buffer (pH7.1) with 10mM NADH.

with their corresponding optical thickness (with the exception of PANI/SPANI), which is due to the different amount of the deposited PANI. In the case of PANI/SPANI system, both components are electroactive, thus it shows the highest electroactivity. As for their catalytic efficiency toward the oxidation of NADH, PANI/SPANI is much better than the other assemblies. The main reason for this is that both PANI and SPANI monolayers of the PANI/SPANI system are electroactive, while for the other three systems only the PANI layer is electroactive. The differences among the catalytic behavior of the four PANI multilayer systems may also originate from differences in the thickness, the density and the morphology of the different films, as a result of different interactions between the PANI and the corresponding poly(anions) under the same conditions.

The catalytic ability of PANI/PAA prepared by LBL method was also compared with that of PANI/PAA copolymers with the same optical thickness prepared by direct electropolymerization method, as shown in Figure 4.2-10 (D). It is clear that the former is much weaker than the latter. We believe this difference arises from the different electrochemical mechanisms of the two films (vide supra). However, if we select the proper system (e.g. PANI/SPANI), their catalytic abilities are comparable.

4.2.6 Conclusions

Self-assembled PANI multilayer films, prepared via the LBL method by doping it with different negatively charged polyelectrolytes, are very stable, reversible and electroactive in a neutral pH solution. It is worth noting that all the films can electrocatalyze the oxidation of NADH, although their catalytic efficiencies are different. Using the LBL method, very uniform PANI multilayer films can be deposited in a highly controlled way. Hence, it is easy and convenient to construct biosensors based on such PANI multilayer films, as will be shown in the later chapters.

4.3 Polyaniline Doped by Modified Gold Nanoparticles

In this section, we use the mercaptosuccinic-acid-capped gold nanoparticles (MSAG$_{NP}$), other than the normally used polyelectrolytes, to dope polyaniline (PANI) via the LBL method to see whether they can form stable multilayer films and whether the obtained PANI/MSAG$_{NP}$ multilayer film could remain electroactive in neutral pH conditions. If we succeed, we are then not limited any longer to use only polyelectrolytes to shift the redox-activity of PANI to neutral conditions. Moreover, it will also provide an alternative method to incorporate metal particles into conducting polymers, which is also a very active research topic nowadays.[14-15]

4.3.1 Preparation and Characterization of the MSAG$_{NP}$

Three MSAG$_{NP}$ samples with different size were prepared, and the details about the preparation process can be found in the experimental part (Chapter 2). Transmission electron microscope (TEM) images and the absorbance of the prepared MSAG$_{NP}$ samples are shown in Figure 4.3-1. From the TEM images, we can see that all the MSAG$_{NP}$ samples are very homogeneous and with no aggregation between the particles. The average particle size was 2.0 ± 0.4 nm, 9.9 ± 0.8 nm and 15.2 ± 1.4nm, for sample (A), (B) and (C), respectively (c.f. inset in (A), (B), (C) for size distribution analysis). Figure (D) shows the UV-vis spectra of MSAG$_{NP}$ samples dispersed in Milli-Q water. For smaller MSAG$_{NP}$ samples (A), a very weak absorption peak is observed at around $\lambda = 520$ nm; while for the bigger ones (B and C), a strong absorbance was observed, with the absorption peak red-shifted to around 528 nm and 532 nm for (B) and (C), respectively. These results are consistent with those reported for particles with similar sizes.[16]

4.3.2 LBL Self-Assembly of PANI with MSAG$_{NP}$

Because the prepared MSAG$_{NP}$ samples are negatively charged when dispersed in Milli-Q water, so it is possible to assemble them with the positively charged PANI by the simple LBL method. For the convenience of further modification and application of the prepared PANI/MSAG$_{NP}$ films, the final layer of every sample we prepared is MSAG$_{NP}$. The scheme of the LBL self-assembly process of PANI with MSAG$_{NP}$ is shown in Figure 4.3-2 (A), and the assembly process was in situ monitored by SPR
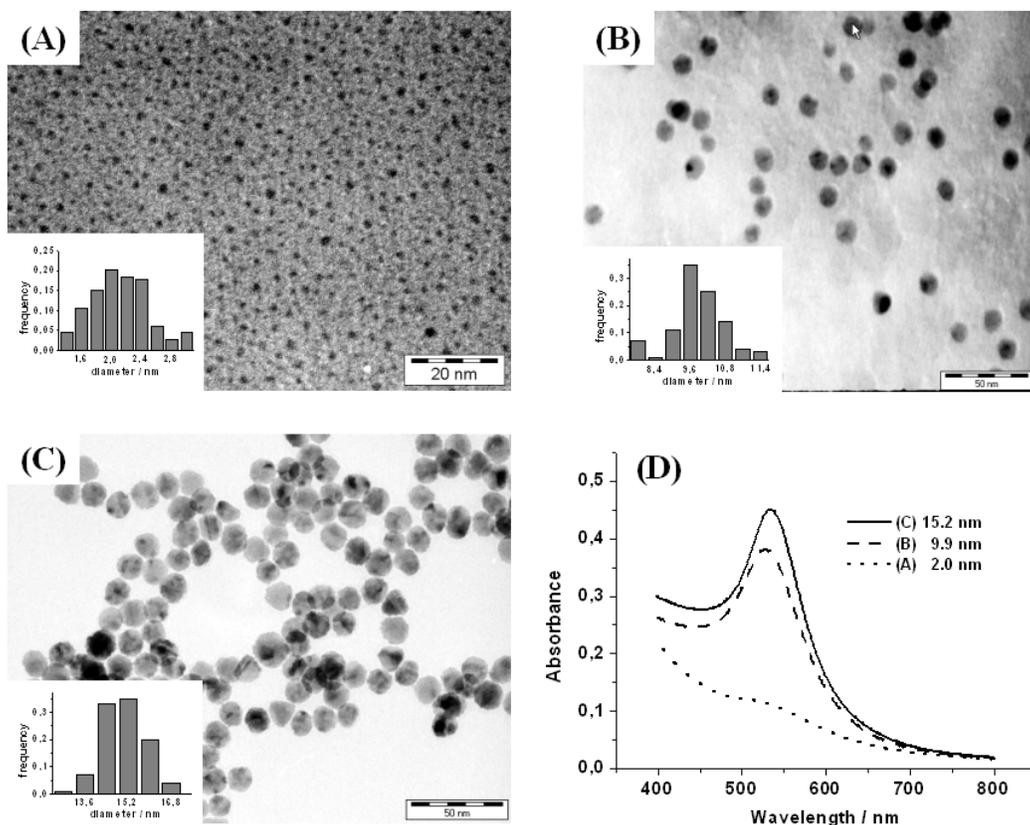
Fig.4.3-1 *(A), (B) and (C) are the TEM images of the prepared MSAG$_{NP}$ samples with a average diameter of 2.0 ± 0.4 nm, 9.9 ± 0.8 nm and 15.2 ± 1.4 nm, respectively. Insets are the corresponding size distribution analysis (50 particles counted in each case). (D) UV-vis spectra of the above MSAG$_{NP}$ samples dispersed in Milli-Q water.*

and electrochemistry, as shown in Figure 4.3-2 (B) to (D). The gradual SPR minimum angle shifts indicate a progressive deposition of PANI and MSAG$_{NP}$ layers onto the Au substrate in each cycle (Fig.4.3-2(B)). An obvious minimum reflectance increase and the broadening of the curve with the increase of the number of deposited bilayers are induced by the absorptivity of both the PANI and the nanoAu particles inside the film, further indicating a stable LBL self-assembly process. *In situ* SPR kinetic measurement (Fig.4.3-2(C)) also shows clearly the incorporation of MSAG$_{NP}$ into the multilayer film. The reason for the seemingly SPR kinetic signal saturation is that the SPR kinetic measurement was carried out at a fixed angle (56.5°) despite the shifting and broadening of the SPR angular curves after deposition of each layer (c.f. Fig.4.3-2(B)). The cyclic voltammetry (CV) measurements (Fig.4.3-2(D)) are nicely consistent with the SPR results. The linear peak current increase with the increase of the number of bilayers suggests a highly reproducible deposition from layer to layer.
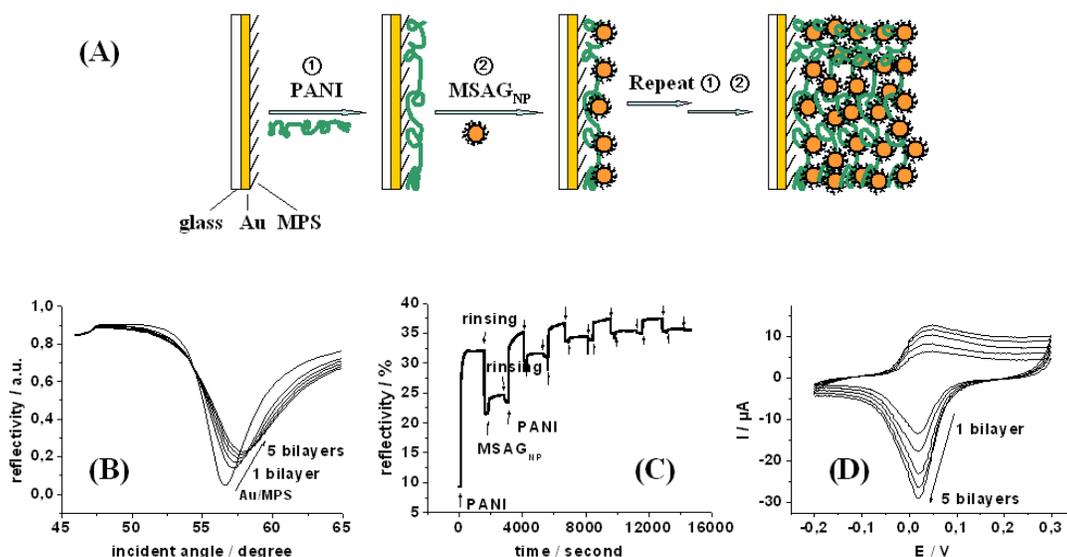
Fig.4.3-2 *(A) Scheme of the LBL assembly of PANI and MSAG$_{NP}$. (B) SPR angular spectra and (D) cyclic voltammograms of different samples with an increasing number of bilayers of PANI/MSAG$_{NP}$ recorded in 0.1M PBS buffer (pH 7.1) after each bilayer was deposited onto the Au subtrate. (C) In situ SPR kinetic measurement during the LBL self-assembly process of PANI/MSAG$_{NP}$ multilayer film at a fixed angle (56.5^o). CV scan rate was 50mV/s.*

4.3.3 Properties of PANI/MSAG$_{NP}$ multilayer films in neutral solution

From the CV curves in Figure 4.3-2(D), it is clear that the PANI/MSAG$_{NP}$ multilayer films show very good redox activity at pH 7.1 in PBS buffer. A broad redox peak is found for different bilayers of PANI/MSAG$_{NP}$, just like those doped by polyelectrolytes (c.f. section 4.2), with the formal potential being around 0.03V. As mentioned before, this redox peak is the overlap of the two redox processes normally found for PANI in acidic conditions (c.f. Chapter 3),[1b] as confirmed by the electrochemical behavior of PANI/MSAG$_{NP}$ multilayer films measured in different pH buffer solutions, as shown in Figure 4.3-3. At low pH, two separate redox peaks appear. As the pH increases, the second redox peak moves toward lower potential with a rate of about –100mV/pH and finally merges with the first one at pH > 5 to show only one redox peak. A similar behavior was also observed in PANI composite films prepared by the afore mentioned methods (c.f. section 4.2).[5b, 6b]

Shown in Figure4.3-4 are 10 consecutive CV curves and the corresponding SPR reflectivity changes of 5 bilayers of PANI/MSAG$_{NP}$ measured in PBS buffer. It can be seen that the multilayer films are very stable in neutral solution upon repeated potential cycling in the potential range between –0.2V and +0.3V, with almost no

observable changes in both the peak current and the peak-to-peak separation after the first cycle. The corresponding SPR signal is also very stable and reproducible during the potential scanning. This excellent stability and reproducibility of the films in
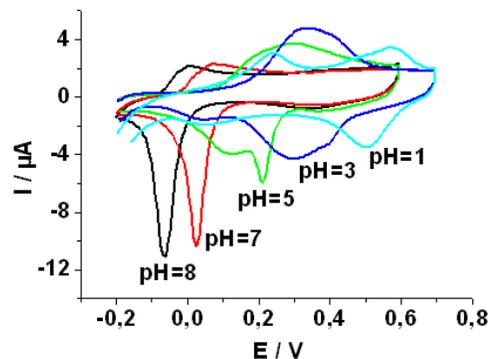
Fig.4.3-3 *Cyclic voltammograms of PANI/MSAG$_{NP}$ measured in buffers with different pH values: for pH 1, HCl solution was used; for pH 3~8, 0.1M citrate phosphate buffer was used. Scan rate was 20mV/s.*
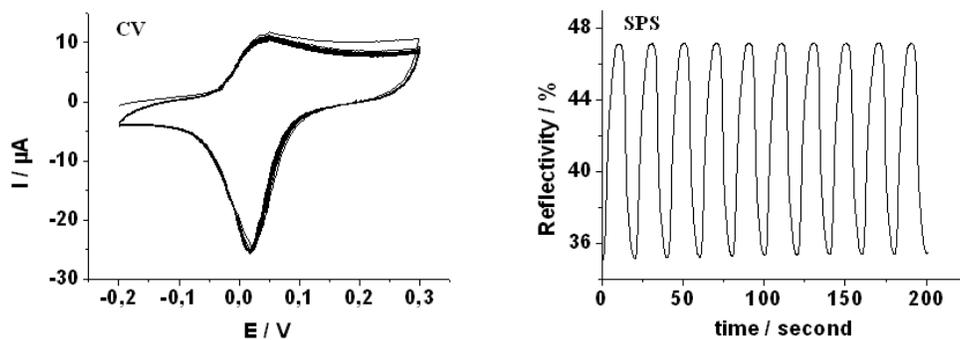
Fig.4.3-4 *Cyclic voltammograms and the corresponding SPR signal changes upon repeated potential scans (-0.2V $\leq E \leq$ +0.3V) of 5 bilayers of PANI/MSAG$_{NP}$ measured in 0.1M PBS buffer, pH7.1. CV scan rate 50mV/s.*

neutral pH environment offer interesting opportunities for practical applications in bioengineering, as will be demonstrated for the stable detection of DNA hybridization in the Chapter 5.

Cyclic voltammograms at different scan rates measured in 0.1M PBS buffer (pH 7.1) showed that the redox peak currents are linearly proportional to the scan rates up to at least 500mV/s, indicating a surface-confined redox process (Fig.4.3-5). However, for PANI multilayer films doped with negatively charged polyelectrolytes

also by the LBL method, this process was diffusion-controlled (c.f. section 4.2). This difference may arise from the different structures due to the different dopants. In the case of PANI/MSAG$_{NP}$ films, the two components form a relatively open and disordered structure, which facilitates both the effective doping of PANI and the fast charge transfer. Moreover, the Au nanoparticle itself may also help the charge transfer across the film. In comparison, PANI and the negatively charged polyelectrolytes form a more compact structure, and the above two processes may be hampered to some extent by the relative rigidity of the polyelectrolyte chain.
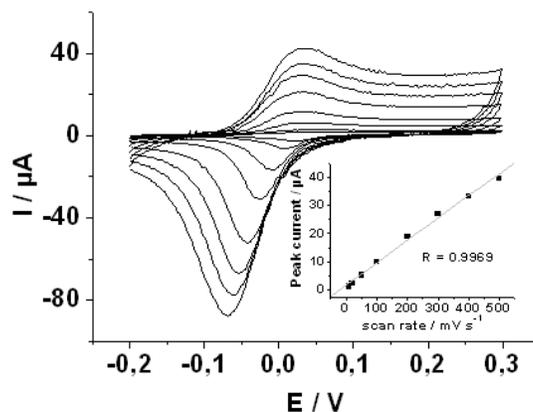
Fig.4.3-5 *Cyclic voltammograms of a PANI/MSAG$_{NP}$ multilayer film (5 bilayers) recorded in 0.1M PBS buffer, pH 7.1 at different scan rates: 10, 20, 50, 100, 200, 300, 400, 500 mV/s. The inset shows the linear relationship between the anodic peak current and the scan rate.*

4.3.4 Size effect of MSAG$_{NP}$ on the electroactivity of PANI/MSAG$_{NP}$ multilayer films

All the results given above are based on the smaller MSAG$_{NP}$ (2.0 ± 0.4 nm). We also prepared PANI/MSAG$_{NP}$ multilayer films with the two bigger MSAG$_{NP}$ samples (9.9 ± 0.8 nm and 15.2 ± 1.4nm), and their electrochemical properties were investigated under the same conditions as those used for the smaller one. We found that the size of MSAG$_{NP}$ had an important effect on the redox activity of the obtained PANI/MSAG$_{NP}$ films with the same number of bilayers, as shown in Figure 4.3-6. The electroactivity of PANI/MSAG$_{NP}$ film decreases with the increase of the size of the corresponding MSAG$_{NP}$, with MSAG$_{NP}$ (2.0 ± 0.4 nm) shows the highest redox activity. This is reasonable, because the surface area per unit volume (S/V) is proportional to the reciprocal of the diameter of MSAG$_{NP}$ if MSAG$_{NP}$ is assumed to

have a spherical shape. Therefore, the smallest MSAG$_{NP}$ sample (2.0 ± 0.4 nm) should have the highest S/V, thus the highest density of –COOH groups per particle, as compared to the larger ones.[17] So the smaller MSAG$_{NP}$ can dope PANI more efficiently than the bigger ones. In our following experiments, we only use the smaller MSAG$_{NP}$ sample (2.0 ± 0.4 nm).
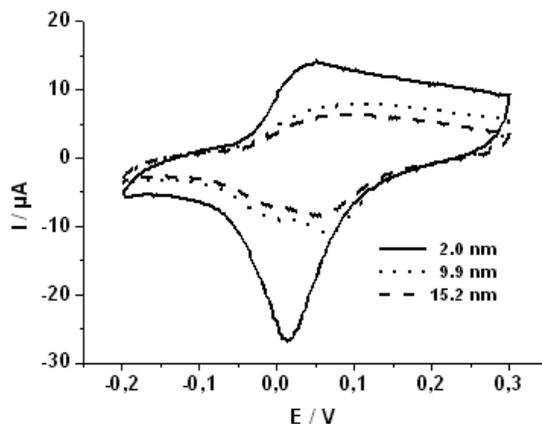
Fig.4.3-6 *Size effect of MSAG$_{NP}$ on the redox activity of the prepared PANI/MSAG$_{NP}$ multilayer films. All the samples are six bilayers, measured in 0.1M PBS buffer, pH7.1. Scan rate 50mV/s.*

4.3.5 Electrocatalytic efficiency of PANI/MSAG$_{NP}$ films toward the oxidation of NADH

It has been shown that PANI doped by negatively charged polyelectrolytes can electrocatalyze the oxidation of NADH (c.f. section 4.2 and references 6 and 7b). Shown in Figure 4.3-7(A) are the cyclic voltammograms of 5 bilayers of PANI/MSAG$_{NP}$ films measured in 0.1M PBS buffer (pH 7.1) in the absence and presence of different amounts of NADH, at a scan rate of 5mV/s. The capability of the PANI/MSAG$_{NP}$ film to electrocatalyze the oxidation of NADH is clearly observed. The anodic catalytic peak current increases with the increase of NADH concentration. Further experiments also show that the catalytic peak current increases with the increase of the film thickness up to at least 12 bilayers (Fig.4.3-7(B)), but not in a strictly linear way. Moreover, there is an offset at n=0, which may arise from the different active reaction sites inside the different layers. This current change is also different from that found for PANI/polyelectrolytes multilayer films. In the latter

case, the catalytic peak currents level off if the films are thicker than 8 bilayers (c.f. Section 4.2).

Figure 4.3-8(A) shows the relative electrocatalytic efficiency of different PANI multilayer systems with the same number of bilayers. Except for the PANI/SPANI system in which every layer is electroactive and has high electrocatalytic ability toward the oxidation of NADH (c.f. Section 4.2), the electrocatalytic efficiency of
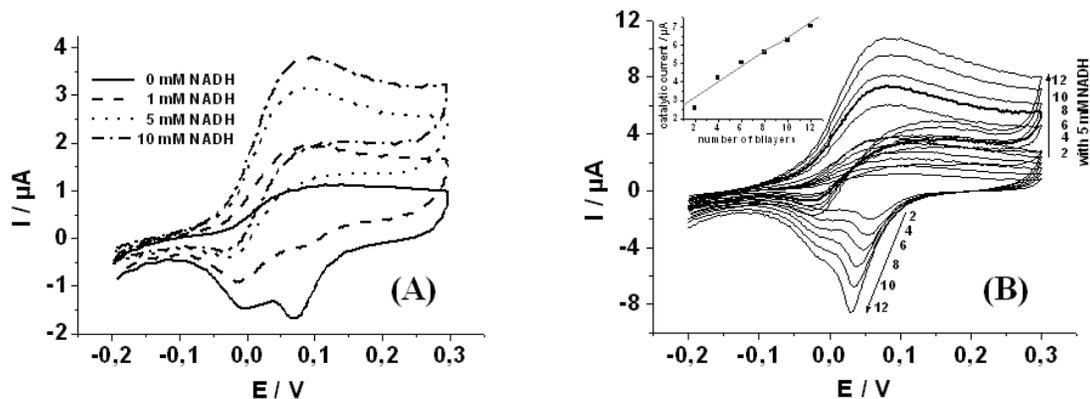
Fig.4.3-7 *(A) Cyclic voltammograms of 5 bilayers of PANI/MSAG$_{NP}$ measured in 0.1M PBS buffer (pH 7.1) in the absence and presence of different concentrations of NADH, scan rate 5mV/s. (B) Cyclic voltammograms of different bilayers of PANI/MSAG$_{NP}$ measured in 0.1M PBS buffer, pH 7.1 without and with 5mM NADH. The inset shows that the electrocatalytic efficiency of the film increases with the increase of the number of bilayers up to at least 12 bilayers.*
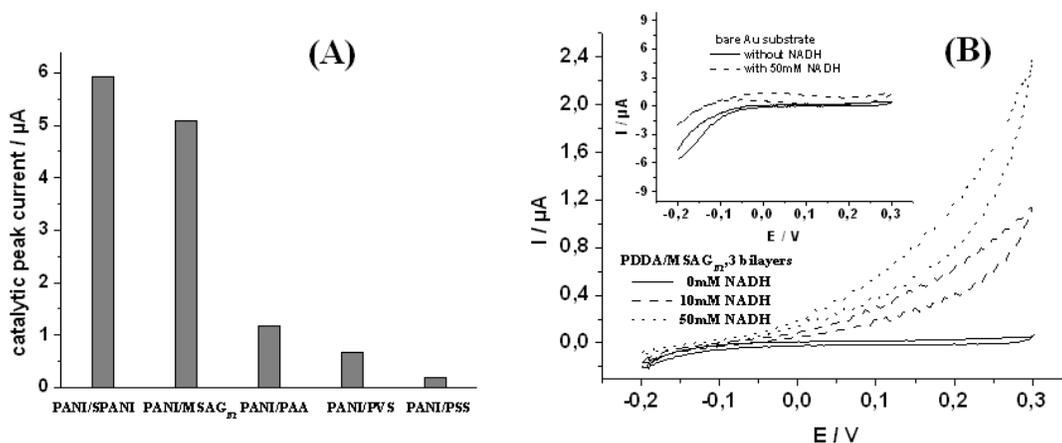
Fig.4.3-8 *(A) Comparison of the electrocatalytic efficiency of different PANI multilayer systems, 6 bilayers each. NADH concentration is 10mM. (B) Control experiment to show that MSAG$_{NP}$ themselves also have electrocatalytic ability towards the oxidation of NADH by using PDDA instead of PANI to construct multilayer film with MSAG$_{NP}$. Inset shows the results of bare Au substrate to exclude the possibility that the catalytic signal comes from the substrate. All the measurements were carried out in 0.1M PBS buffer, pH7.1 with different amount of NADH. Scan rate 5mV/s.*

PANI/MSAG$_{NP}$ is higher than that of PANI doped by polyelectrolytes. The relatively higher electrocatalytic efficiency of PANI/MSAG$_{NP}$ originates mainly from the following aspects: firstly, the surface charge density of MSAG$_{NP}$ is higher compared to that of the corresponding polyelectrolytes, which enables them to dope PANI more effectively than polyelectrolytes; secondly, MSAG$_{NP}$ inside the multilayer film facilitate the charge transfer across the film (vide supra); thirdly, MSAG$_{NP}$ themselves show some electrocatalytic ability towards the oxidation of NADH, as confirmed by a control experiment done under the same conditions using poly(diallyldimethylammonium chloride)(PDDA) instead of PANI to construct multilayer film with MSAG$_{NP}$, as shown in Figure 4.3-8(B). The differences among the catalytic behavior of different PANI multilayer systems may also originate from differences in the thickness, the density and the morphology of the different films, as a result of different interactions between the PANI and the corresponding poly(anions) or MSAG$_{NP}$ under the same conditions (c.f. Section 4.2).

4.3.6 Conclusions

In summary, we have demonstrated successfully that PANI and MSAG$_{NP}$ can form stable multilayer films by the LBL method. The obtained PANI/MSAG$_{NP}$ multilayer films were very stable and show very good electroactivity in a neutral pH enviroment, just like those doped by polyelectrolytes. PANI/MSAG$_{NP}$ multilayer films can also electrocatalyze the oxidation of NADH, and their electrocatalytic efficiency is even higher as compared to those of PANI/polyelectrolytes systems (except for PANI/SPANI system). Besides, the method we used here also offers an alternative approach to incorporate Au nanoparticles into conducting polymers.

Another advantage of doping PANI with MSAG$_{NP}$ is that the carboxyl groups on the MSAG$_{NP}$ can be used to link enzymes or other biomolecules to the PANI/MSAG$_{NP}$ film. We will demonstrate their application in this aspect by linking amino-terminated DNA probes to PANI/MSAG$_{NP}$ film and detecting hybridization event by both electrochemical and optical techniques, as will be shown in Chapter 5.

Moreover, the PANI/MSA-nanoAu films combine the properties of PANI and nano-Au particles, each of which has its unique electrical, optical, and optoelectrical properties, they should also find potential applications in other fields such as microelectronics, or for electrochromic and photovoltaic devices. However,

investigation on the properties and applications in this aspect is out of the scope of the present study and will not be discussed here.

4.4 Polyaniline Doped by Modified Carbon Nanotubes and Their Application for Stable Low-Potential Detection of NADH

4.4.1 Motivation

Carbon Nanotubes (CNTs), as one of the most interesting carbon materials, has attracted an enormous interest over the past years, mainly due to their exceptional electrical, chemical and mechanical properties which make them attractive candidates for diverse applications such as in nanoelectronics, biosensors, and so on.[18,19] Recently, fabrication of CNTs/conducting polymers (CPs) composites has gained great interest, and it has been demonstrated that the obtained CNTs/CPs composites possess the properties of each of the constituents with a synergistic effect.[20] Different CPs have been used, such as polypyrrol(Ppy),[20a,20b] poly(phenylene vinylene) (PPV),[20c,20d] polythiophene and its derivatives.[20e,20f] Polyaniline (PANI)/CNTs composites were also prepared and investigated by many researchers.[21,22] Almost all the reported PANI/CNTs composites show enhanced electronic properties, with some of them finding practical applications as printed electrodes in transistors with high-performance contacts and logic gates.[22] However, the reported methods for preparing the CNTs/CPs composites are almost the same, i.e., by polymerisation of the corresponding monomer in the presence of CNTs, either by chemical method or by the electrochemical techniques. In addition, until now no reports were available about the properties of PANI/CNTs composites in neutral conditions, which is an important aspect to learn for their potential biological applications. Here we report another simple way of incorporating CNTs into CPs by using the layer-by-layer (LBL) method. Recently, the LBL method has been demonstrated very successfully in the preparation of CNTs/non-conducting polymer (e.g. PDDA) composites.[23] The obtained multilayer films were highly homogeneous and showed drastically improved mechanical properties as compared to those prepared by other methods,[23a,23b] or acted as potential candidates for development of environmentally benign non-platinum alkaline air electrodes for energy conversions.[23d] Here we first demonstrated, by the LBL method, the preparation of CNTs composites with a conducting polymer, polyaniline (PANI). PANI was successfully assembled with a commercially available polyaminobenzene sulfonic acid-modified single-walled carbon nanotubes (PABS-SWNTs) via the LBL approach. It was found that PABS-SWNTs inside the multilayer

film can dope PANI effectively and shift its electroactivity to a neutral pH condition. The obtained PANI/PABS-SWNTs multilayer films are very stable and show a high electrocatalytic efficiency toward the oxidation of β-nicotinamide adenine dinucleotide (NADH) at a much lower overpotential (about -50mV vs. Ag/AgCl), which makes it an ideal substrate for constructing a NADH sensor.

NADH and its oxidized form (NAD$^+$) are important coenzymes that take part in a lot of dehydrogenase enzymatic reactions. They show a key role in developing amperometric enzyme sensors or biofuel cells that use dehydrogenase dependent enzymes. However, the direct oxidation of NADH at bare electrodes in a neutral environment normally requires high overpotentials up to 1.0V.[24] Consequently, different redox mediators have been used to reduce the overpotential for NADH oxidation. Among them, PANI doped with polyanions either by the electropolymerisation method [6,7b] or by the LBL method (c.f. Section 4.2) have been shown to be good candidates. We also showed in the previous section that PANI doped by modified gold nanoparticles (MSAG$_{NP}$) can also electrocatalyze the oxidation of NADH at a low potential in a neutral environment (c.f. Section 4.3). Recently, Wang's group reported that CNTs-modified glassy carbon electrodes can also offer a stable low-potential amperometric detection of NADH.[25] This idea was optimised by Cai's group by using the ordered CNTs (OCNTs) instead, and a diminution of the overpotential of 645mV was reported, with a detection limit of 5×10^{-7} M.[26] However, the template method for preparing the OCNTs and the following casting them onto electrode are a little complex. Here we show that PANI/PABS-SWNTs multilayer films prepared by the simple LBL technique show a sensitivity comparable to that of OCNTs. For a six-bilayer sample, the detection limit can go down to 1×10^{-6} M as detected by the simple cyclic voltammetry method (this limit can go down further by using other more sensitive detection techniques or building up thicker films), with a linear range between 5×10^{-6} M and 1×10^{-3} M. The substrate can be used repeatedly for consecutive detection of NADH with a very stable signal.

4.4.2 LBL self-assembly of PANI with PABS-SWNTs

The LBL self-assembly process of PANI with PABS-SWNTs was monitored in situ by surface plasmon resonance spectroscopy (SPR) and cyclic voltammetry (CV), as

shown in Figure 4.4-1. The regular minimum angle shift as well as the broadening of the SPR curves with the deposition of each bilayer of PANI/PABS-SWNTs indicates a very stable self-assembly process. CV measurement also confirms the LBL process. It is clear that after the assembly of each bilayer, the peak current increases gradually.
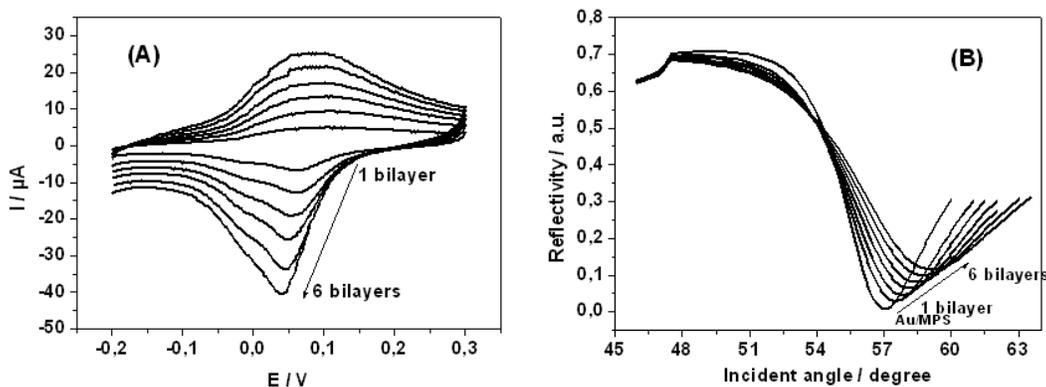
Fig.4.4-1 *Cyclic voltammograms (A) and SPR spectra (B) of different bilayers of PANI/PABS-SWNTs multilayer films self-assembled on Au substrates recorded in 0.1M PBS buffer, pH=7.2. Scan rate 50mV/s.*

4.4.3 Properties of PANI/PABS-SWNTs multilayer films in neutral solution

It is well known that PANI is electroactive only in acidic conditions.[4] However, after incorporation PABS-SWNTs into the PANI films by the LBL technique, the formed PANI/PABS-SWNTs multilayer films remain electroactive in pH7.2 PBS buffer, as can be seen clearly in Figure 4.4-1(A). A broad redox peak is found for each sample with different bilayers, with the redox potential around 0.05V. This
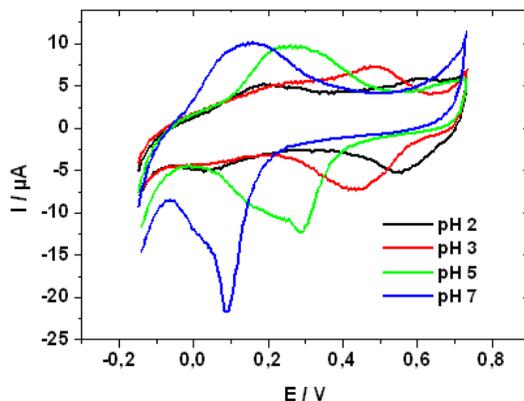
Fig.4.4-2 *Cyclic voltammograms of PANI/PABS-SWNTs multilayer films (6 bilayers) measured in different pH buffers: for pH 2, HCl solution was used; for pH 3~7, 0.1M citrate phosphate buffer was used. Scan rate was 20mV/s.*

redox peak is the overlapping of the two redox processes normally found for PANI system in acidic conditions (c.f. Chapter 3), as confirmed by the redox behavior of PANI/PABS-SWNTs multilayer films measured in different pH buffer solutions (Figure 4.4-2). This electrochemical behavior of PANI/PABS-SWNTs multilayer film is also similar to those of PANI doped by polyanions or modified Au nanoparticles via the same LBL method (c.f. Sections 4.2 and 4.3).

The stability of the prepared PANI/PABS-SWNTs multilayer films is a key aspect to learn for their practical applications. Shown in Figure 4.4-3 are the SPR kinetic signal changes during the repeated cyclic potential scanning in PBS buffer. In the potential range between –0.2V and +0.3V, the SPR signal is very stable and reproducible during potential scanning. At the same time, almost no changes are observed in the CV curves in both the peak current and the peak-to-peak separation after the first cycle. All this indicates that PANI/PABS-SWNTs multilayer films are very stable and reproducible in neutral solution, which offers attractive opportunities for their practical applications in bioassays.
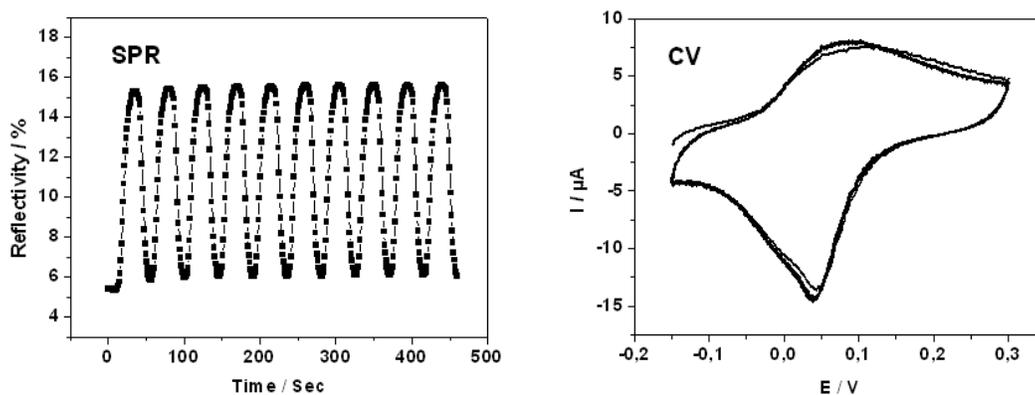
Fig.4.4-3 *SPR reflectivity changes of PANI/PABS-SWNTs multilayer films (6 bilayers) measured at a fixed angle (58°) upon repeated cyclic potential scanning (10 cycles) in 0.1M PBS buffer, pH = 7.2. CV scan rate 20mV/s.*

The cyclic voltammograms of a six-bilayer PANI/PABS-SWNTs sample measured at different scan rates showed that the peak currents increase linearly with the scan rates (Figure 4.4-4), indicating a fast surface-controlled redox process. This fast electron transfer behavior is the same as that of PANI/MSAG$_{NP}$ multilayer films (c.f. Section 4.3), but different from that of PANI/polyelectrolytes system which show a diffusion-controlled mechanism (c.f. Section 4.2). The fast redox behavior of

PANI/PABS-SWNTs films may originate from the fact that both PANI and PABS-SWNTs are conducting, which facilitates a fast charge transfer across the film.
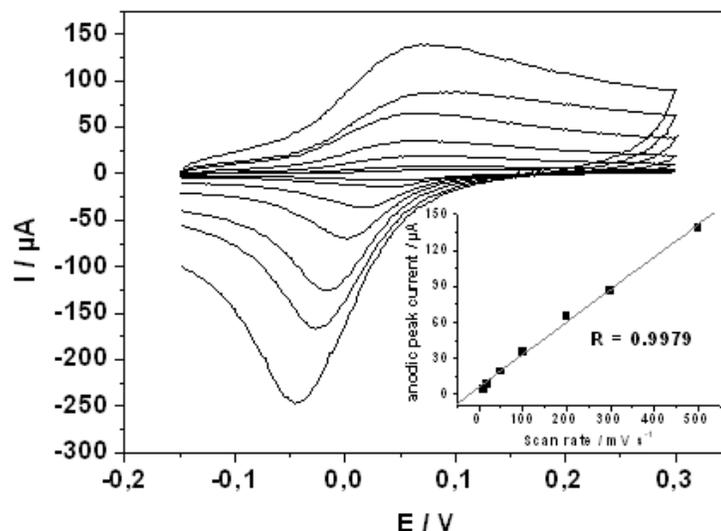
Fig.4.4-4 *Cyclic voltammograms of 6 bilayers of PANI/PABS-SWNTs in 0.1M PBS buffer, pH7.2, at a scan rate of 10, 20, 50, 100, 200, 300, 500mV/s, respectively. Inset shows the linear relationship between anodic peak currents and the scan rates.*

4.4.4 Application of PANI/PABS-SWNTs multilayer film for the stable low-potential detection of NADH

As mentioned above, both PANI composites and CNTs have been reported to be able to electrocatalyze the oxidation of NADH. Figure 4.4-5(A) shows the cyclic
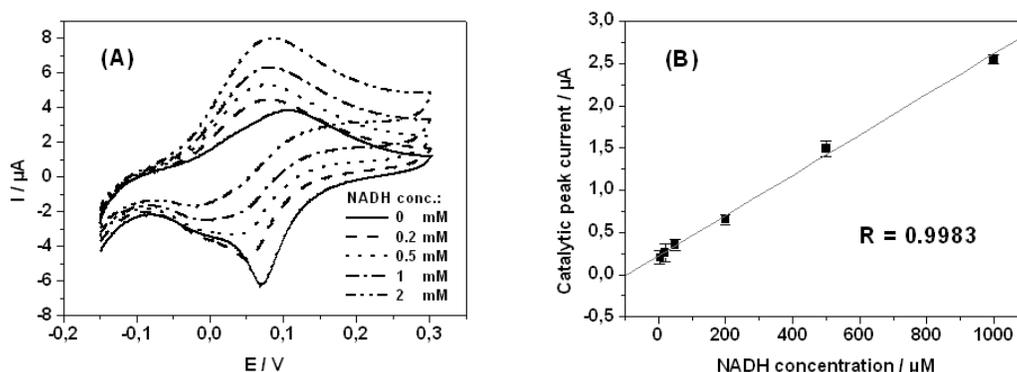
Fig.4.4-5 *(A) Cyclic voltammograms of 6 bilayers of PANI/ PABS-SWNTs measured in 0.1M PBS buffer (pH=7.2) containing different concentrations of NADH. Scan rate was 5mV/s. (B) The linear relationship between the catalytic peak current and NADH concentration in the range between 5×10^{-6} M and 1×10^{-3} M. The error bars show the data range of three parallel experiments.*

voltammograms of a 6 bilayer PANI/PABS-SWNTs multilayer film measured in 0.1M PBS buffer (pH7.2) in the absence and presence of different amounts of NADH. It can be seen clearly that PANI/PABS-SWNTs multilayer film can also electrocatalytize the oxidation of NADH. The oxidation process starts at about – 0.05V, much lower than the reported potential for NADH oxidation at a bare electrode.[24] As can also be seen the catalytic peak currents increase gradually with the increase of the concentration of NADH. Detailed studies indicate that the catalytic peak currents show a linear relationship with the concentration of NADH in the range of 5×10^{-6} M and 1×10^{-3} M, with a detection limit of 1×10^{-6} M (Fig.4.4-5(B)). This sensitivity is comparable to that obtained on a OCNTs-modified glass carbon electrode.[26] Compared with our previous results for other polyaniline systems, the electrocatalytic efficiency of PANI/PABS-SWNTs is more than twice that of PANI/SPANI, nearly three times that of PANI/MSAG$_{NP}$, and much higher than those of the other PANI systems doped by non-electroactive polyelectrolytes (i.e. PANI/PAA, PANI/PVS and PANI/PSS), as shown in Figure 4.4-6. Further experiments also showed that the catalytic efficiency of PANI/PABS-SWNTs multilayer films increase almost linearly with the increase of the film thickness up to at least 12 bilayers (Figure 4.4-7), which means that even higher catalytic signal can be achieved by building up thicker films. This good electrocatalytic efficiency of PANI/PABS-SWNTs multilayer films at such a low potential makes it an excellent candidate for constructing a NADH sensor.
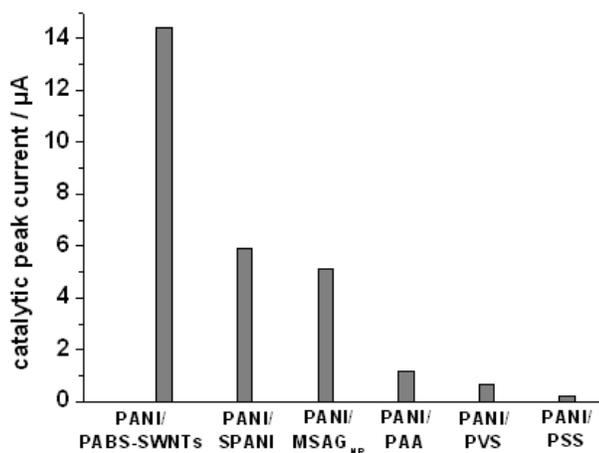
Fig.4.4-6 *Comparison of the electrocatalytic efficiency of different PANI multilayer systems (6 bilayers each) toward the oxidation of NADH. NADH concentration is 10mM.*
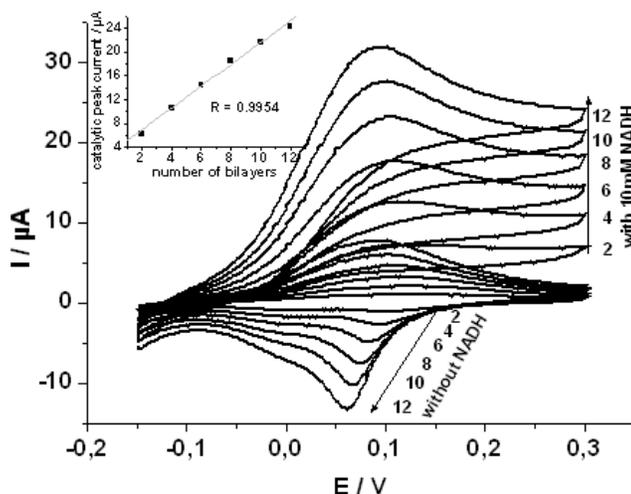
Fig.4.4-7 *Cyclic voltammograms of different bilayers of PANI/PABS-SWNTs measured in 0.1M PBS buffer, pH 7.2 without and with 10mM NADH. The inset shows that the electrocatalytic efficiency of the film increases almost linearly with the increase of the number of bilayers up to at least 12 bilayers.*

The catalytic efficiency of PANI/PABS-SWNTs multilayer films for the oxidation of NADH is very stable upon repeated use, as shown by the flow-injection experiment (Figure 4.4-8). If the potential is held at +0.2V where the film is in its oxidised state, 0.5 mM NADH was flow-injected sequentially (1ml per time). It can be seen clearly that both the catalytic current and the response time are all very stable and reproducible, showing the suitability of PANI/PABS-SWNTs multilayer film for repeated stable detection of NADH.
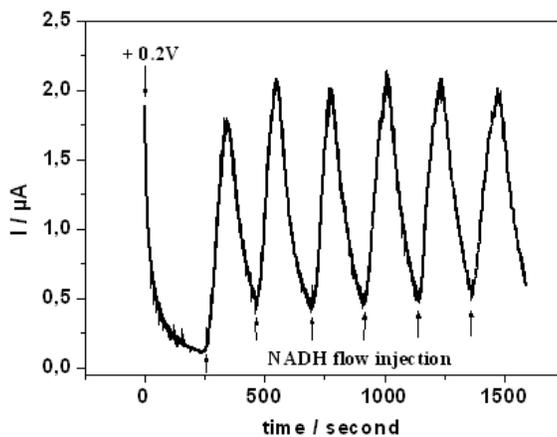
Fig.4.4-8 *Current changes during the repeated flow-injection of 0.5mM NADH (1ml per time) while keeping the PANI/PABS-SWNTs multilayer film (12 bilayers) in its oxidised state (+0.2V).*

4.4.5 Conclusions

In summary, PANI/CNTs composite films were successfully prepared via the LBL method for the first time. The obtained films were very stable and electroactive in neutral solution. They also showed a stable and high electrocatalytic efficiency toward the oxidation of NADH at a much lower potential, which makes it a good candidate as a NADH sensor.

4.5 Chapter Concluding Remarks

In this chapter, different PANI multilayer films were successfully prepared via the LBL method with different materials, which include not only the normally used negatively charged polyelectrolytes, but also some other novel materials like modified Au nanoparticles or carbonnanotubes. It was found that all the used dopants could effectively dope PANI and shift its redox activity to a neutral pH environment. All the prepared PANI multilayer films are very stable and show catalytic ability toward the oxidation of NADH at a low potential, with PANI/PABS-SWNTs having the highest catalytic efficiency which makes it an ideal candidate for constructing a NADH sensor. Besides, because PANI/MSAG$_{NP}$ multilayer films were terminated with – COOH groups, we can link amino-modified DNA probes to this film and use it as a sensing surface for DNA hybridization detection, as will be shown in the next chapter.

4.6 References

1. a) A. G.MacDiarmid, J. C.Chiang, M. Halpern, W. S. Huang, S. L. Mu, N. L. D. Somasiri, W. Wu, S. I. Yaniger, *Mol. Cryst. Liq. Cryst.* **1985**, *121*, 173. b) W.-S. Huang, B. D. Humphrey, A. G. MacDiarmid, *J Chem. Soc., Faraday Trans. 1*, **1986**, *82*, 2385.

2. a) A. G. MacDiarmid, *Synth. Met.* **1997**, *84*, 27. b) Alan G. MacDiarmid, *Synth. Met.* **2002**, *125*, 11. c) A. J. Heeger, *Synth. Met.* **2002**, *125*, 23.

3. a) D. Nicolas-Debarnot, F. Poncin-Epaillard, *Anal. Chim. Acta* **2003**, *475*, 1. b) A. Malinauskas, *Synth. Met*. **1999**, *107*, 75. c) P. N. Bartlett, J. M. Cooper, *J. Electroanal. Chem.* **1993**, *362*, 1. d) J. Bobacka, A. Ivaska, A. Lewenstam, *Electroanalysis*, **2003**, *15*, 366. e) G. G. Wallace, M. Smyth, H. Zhao, *Trends in Anal. Chem.* **1999**, *18*, 245. f) S. Cosnier, *Biosen. Bioelectron*., **1999**, *14*, 443.

4. a) A. F. Diaz, J. A. Logan, *J. Electroanal. Chem*., **1980**, *111*, 111. b) T. Ohsaka, Y. Ohnuki, N. Oyama, K. Katagiri, K. Kamisako, *J. Electroanal. Chem.* **1984**, *161*, 399. c) S. Y.Cui, S. M. Park, *Synth. Met.* **1999**, *105*, 91.

5. a) J. Yue, A. J. Epstein, A. G. MacDiarmid, *Mol. Cryst. Liq. Cryst.* **1990**, *189*, 255. b) A. A. Karyakin, A. K. Strakhova and A. K. Yatsimirsky, *J. Electroanal. Chem*., **1994**, *371*, 259.

6. a) P. N. Bartlett, P. R. Birkin, E. N. K. Wallace, *J. Chem. Soc., Faraday Trans.* **1997**, *93*, 1951. b) P. N. Bartlett, E. Simon, *Phys. Chem. Chem. Phys.* **2000**, *2*, 2599. c) P. N. Bartlett, E. N. K. Wallace, *J. Electroanal. Chem.* **2000**, *486*, 23.

7. a) E. Simon, C. M. Halliwell, C. S. Toh, A. E. G. Cass, P. N. Bartlett, *Bioelectrochemistry*, **2002**, *55*, 13. b) O. A. Raitman, E. Katz, A. F. Bückmann, I. Willner, *J. Am. Chem. Soc.* **2002**, *124*, 6487.

8. a) G. Decher, J. D. Hong, J. Schmitt, *Thin Solid Films* **1992**, *210-211*, 831. b) G. Decher, *Science* **1997**, *277*, 1232.

9. a) M. Ferreira, J. H. Cheung, M. F. Rubner, *Thin Solid Films* **1994**, *244*, 806. b) J. H. Cheung, A. F. Fou, M. F. Rubner, *Thin Solid Films* **1994**, *244*, 985. c) J. H. Cheung, W. B. Stockton, M. F. Rubner, *Macromolecules* **1997**, *30*, 2712. d) W. B. Stockton, M. F. Rubner, *Macromolecules* **1997**, *30*, 2717.

10. a) M. K. Ram, M. Salerno, M. Adami, P. Faraci, C. Nicolini, *Langmuir* **1999**, *15*, 1252. b) D. Li, Y. Jiang, C. Li, Z. Wu, X. Chen, Y. Li, *Polymer* **1999**, *40*, 7065. c) D. Li, Y. Jiang, Z. Wu, X. Chen, Y. Li, *Thin Solid Films* **2000**, *360*, 24. d) D. DeLongchamp, P. T. Hammond, *Adv. Mater.***2001**, *13*, 1455. e) A. Baba, M.-K. Park, R. C. Advincula, W. Knoll, *Langmuir* **2002**, *18*, 4648.

11. a) M. Ferreira, M. F. Rubner, *Macromolecules* **1995**, *28*, 7107. b) J. Sun, Tao Wu, F. Liu, Z. Wang, X. Zhang, J. Shen, *Langmuir* **2000**, *16*, 4620.

12. a) D. Orata, D. A. Buttry, *J. Am. Chem. Soc.* **1987**, *109*, 3574. b) D. A. Buttry, M. D. Ward, *Chem. Rev.* **1992**, *92*, 1355.

13. a) S. Cordoba-Torresi, C. Gabrielli, M. Keddam, H. Takenouti, R. Torresi, *J. Electroanal. Chem.* **1990**, *290*, 269. b) M. J. Brown, A. R. Hillman, S. J. Martin, R. W. Cernosek, H. L. Bandey, *J. Mater. Chem.* **2000**, *10*, 115.

14. R. Krishnamoorti, R. A. Vaia, *Polymer Nanocomposites*, Vol.804, Washington, DC: ACS, **2002**.

15. See recent reviews: a) R. Gangopadhyay, A. De, *Chem. Mater.* **2000**, *12*, 608. b) G. Schmidt, M. M. Malwitz, *Curr. Opin. Coll. Interface Sci.* **2003**, *8*, 103.

16. a) S. Chen, K. Kimura, *Langmuir* **1999**, *15*, 1075. b) T. Zhu, K. Vasilev, M. Kreiter, S. Mittler, W. Knoll, *Langmuir*, **2003**, *19*, 9518.

17. K. Kimura, S. Takashima, H. Ohshima, J. Phys. Chem. B 2002, 106, 7260.

18. a) T. W. Ebbesen, *Carbon nanotubes: Preparation and Properties*, CRC Press: Boca Raton, FL, **1997**. b) A. B. Kaiser, *Adv. Mater.* **2001**, 13, 927. c) R. H. Baughman, A. A. Zakhidov, W. A. D. Heer, *Science*, **2002**, 297, 787. d) Q. Zhao, Z. Gan, Q. Zhuang, *Electroanalysis* **2002**, 14, 1609. e) M. Terrones, *Annu. Rev. Mater. Res.* **2003**, 33, 419. f) P. M. Ajayan, *Chem. Rev.* **1999**, 99, 1787.

19. a) J.N. Wohlstadter, J. L. Wilbur, G. B. Sigal, H. A. Biebuyck, et al, *Adv. Mater.* **2003**, 15, 1184. b) J. Wang, M. Musameh, Y. Lin, *J. Am. Chem. Soc.*, **2003**, 125, 2408. c) J. Wang, G. Liu, M. R. Jan, *J. Am. Chem. Soc.*, **2004**, 126, 3010. d) H. Hu, Y. Ni, V. Montana, R. C. Haddon, and V. Parpura, *Nano Lett.* **2004**, 4, 507.

20. a) M. Hughes, G. Z. Chen, M. S. P. Schaffer, D. J. Fray and A. H. Windle, *Chem. Mater.* **2002**, 14, 1610. b) K. H. An, S. Y. Jeong, H. R. Hwang, Y. H. Lee, *Adv. Mater.* **2004**, 16, 1005. c) E. Kymakis, G. A. J. Amaratunga, *Appl. Phys. Lett.* **2002**, 80, 112. d) H. S. Woo, R. Czerw, S. Webster, D. L. Carroll, J. W. Park, J. H. Lee, *Synth. Met.* **2001**, 116, 369. e) I. Musa, M. Baxendale, G. A. J. Amaratunga, W. Eccleston, *Synth. Met.* **1999**, 102, 1250. f) J. N. Coleman, S. Curran, A. B. Dalton, A. P. Davey, B. McCarthy, W. Blau, R. C. Barklie, *Synth. Met.* **1999**, 102, 1174.

21. a) H. Zengin, W. Zhou, J. Jin, R. Czerw, D. W. Smith, Jr, L. Echegoyen, D. L. Carroll, S. H. Foulger and J. Ballato, *Adv. Mater.* **2002**, 14, 1480. b) M. Cochet, W. K. Maser, A. M. Benito, M. A. Callejas, M. T. Martinez, J-M. Benoit, J. Schreiber and O. Chauvet, *Chem. Commun.* **2001**, 1450. c) M. Gao, S. Huang, L Dai, G. Wallace, R. Gao, and Z. Wang, *Angew. Chem. Int. Ed.* **2000**, 39, 3664. d). Z. Wei, M. Wan, T. Lin and L. Dai, *Adv. Mater.* **2003**, 15, 136. e) P. C. Ramamurthy, W. R. Harrell, R. V. Gregory, B. Sadanadan, A. M. Rao, *Synth. Met.* **2003**, 137, 1497. f) I. A. Tchmutin, A. T. Ponomarenko, E. P. Krinichnaya, G. I. Kozub, O. N. Efimov, *Carbon*, **2003**, 41, 1391. g) J. Deng, X. Ding, W. Zhang, Y. Peng, J. Wang, X. Long, Pei Li, A. S. C. Chan, *Eur. Polym. J.* **2002**, 38, 2497. h) J-E Huang, X-H Li, J-C. Xu, H-L. Li, *Carbon*, **2003**, 41, 2731.

22. M. Lefenfeld, G. Blanchet and J. A. Rogers, *Adv. Mater.* **2003**, 15, 1188.

23. a) A. A. Mamedov, N. A. Kotov, M. Prato, D. M. Guldi, J. P. Wicksted, A. Hirsch, *Nat. Mater.* **2002**, *1*, 190. b) M. Olek, J. Ostrander, S. Jurga, H. Möhwald, N. Kotov, K. Kempa, M. Giersig, *Nano Lett.* **2004**, *4*, 1889. c) J. H.

Rouse, P. T. Lillehei, *Nano Lett.* **2003**, *3*, 59. d) M. Zhang, Y. Yan, K. Gong, L. Mao, Z. Guo, Y. Chen, *Langmuir* **2004**, *20*, 8781.

24. a) J. Moiroux, P. J. J. Elving, *Anal. Chem.* **1978**, 50, 1056. b) H. Jaegfeldt, *J. Electroanal. Chem.* **1980**, 110, 295.

25. M. Musameh, J. Wang, A. Merkoci, Y. Lin, *Electrochem. Commun.* **2002**, 4, 743.

26. J. Chen, J. C. Bao, C. X. Cai, T. H. Lu, *Anal. Chim. Acta* **2004**, 516, 29.

Chapter 5

DNA Hybridization Detection Based on Polyaniline

Multilayer Films

5.1 Motivation

The detection of specific base sequences in human, viral and bacterial nucleic acids is becoming increasingly important in the diagnosis of diseases. DNA hybridisation based on the Watson-Crick base-pair recognition is among the most often used methods for genetic diagnosis. Over the past years, great advances have been made in designing fast, easy-to-use and inexpensive DNA biosensors in different formats, based on electrochemical,[1] optical [2-4] or microgravimetric [5] techniques. In particular, electrochemical techniques have drawn greatest interest due to their high sensitivity, low cost and compatibility with microfabrication technologies. In addition, they offer a unique route for electrical control of DNA hybridisation and for the use of specific DNA interactions to induce electrical signals.[1c]

When designing an electrochemical DNA sensor, a key factor that has to be taken into consideration is to achieve an efficient interface between the nucleic acid system and the electrode surface and to prevent non-specific interactions at the electrode surface which can obscure the hybridisation signals.[1] Conducting polymers, which have been shown to be particular attractive in designing chemo- and biosensors,[6] were also found to be particularly suitable for blocking and interfacing the transducer, for modulating DNA interactions at interfaces, and for inducing electrical signals derived from such interactions.[1d] Until now, applications in this aspect have been reported for many conducting polymers, such as polypyrrole, polythiophene and their derivatives.[7,8] However, as one of the most important conducting polymers, polyaniline (PANI) has not been applied to such kind of purpose. One main reason may be that, as mentioned before, PANI is only redox-active in acidic conditions, whereas DNA detection can only be performed in a neutral pH environment.

We demonstrated in the previous chapter that PANI multilayer films were very stable and showed good redox-activity in a neutral pH environment. In this Chapter,

detection of DNA hybridization based on PANI/MSAG$_{NP}$ multilayer film was demonstrated. Firstly, amino-terminated DNA catcher probes (NH$_2$-DNA) were covalently attached to the carboxyl groups of the MSAG$_{NP,}$ and then their hybridization with different DNA target strands was monitored (the sequences of both DNA probe and targets can be found in Chapter 2), using electrochemical methods (with and without enzyme amplification) and the surface plasmon enhanced fluorescence spectroscopy (SPFS).[9] All methods can effectively discriminate complementary DNA from non-complementary DNA, even at a single-base mismatch level. To our best knowledge, this is the first report of DNA hybridization detection based on PANI films.

5.2 Covalent Attachment of NH$_2$-DNA to PANI/MSAG$_{NP}$ Multilayer Film

The details about the covalent attachment of the amino-terminated DNA catcher probes NH$_2$-DNA to the carboxyl groups of the MSAG$_{NP}$ can be found in Chapter 2, see also the scheme in Fig.5-1. The whole attachment process was monitored in situ
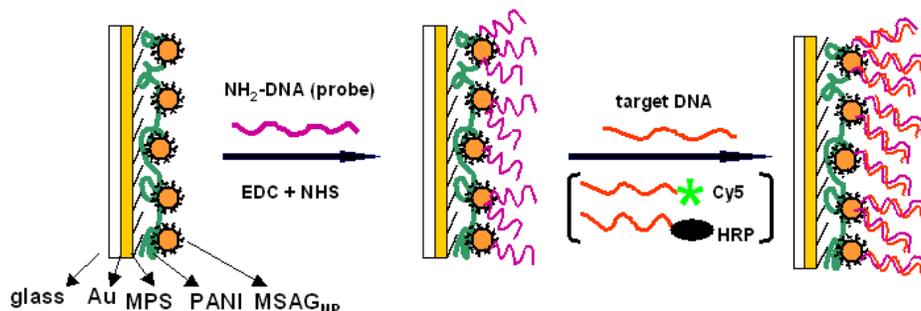
Fig.5-1 *Scheme showing the attachment of NH$_2$-DNA probes to PANI/MSAG$_{NP}$ film and their following hybridization with target DNA either unlabeled or labeled with a Cy5 dye or a horseradish peroxidase (HRP).*

by SPR and by cyclic voltammetry, as shown in Figure 5-2. From the SPR measurements, we can see that the reflectivity increases a little after the attachment of NH$_2$-DNA to the PANI/MSAG$_{NP}$ film (A). The minimum resonance angle also shifts a little after the attachment (B), clearly indicating that DNA probes was successfully linked to the PANI/MSAG$_{NP}$ surface. Cyclic voltammetry measurements (C) showed that after the linking of NH$_2$-DNA to the PANI/MSAG$_{NP}$ film, the redox activity of

PANI/MSAG$_{NP}$ film decreased significantly, while at the same time the peak-to-peak separation increased. This may be caused by the steric effect and possible conformational changes of the polymer backbone induced by the attachment of DNA probes to the PANI/MSAG$_{NP}$ surface. However, the redox activity of PANI/MSAG$_{NP}$/NH-DNA is still good enough to be used for the detection of the following hybridization event, as will be demonstrated in the later parts.
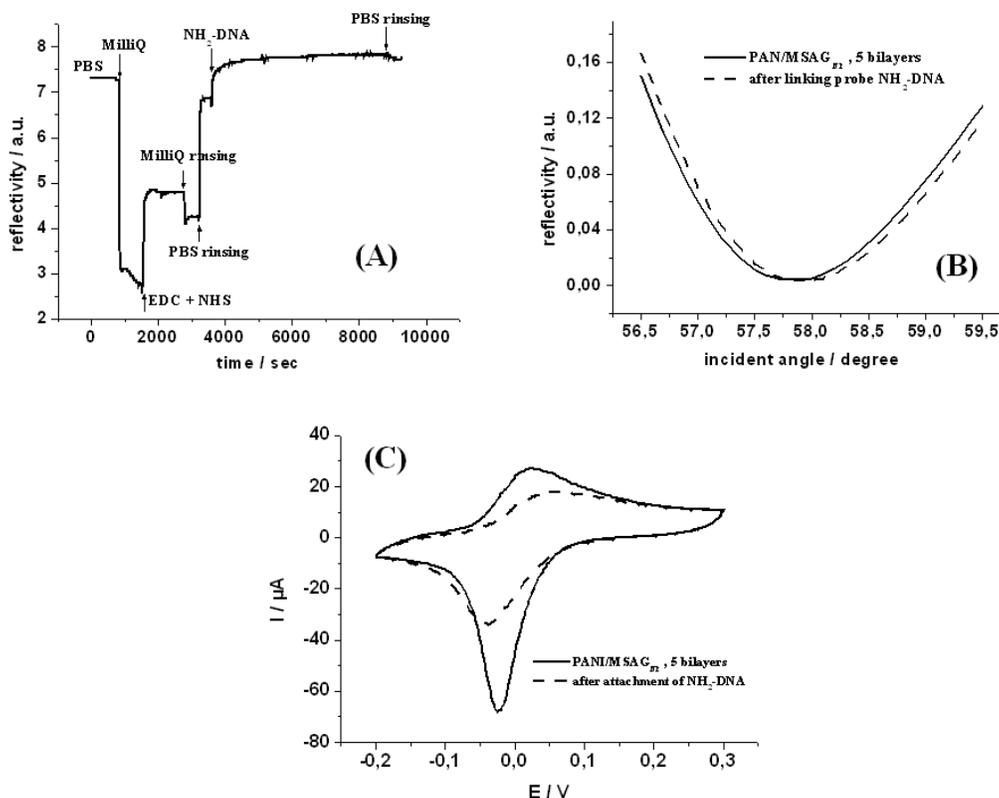
Fig.5-2 *(A) In situ SPR kinetic measurement during the attachment of NH2-DNA to PANI/MSAG$_{NP}$ film. (B) SPR angular scan and (C) Cyclic voltammograms before and after the attachment of NH2-DNA to PANI/MSAG$_{NP}$ film measured in 0.1M PBS buffer, pH 7.1.*

5.3 DNA Hybridization Detection Based on PANI/MSAG$_{NP}$/NH-DNA

5.3.1 Direct electrochemical detection

Figure 5-3 (A) shows the cyclic voltammograms of NH$_2$-DNA modified PANI/MSAG$_{NP}$ multilayer films (5 bilayers) before and after the hybridization with different DNA targets. The electrochemical signal remains almost unchanged after incubation with the completely non-complementary target DNA (same sequence as

the probe DNA, MM15, 500nM) for 1 hour (curve b). This means that no interaction occurred between the probe DNA and the non-complementary target DNA. However, hybridization with perfectly complementary target DNA (MM0) under the same conditions induces both a decrease in the peak current and a wider peak-to-peak separation (curve d). These changes were caused by the different doping levels and steric effects induced by the hybridization process. Possible conformational changes inside the film may also play a role. Similar effects were also observed in other functionalized conducting polymers.[7a,7b] The electrochemical signal change is smaller
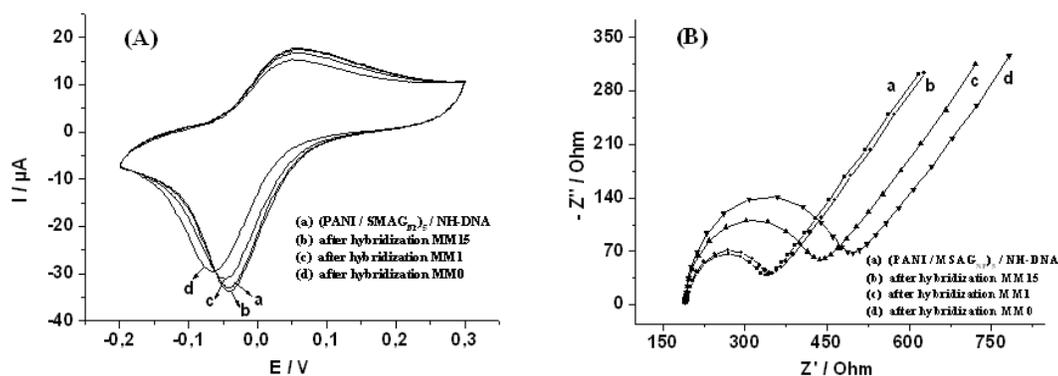
Fig.5-3 (A) Cyclic voltammograms and (B) Electrochemical impedance spectra of NH_2-DNA modified PANI/MSAG$_{NP}$ multilayer films (5 bilayers) before and after hybridization with different target DNA measured in 0.1M PBS buffer. The concentration for all DNA targets is 500nM, and the hybridization time is 1 hour. CV scan rate: 50mV/s. For the EIS measurements, 1mM/1mM $Fe(CN)_6^{3-/4-}$ was added as a redox indicator.

if one-base-mismatched target DNA (MM1) was used for the hybridization process (curve c), indicating the feasibility for the detection of a single-base mismatch.

The hybridization process can also be detected by electrochemical impedance spectroscopy (EIS) in the presence of a redox indicator, such as $Fe(CN)_6^{3-/4-}$. Once the target DNA is hybridized with the probe DNA on the PANI/MSAG$_{NP}$ film, the surface charge density of the film will increase, which will result in an increased electrostatic repulsion toward the negatively charged redox couple $Fe(CN)_6^{3-/4-}$, thus increasing the charge transfer resistance (R_{ct}, the diameter of the semicircle in the Nyquist plot, cf. Fig.5-3(B)). Shown in Fig.5-3(B) are the EIS spectra (Nyquist plots) of the NH_2-DNA functionalized PANI/MSAG$_{NP}$ film before and after hybridization with DNA targets of different sequences. If the MM15 target DNA was used, a very small R_{ct} change (if any) was detected (curve b), indicating that no hybridization

occurred, with almost no non-specific adsorption of target DNA onto the film. However, if MM0 was added, R_{ct} increases significantly (curve d), showing that the target DNA hybridized with the probe DNA. This method can also differentiate a single-base mismatch, as it is demonstrated by curve (c).

5.3.2 Enzyme-amplified electrochemical detection

Although it is feasible to directly detect the hybridization event on PANI/MSAG$_{NP}$/NH-DNA film (vide supra), the signal differences between different DNA targets are not so significant. To increase the sensitivity and the detection limit, enzymes are often used as biocatalysts for the amplified detection of DNA by labeling enzymes either to the target DNA or to the detection probe DNA in a sandwich format.[10,11] Different enzymes have been used for DNA labeling with electrochemical transduction of hybridization event, such as horseradish peroxidase (HRP),[11b,11c] glucose oxidase (GOx),[11d,11f] soybean peroxidase (SBP),[10b] bilirubin oxidase (BOD),[12] alkaline phospatase,[13] β-galactosidase,[14] glucose dehydrogenase,[15] etc.

Hereby we also adopt this method to enhance the sensitivity and selectivity of our system, by labeling the DNA targets used above with HRP enzyme (c.f. Fig.5-4(A)). If the hybridization event occurs, the HRP labels get electrically contacted with the Au electrode via the PANI/MSAG$_{NP}$ film, then the whole film becomes an electrocatalyst for the reduction of H_2O_2 to H_2O through the cycle shown in Figure 5-4 (B), thus the hybridization event is translated into the current of H_2O_2 electroreduction.
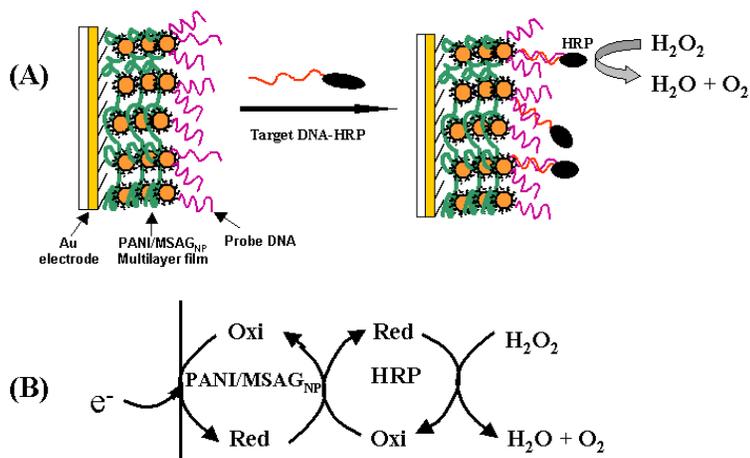
Fig.5-4 *Schematic diagrams of the detection mechanism (A) and the corresponding electron transfer in the electrocatalytic redox cycle (B).*

It has been demonstrated previously that the catalytic efficiency of the enzyme is closely associated with the concentration of H_2O_2 used in the assays. Too high a H_2O_2 concentration will denature the enzyme immediately.[11b,11d,16] So firstly, the H_2O_2 concentration that is allowed in the present system was optimized. Figure5-5 shows the dependence of the electrocatalytic response on the concentration of H_2O_2 used in the assays. After the hybridization of the HRP labeled fully complementary target DNA (MM0) with the electrode-bound probe DNA for about 30 min, the electrode
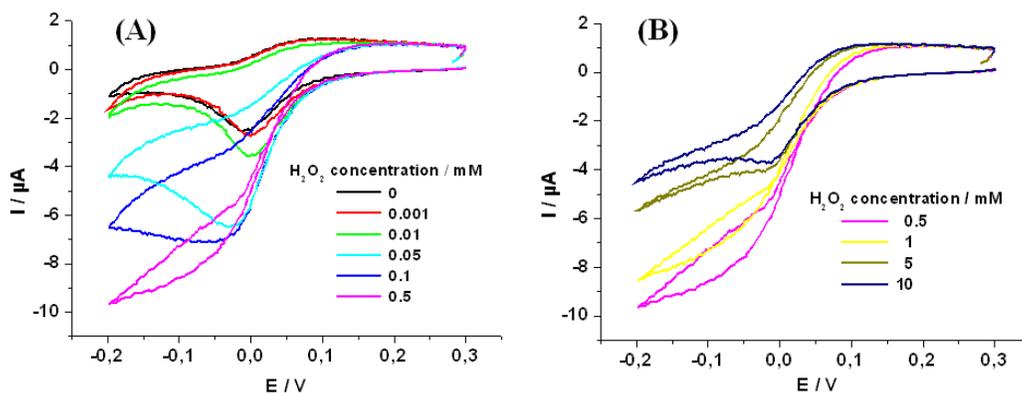
Fig.5-5 *Dependence of the electrocatalytic response on the H_2O_2 concentration. Experimental conditions: Au/(PANI/MSAG$_{NP}$)3/NH-DNA/DNA-HRP(MM0). H_2O_2 was dissolved in 0.1M PBS buffer, pH 7.1. Scan rate 5 mV/s.*

was rinsed thoroughly with PBS buffer, and then measured in PBS buffer with different amount of H_2O_2. Clearly, at lower H_2O_2 concentrations, the electrocatalytic reduction peak current increases with the increase of H_2O_2 concentration (c.f. Fig.5-5(A)). However, if the H_2O_2 concentration is too high (above 0.5 mM), then the peak current decreases with the increase of H_2O_2 concentration (c.f. Fig.5-5(B)). So in our later experiments, 0.5 mM H_2O_2 was used in all cases.

Figure 5-6 (A) shows the cyclic voltammograms of Au/(PANI/MSAG$_{NP}$)3/NH-DNA electrode before and after hybridization with different HRP-labeled DNA targets with different sequences for 30 min, and then measured in 0.1M PBS buffer with 0.5 mM H_2O_2. For the complementary HRP-labeled target DNA (MM0), a sharp increase in the reduction peak current was observed upon adding H_2O_2, indicating the DNA targets hybridized with the surface-bound DNA probes. However, if the noncomplementary HRP-labeled target DNA (MM15) was used instead of MM0, the change in the reduction peak current was almost negligible upon adding H_2O_2. This

84

means that no hybridization event occurred. And it also further confirmed that there was no non-specific adsorption on our sensing surface. Compared to the unlabeled case (c.f. Fig.5-3(A)), the signal-to-noise ratio (i.e.the sensitivity) was greatly enhanced by the enzyme-amplification. In addition, with enzyme-amplification, the single-base mismatched case can also be differentiated very easily, as also shown in Figure 5-6 (A).

The enhanced sensitivity by enzyme-amplification also allowed us to do the titration experiment, as shown in Figure 5-6 (B) for the complementary HRP-labeled target DNA (MM0). It can be seen that the electrocatalytic reduction signal increases with the increase of target DNA concentration. With enzyme-amplification, the catalytic signal for target concentration down to 1 nM can still be detected by the simple cyclic voltammetry method.
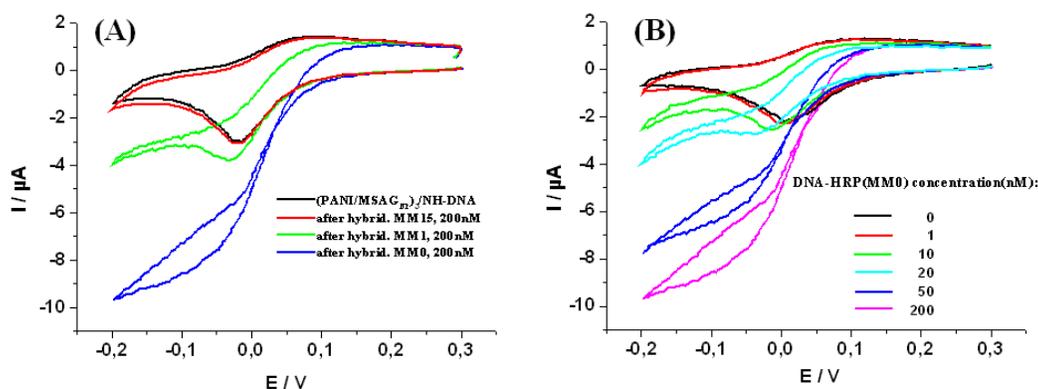
Fig.5-6 *(A) Voltammetric response changes of Au/(PANI/MSAG$_{NP}$)3/NH-DNA electrode upon adding 0.5mM H$_2$O$_2$ after hybridization with (A) DNA targets with different sequences (target concentration 200 nM); (B) full complementary target DNA (MM0) with different concentrations. Scan rate, 5mV/s.*

5.3.3 Surface plasmon enhanced fluorescence spectroscopy (SPFS) detection

SPFS is a novel technique recently developed by our group offering an increased sensitivity for monitoring interfacial binding events in biosensor formats.[9,17] Here we also apply this technique to confirm the hybridization process on the NH$_2$-DNA modified PANI/MSAG$_{NP}$ film. The sequences of the DNA targets are the same as those used in the EC experiments, but labeled with a Cy5 dye at their 5' ends. Fig.5-7 shows the in situ kinetic measurement during the hybridization process and the corresponding angular scans after hybridization. It can be seen that the hybridization

reactions for different mismatch situations, MM0, MM1 and MM2, respectively, can be clearly discriminated. For MM2, the fluorescence signal is almost gone after a short rinse, indicating that no hybridization and no non-specific binding occurred. However, for the MM1 case, there is still some signal left after rinsing, showing that some of the target DNA strands bind to the catcher probe strands. If MM0 is further added, the fluorescence intensity increases further after rinsing, which means that more target DNA strands hybridized with the probe DNA strands. In addition, regeneration experiments show that the NH_2-DNA modified PANI/MSAG$_{NP}$ film can be regenerated and used repeatedly (Fig.5-8). After regeneration with 50mM HCl, the
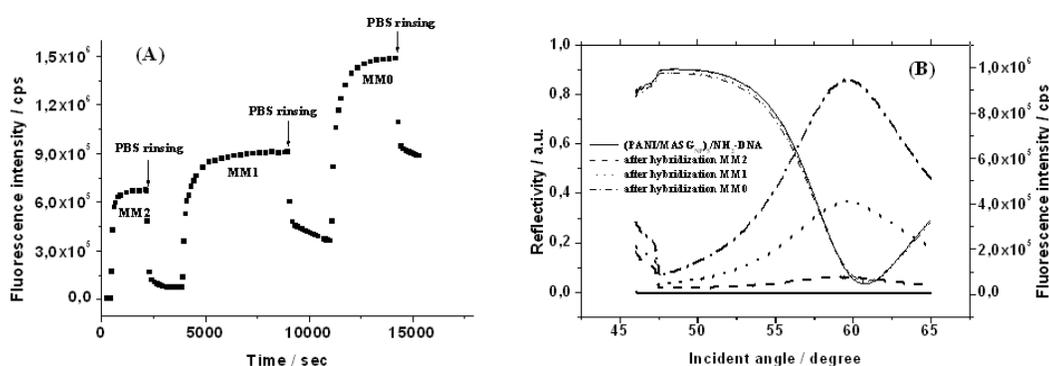
Fig.5-7 *Fluorescence kinetic curves during the hybridization process (A) and the corresponding angular scan curves after hybridization (B) for different DNA targets with different base mismatches. The concentration for all DNA targets is 200 nM.*
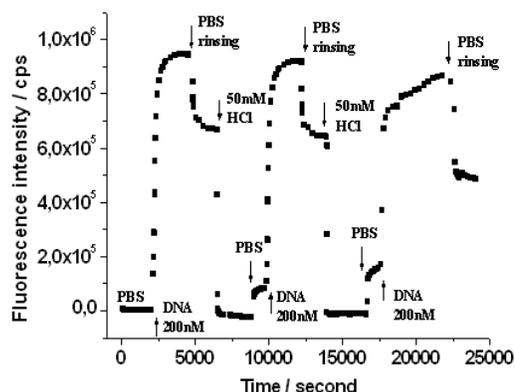
Fig. 5-8 *Regeneration experiment for MM0 using 50mM HCl. DNA concentration 200nM.*

hybridization was again observed with MM0 targets (200nM), with the SPFS signal reaching its original level.

By SPFS, we can also get the corresponding affinity constant, K_A, by carrying out titration measurement. Shown in Fig.5-9 (A) and (B) are a series of angular fluorescence intensity scans taken after the addition and binding of DNA targets with increasing concentrations for MM0 and MM1, respectively. In both cases, the fluorescence intensity increases with the increase of the concentration of DNA target and finally reaches an equilibrium level (c.f. Fig.5-9 (C) and (D)). If we assume that the hybridization process follows a Langmuir behavior (c.f. Fig.5-9 (C) and (D), solid lines), the fits to the experimental data then yield affinity constants $K_{A0} = 5.4 \times 10^7$ M^{-1} and $K_{A1} = 1.03 \times 10^7$ M^{-1} for MM0 and MM1, respectively.
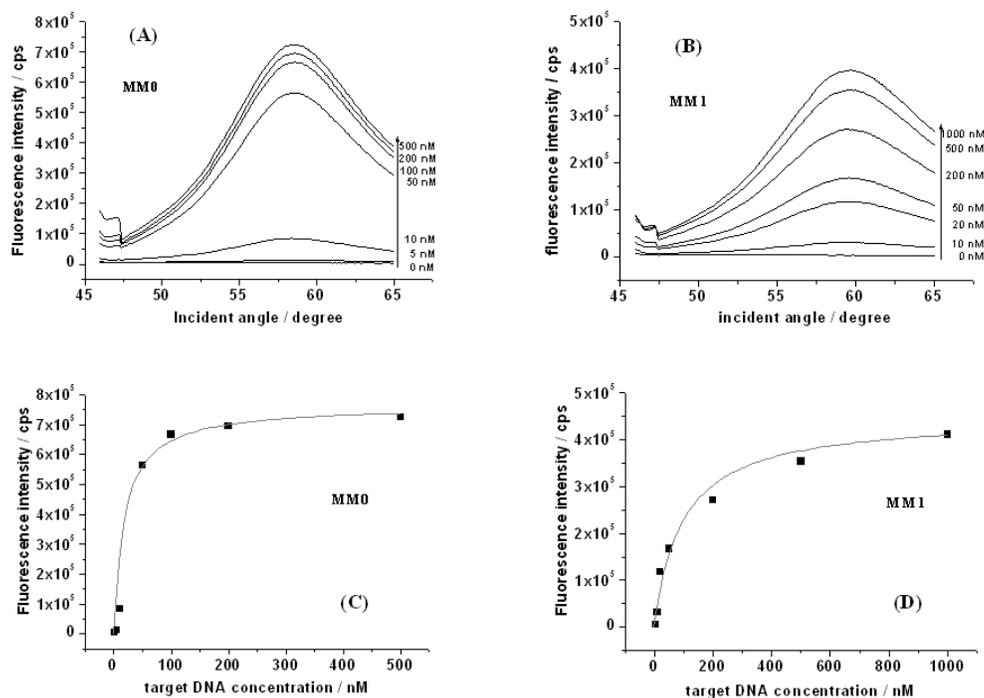
Fig.5-9 _Fluorescence intensity scans measured in equilibrium with increasing bulk target concentrations for MM0 (A) and MM1 (B), respectively. (C) and (D) are the corresponding theoretical fit (line) to the experimental data (solid square) based on the Langmuir isotherm model._

5.4 Conclusions

Amino-terminated DNA probes were successfully linked to the surface of the prepared PANI/MSAG$_{NP}$ multilayer film by the formation of an amide bond in the presence of EDC and NHS. The obtained sensing surface is resistant to the non-specific adsorption, and can be regenerated for repeated use. Hybridization detection could be realized by different schemes, such as direct electrochemical detection, enzyme-amplified electrochemical detection, or detection based on SPFS technique. All methods can effectively discriminate complementary from non-complementary DNA sequences, even at the single-base mismatch level.

5.5 References

1. See recent reviews: a) S. R. Mikkelsen, _Electroanalysis_ **1996**, _8_, 15. b) H. H. Thorp, _Trends Biotechnol._ **1998**, _16_, 117. c) J. Wang, _Chem. Eur. J._ **1999**, _5_, 1681. d) E. Palecek, M. Fojta, _Anal. Chem._ **2001**, _73_, 74A.

2. a) D. Piscevic, R. Lawall, M. Veith, M. Liley, Y. Okahata, W. Knoll, _Appl. Surf. Sci._ **1995**, _90_, 425. b) T. Liebermann, W. Knoll, P. Sluka, R. Hermann, _Colloids and surfaces: A_. **2000**, _169_, 337. c) T. Neumann, M.-L. Johansson, D. Kambhampati, W. Knoll, _Adv. Funct. Mater._ **2002**, _12_, 575. d) K. A. Peterlinz, R. Georgiadis, T, M. Herne, M. J. Tarlov, _J. Am. Chem. Soc._ **1997**, _119_, 3401.

3. a) P. A. F. Piuuno, U. J. Krull, R. H. E. Hodson, M. J. Damha, H. Cohen, _Anal. Chem._ **1995**, _67_, 2635. b) K. Dore, S. Dubus, H.-A. Ho, I. Levesque, M. Brunette, G. Corbeil, M. Boissinot, G. Boivin, M. G. Bergeron, D. Boudreau, M. Leclerc, _J. Am. Chem. Soc._ **2004**, _126_, 4240. c) K. P. R. Nilsson, O. Inganäs, _Nat. Mater._ **2003**, _2_, 419. d) R. Jenison, S. Yang, A. Haeberli, B. Polisky, _Nat. Biotechnol._ **2001**, _19_, 62

4. a) A. J. Thiel, A. G. Frutos, C. E. Jordan, R. M. Corn, L. M. Smith, _Anal. Chem._ **1997**, _69_, 4948. (b) H. J. Lee, T. T. Goodrich, R. M. Corn, _Anal. Chem._ **2001**, _73_, 5525.

5. a) F. Caruso, E. Rodda, D. N. Furlong, K. Niikura, Y. Okahara, *Anal. Chem.* **1997**, *69*, 2043. b) A. Bardea, A. Dagan, I. Ben-Dov, B. Amit, I. Willner, *Chem. Commun.* **1998**, 839. c) F. Patolsky, A. Lichtenstein, I. Willner, *J. Am. Chem. Soc.* **2000**, *122*, 418. d) C. Larsson, M. Rodahl, F. Höök, *Anal. Chem.* **2003**, *75*, 5080.

6. a) P. N. Bartlett, J. M. Cooper, *J. Electroanal. Chem.* **1993**, *362*, 1. b) G. G. Wallace, M. Smyth, H. Zhao, *Trends in Anal. Chem.* **1999**, *18*, 245. c) S. Cosnier, *Biosen. Bioelectron*., **1999**, *14*, 443. d) J. Bobacka, A. Ivaska, A. Lewenstam, *Electroanalysis*, **2003**, *15*, 366.

7. a) H. Korri-Youssoufi, F. Garnier, P. Srivastava, P. Godillot and A. Yassar, *J. Am. Chem. Soc.*, **1997**, *119*, 7388. b) F. Garnier, H. Korri-Youssoufi, P. Srivastava, B. Mandrand, T. Delair, *Synth. Met.*, **1999**, *100*, 89. c) J. Wang, M. Jiang, A. Fortes, B. Mukherjee, *Anal. Chim. Acta,* **1999**, *402*, 7.

8. a) P. Bäuerle, A. Emge, *Adv. Mater.* **1998**, *10*, 324. b) T.-Y. Lee and Y.-B. Shim, *Anal. Chem.*, **2001**, *73*, 5629. c) L. A. Thompson, J. Kowalik, M. Josowicz and J. Janata, *J. Am. Chem. Soc.*, **2003**, *125*, 324.

9. a) T. Neumann, M.L. Johansson, D. Kambhampati, W. Knoll, *Adv. Funct. Mater.* **2002**, *12*, 575. b) F. Yu, D. F. Yao, W. Knoll, *Anal. Chem.* **2003,** *75*, 2610.

10. a) T. de Lumley-Woodyear, C. N. Campbell, A. Heller. *J. Am. Chem. Soc.* **1996**, *118*, 5504. b) D. J. Caruana, A. Heller. *J. Am. Chem. Soc.* **1999**, *121*, 769.

11. a) C. N. Campbell, D. Gal, N. Cristler, C. Banditrat, A. Heller, *Anal. Chem.* **2002**, *74*, 158. b) M. Dequaire, A. Heller, *Anal. Chem.* **2002**, *74*, 4370. c) L. Alfonta, A. K. Singh, I. Willner, *Anal. Chem.* **2001**, *73*, 91. d) H. Xie, C. Zhang, Z. Gao, *Anal. Chem.* **2004**, *76*, 1611. e) V. Pavlov, Y. Xiao, R. Gill, A. Dishon, M. Kotler, I. Willner, *Anal. Chem.* **2004**, *76*, 2152. f) E. Dominguez, O. Rincon, A. Narvaez, *Anal. Chem.* **2004**, *76*, 3132.

12. Y. Zhang, A. Pothukuchy, W. Shin, Y. Kim, A. Heller, *Anal. Chem.* **2004**, *76*, 4093.

13. a) Z. P. Aguilar, I. Fritsch, *Anal. Chem.* **2003**, *75*, 3890. b) F. Patolsky, A. Lichtenstein, I. Willner, *Chem.- Eur. J.* **2003**, *9*, 1137.

14. J. Wang, A. N. Kawde, M. Musameh, G. Rivas, *Analyst* **2002**, *127*, 1279.

15. K. Ikebukuro, Y. Kohiki, K. Sode, *Biosens. Bioelectron.* **2002**, *17*, 1075.

16. a) Y. Zhang, H.-H. Kim, N. Mano, M. Dequaire, A. Heller, *Anal. Bioanal. Chem.* **2002**, *374*, 1050. b) Y. Zhang, H.-H. Kim, A. Heller, *Anal. Chem.* **2003**, *75*, 3264.

17. a) Liebermann, T.; Knoll, W., *Colloids Surf. A* **2000**, *171*, 115. b) Liebermann, T.; Knoll, W.; Sluka, P.; Herrmann, R., *Colloids Surf. A* **2000**, *169*, 337

Chapter 6

Patterned Polyaniline Films and Their Sensing Applications

6.1 Introduction

Patterning has becoming more and more important in many areas of modern science and technology, with applications ranging from the production of integrated circuits, information storage devices, and display units, to the fabrication of microelectromechanical systems, miniaturized sensors, microfluidic devices, biochips, photonic bandgap crystals, micro-optical components, diffractive optical elements, and so on[1-2] The patterning process is usually termed "lithography". The different patterning techniques that have been reported can be divided into the following several categories: (1) photo lithography;[3] (2) writing based lithography, such as micromachining,[4] electron-beam (e-beam) lithography,[5] focused ion beams (FIBs) lithography,[6] lithography based on near-field scanning optical microscopy (NSOM),[7] electrical writing,[8] magnetic writing,[9] and the so-called add-on writing (like laser-induced chemical vapor deposition (LCVD),[10] injekt printing (IJP),[11] and dip-pen nanolithography (DPN)[12]); (3) self-assembly, this includes i) the molecular level self-assembly,[13] such as the formation of SAMs, crystals, lipid bilayers, phase-separated block copolymers, etc.; ii) the assembly of nanoscale objects (such as colloidal particles, nanowires, nanotubes, etc.) into ordered arrays or lattices, like nanosphere lithography;[14] iii) the assembly of objects with meso- to macroscale dimensions;[15] (4) mask etching or deposition;[16] (5) soft lithography;[17] (6) edge lithography;[18] (7) holographic patterning;[19] (8) gray-scale lithography;[20] and (9) the derived combination of the above mentioned patterning techniques.

Among the above mentioned patterning methods, soft lithography based techniques pioneered by Whitesides' group has recently attracted great interest due to their simplicity, versatility and cost-efficiency. These techniques rely on the use of an elastomer, usually poly(dimethylsiloxane) (PDMS), either as a mask , mold or stamp, to generate or transfer the pattern. They can be applied for both flat and curved surfaces over a large area. The reported soft lithographic techniques include replica

molding (RM),[21] microtransfer molding (μTM),[22] solvent-assisted micromolding (SAMIM),[23] micromolding in capillaries (MIMIC),[24] microcontact printing (μCP),[25] and microfluidic networks (μFNs),[26] and so on. The combination of these techniques with other techniques, like electrochemistry,[27] layer-by-layer (LBL) self assembly technique,[28] etc., has also been reported, which makes their application more variable.

Along with the evolution of the patterning techniques, patterning of polymers have been drawing great attention due to their promising application as components in molecular electronics,[29] optical devices,[30] etch resists,[31] biosensors,[32] and even as scaffolds for tissue engineering and for fundamental studies in cell biology[33-34]. Among the polymers studied, conjugated organic polymers are especially attractive because of their intriguing advantages compared to metals and conventional inorganic semiconductors, such as relatively more facile processing and ease of adjusting their conductivity in a wide range by just changing the dopant and/or the doping level. They are being evaluated as potential alternatives to metals or semiconductors as connecting wires and conductive channels, which can be used as active materials in optoelectronics,[35] microelectronics,[36] microelectromechanical systems (MEMS),[37] sensors,[38] and related areas.[39]

Until now, many well-patterned conjugated conducting polymers have been successfully demonstrated on various substrates (e.g. glass, silicon, ITO, Au, etc.) by using a variety of patterning techniques described above. These include: polyaniline (PANI) and its derivatives,[27b,40] polypyrrole (PPy),[27a, 40b-d, 41] polythiophene and its derivatives,[42] and others.[43] Some of the obtained patterned polymers have found practical applications, such as for fabricating polymer dispersed liquid crystal displays (PDLCD),[40d] as all-polymer circuit (board),[27a,40e,42d] high-performance organic transistors,[42d] organic light-emitting diodes (OLED),[42e] optical diffraction gratings,[27b,43a] and for immunoassays.[40g] However, most of the above reported examples dealt with only one pure conducting polymer, with only a few exceptions dealing with polymer composites, i.e. doped with some special dopants which in some case is a necessity for some special purposes or applications.[40e,40g, 41,42e]

In this chapter, well-patterned polyaniline (PANI) and its composites were successfully fabricated by the combination of several patterning techniques. Because the prepared PANI composites remain redox-active in neutral solution, their potential sensing applications (especially biosensing aspect) were also explored.

In the first part of this chapter, two approaches were used to fabricate parallel-line-shaped PANI composite films. One way is to combine electrocopolymerization with micromolding in capillaries (EP-MIMIC); the other one combines microcontact printing with the layer-by-layer technique (μCP-LBL). Both methods produce relatively nice patterns. Later, we demonstrated that these line-shaped PANI could be used as optical diffraction gratings based on the surface-plasmon-enhanced diffraction mode. Based on this, an electrotunable surface-plasmon-enhanced diffraction (ESPD) sensor was constructed. The diffraction efficiency (DE) of the sensor can be easily modulated by either changing the potential, or the pH, or by an electrocatalytic event.

In the second part of this chapter, inverse opals of PANI and its composites were fabricated by an electrochemical method by using ordered polystyrene (PS) colloidal assemblies as template. The quality of the obtained inverse opaline films was much higher than those reported by chemical synthesis methods. Because the prepared inverse opals possess a three-dimensional (3D) macroporous structure that comprises highly ordered air spheres interconnected to each other by small channels, they are promising candidates as photonic bandgap (PBG) crystals.[44] And also because of the huge surface area of such structures, the prepared PANI inverse opals are also ideal candidates as advanced adsorbents, catalysts and bioreactors. Our efforts here are mainly focused on their potential applications in the latter case.

6.2 Electrochemically Tunable Surface Plasmon Enhanced Diffraction Gratings and Their Sensing Applications

6.2.1 Background and motivation

During the past decade, optical diffraction gratings and diffraction-based optical assays have attracted great interest.[27b,43a,45-57] Diffraction occurs when light hits a periodically patterned surface due to a periodic variation of the contrast in the refractive index between the patterned lattice and the surrounding medium (normally air or water). Any event that induces a change in the refractive index contrast will result in a modulation in the diffracted light intensity, thus the change in the diffraction efficiency (DE).[58] Different materials have been used to fabricate the gratings, such as liquid crystals,[46-48] redox polymers,[27b,43a,49] microporous supramolecular coordination compounds,[50b] gelatin films containing a pH indicator,[52] biomolecules,[51-55, 57] and even condensed water drops (condensation figures, CFs).[45] The diffraction-based transduction mechanism has successfully been demonstrated in the sensing of environmental humidity,[45] pH,[52] volatile organic compounds,[50] aqueous phase metal ions,[50b] DNA hybridisation,[57b] proteins[51,55,57a,57c] and even whole cells.[53-54]

Among the above reported diffraction-based sensing schemes, most are based on the traditionally transmitted or reflected configurations. Our group once reported a surface-plasmon-enhanced diffraction (SPD) configuration.[56] In this scheme (c.f. Fig.6.2-5(A)), the light was coupled to surface plasmon modes through a prism, and a dielectric grating on the planar metal surface (normally Au or Ag) diffracted the nonradiative plasmon surface plariton (PSP) field into light radiation. The grating structure with a periodicity Λ provides an additional multiple of a small momentum g with $|g| = 2\pi/\Lambda$ and diffracts the surface plasmon field, generating a typical diffraction pattern. The DE of this SPD configuration was shown to be strongly enhanced as compared with that of the conventional diffraction schemes like the total internal reflection (TIR).[56a] Recently, this SPD scheme has been successfully used to construct biosensors for the label-free detection of protein and DNA hybridisation.[57]

Here, a redox-active polymer composite grating (e.g. PANI/PSS) was successfully prepared via soft lithography based patterning techniques and was investigated by the combination of electrochemistry with the above SPD scheme (ESPD). Pure PANI gratings based on the traditionally transmitted configuration and its chemo- and electrochemical response was once reported by Hupp's group.[27b] However, due to the inherent loss of redox activity of PANI in neutral solution,[59,60] such a pure PANI grating can not be used for biosensing purpose. It has been demonstrated that the redox activity of PANI can be shifted to a neutral environment by doping it with different polyanions (such as PSS, c.f. Chapter 4, section 4.2)[61-63] or modified gold nanoparticles (c.f. Chapter 4, section 4.3).[64] Hence, we use a PANI composite instead of pure PANI for the fabrication of the grating in order to probe its potential biosening applications. Using PANI/PSS composite grating as an example, we demonstrate that the DE of the obtained PANI/PSS grating based on the SPD mode can be electrochemically tuned in a neutral pH environment, which shows the possibility for bioassays. The DE is also very sensitive to environmental pH changes. The DE response to a pH change strongly depends on the redox state of PANI/PSS, and they show almost a linear relationship if the PANI/PSS composite is in its reduced state. Moreover, we demonstrate that PANI/PSS composite gratings can also be used to monitor an electrocatalytic event: by keeping PANI/PSS in its oxidised form, the DE can be modulated by adding β-nicotinamide adenine dinucleotide (NADH) due to the electrocatalytic oxidation of NADH by PANI, and the DE increases with the increase of the NADH concentration, which points to the possibility of the present system for developing ESPD-based biosensors.

6.2.2 Fabrication of PDMS stamp

The procedure for making PDMS stamps used here is shown in Figure 6.2-1(A), according to the method reported by Whitesides' group.[65] After liquid PDMS base and curing agent (Sylgard 184, Dow Corning) was mixed in a 10:1 weight ratio and thoroughly degassed, the mixture was cast onto a silicon master, and then cured for 2 hours at 70 °C. Before use, the PDMS was removed from the master. Using this method, three stripe-type PDMS stamps were fabricated, and their features and periodicity are shown in Figure 6.2-1 (B).
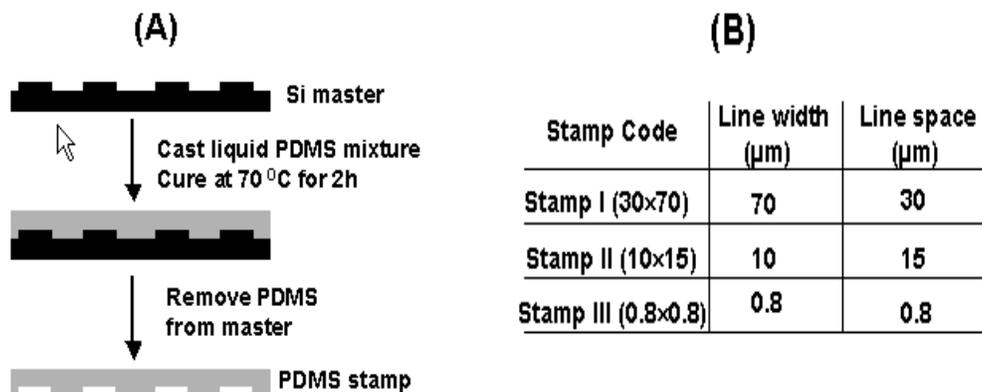
Fig.6.2-1 *(A) Schematic of the procedure used for fabricating PDMS stamps. (B) The features of the three stamps prepared and used in the present work.*

6.2.3 Fabrication of PANI composite polymer gratings

The well-defined PANI composite films used here were fabricated via two different approaches, as shown in Figure 6.2-2.

Method I --- EP-MIMIC This method combines electropolymerisation with micromolding in capillaries (EP-MIMIC). In brief, a freshly prepared PDMS stamp
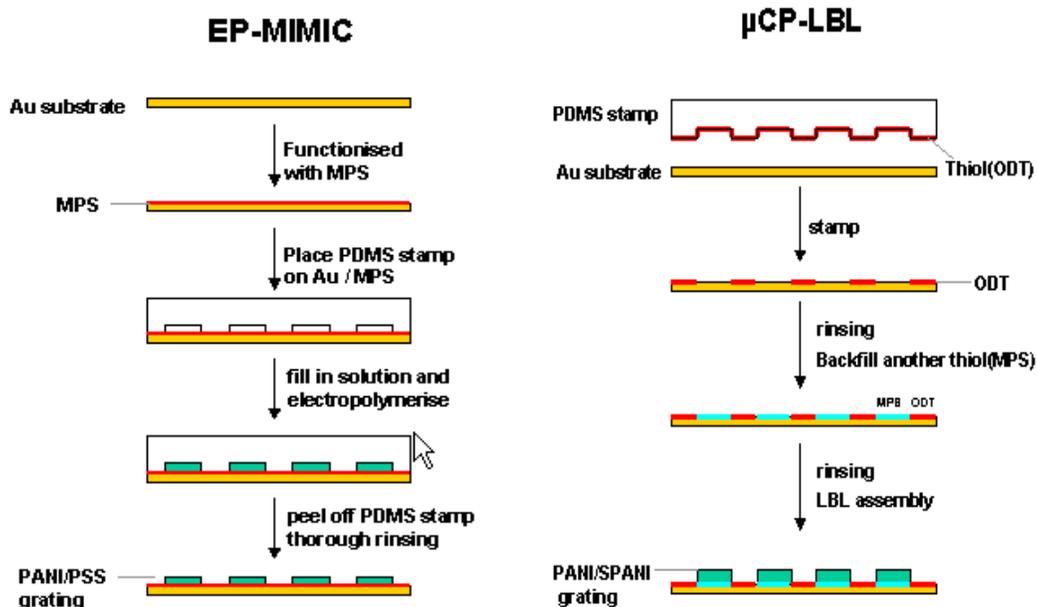
Fig.6.2-2 *Schematic illustration of the two methods used to fabricate PANI composite polymer gratings. The first method combines electropolymerisation with micromolding in capillaries (EP-MIMIC), while the second is the combination of microcontact printing with the layer-by-layer self-assembly technique (μCP-LBL).*

96

was placed on an Au substrate to form many micro-channels. To facilitate the following filling by the polymer solution, the Au substrate was previously functionalised with a layer of a hydrophilic thiol, 3-mercapto-1-propanesulfonic acid (MPS). After filling in the polymer solution (0.02M Aniline in 0.5M H_2SO_4 with 0.01M PSS) by capillary force and carrying out electropolymerisation, the PDMS stamp was carefully peeled off, and well-shaped PANI/PSS gratings were obtained (c.f. Fig.6.2-3). The grating was rinsed carefully first with 0.5M H_2SO_4, followed by 0.1M PBS buffer (pH7.2), and then used for the diffraction measurements.

The optical and AFM height images of some typical examples prepared via this method are shown in Figure 6.2-3. (A) to (C) are optical and AFM images of a polymer grating made from Stamp II (10 × 15) by applying 6 cycles of potential scanning between –0.2V and 0.9V at a scan rate of 20mV/s, while (D) to (F) were made from Stamp I (30 × 70) by applying 15 cycles of potential scanning under the same conditions. The optical images reveal a highly periodic polymer structure over a
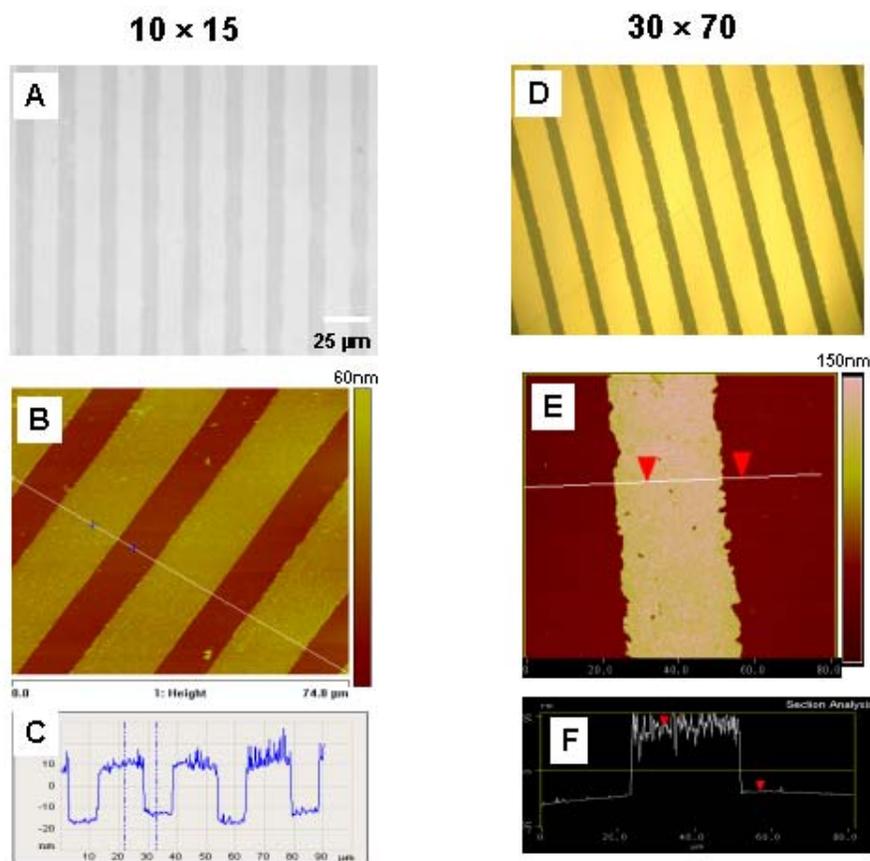
Fig.6.2-3 *Optical and AFM images of two examples fabricated via the EP-MIMIC method from Stamp II (10×15, A to C) and Stamp I (30×70, D to F), respectively. Electropolymerisation conditions: 0.02M Aniline in 0.5M H_2SO_4 with 0.01M PSS, CV scan rate 20mV/s, 6 cycles for sample (A), 15 cycles for sample (D).*

large area (sample up to 1cm × 1cm was successfully fabricated with only a few defects). Further AFM measurements confirmed the well-shaped micropatterns, which are exactly the reverse replica of the used PDMS stamps, with an average thickness of 25nm and 110nm for sample (A) and (D) respectively (c.f. section analysis (C) and (F) respectively).

   Method II --- μCP-LBL This method combines microcontact printing with the layer-by-layer technique (μCP-LBL), which was pioneered by Hammond and her coworkers.[28] In this method, polymeric thin films were patterned through the use of chemically patterned surfaces as templates for ionic multilayer assemblies. Selective deposition was achieved by introducing alternating regions of two different chemical functionalities on a surface: one which promotes adsorption and a second which effectively resists adsorption of polyions on the surface. Here we use alkanethiols to create a functionalised self-assembled monolayer (SAM) on gold. Firstly, we stamped a hydrophilic thiol MPS on the Au substrate, which promotes the adsorption. After a thorough rinse with ethanol, the substrate was backfilled with another thiol,
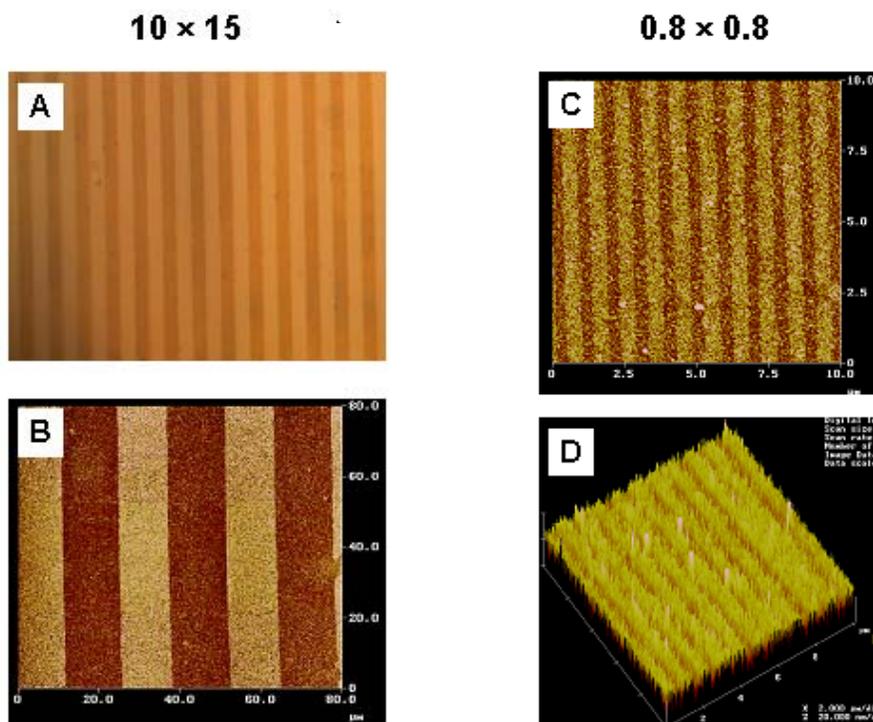
Fig.6.2-4 *Optical and AFM images of two examples fabricated via the μCP-LBL method from Stamp II (10×15, A and B) and Stamp III (0.8×0.8, C and D), respectively. A is the optical image, B is AFM phase image; C is AFM height image, while D the side view of C. LBL assembly conditions:PANI or SPNI 1mM, pH2.6. Sampe A, 6 bilayers, sample C, 4 bilayers.*

octadecanthiol (ODT), which passivates the rest of the Au substrate. Then after rinsing completely with ethanol, the LBL self-assembly was carried out. Due to the highly hydrophilic and hydrophobic regions generated by MPS and ODT, the LBL assembly event occurs, in principle, only in the MPS regions. Figure 6.2-4 shows two samples of patterned PANI/SPANI prepared via this method from Stamp II. (10×15, A and B) and Stamp III (0.8×0.8), respectively. It can be seen that the PANI/SPANI mainly adsorbed in the MPS-functionalised regions as expected, even at the submicron scale (C and D). However, in the passivated ODT regions, some PANI/SPANI also exists, which reduces the resolution and the refractive index contrast within the film a little bit. Furthermore, the surface of the obtained film is not as smooth as those prepared by EP-MIMIC method. So in the later diffraction experiments, only the samples prepared via EP-MIMIC method were used.

6.2.4 Diffraction Experiments

The scheme of the ESPD setup is shown in Figure 6.2-5(A). An electrochemical flow cell is combined with a SPR set up based on the Kretschmann configiration, which has been described in detail elsewhere.[66] The Au substrate coated with the polymer grating was used both for the coupling of the PSP and as the working electrode for the electrochemistry measurement. A p-polarized HeNe laser (632.8nm)
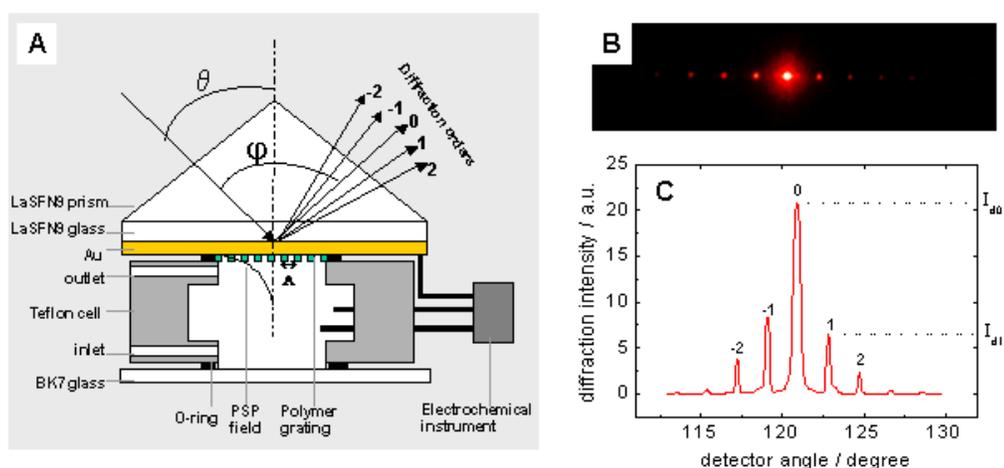
Fig.6.2-5 *(A) Schematic of the electrochemically tunable surface-plasmon-enhanced diffraction (ESPD) setup. (B) and (C) are the digital and SPD diffraction images, respectively, of the PANI/PSS grating prepared by EP-MIMIC method as shown in Fig.6.2-3(A)-(C).*

was used for the excitation of the PSP. The reflected or diffracted light was measured by photodiodes. The electrochemical measurements were carried out on a potentiostat (EG&G 263A), with a coiled platinum wire being used as the counter electrode, and an Ag/AgCl (3M NaCl) electrode as the reference electrode. All potentials reported here are with respect to this reference electrode.

For the reasons mentioned above, we only use PANI gratings prepared from the EP-MIMIC method for diffraction measurements. Here we take PANI/PSS gratings made from stamp II as shown in Figure 6.2-3 (A)-(C) as an example. The digital and SPD diffraction images from this grating are shown in Figure 6.2-5 (B) and (C), respectively. Very nice diffraction images were obtained. The diffraction efficiency (DE) can be easily calculated from the SPD signal by using the approximate relationship DE = I_{d1}/I_{d0}.[50a,50c] It should be noted that, for the calculation of DE, we are interested only in the first few diffraction orders, so we deliberately reduced the laser intensity to avoid the saturation of diffraction signals of the first few orders. If we increase the laser intensity, at least over 15 orders of diffraction can be observed even with the naked eyes.

6.2.4.1 Electrochemical Modulation of the Diffraction Efficiency

The cyclic voltammograms (CV) of the prepared PANI/PSS polymer grating (Fig.6.2-3(A)-(C)) measured in 0.1M PBS buffer (pH7.2) is shown in Figure 6.2-6(A). It is clear that the polymer grating can remain redox-active in a neutral pH environment, with the redox potential around +0.04V v.s. Ag/AgCl at 20mV/s. The redox behavior is similar to those reported previously and the redox peak is ascribed to the overlap of the two redox processes of PANI normally found in acidic conditions (c.f. Fig.6.2-7(C)).[61-63] The DE of the grating changes with the change of the applied potential (Fig.6.2-6(B)), with a relatively good signal reproducibility after the first cycle. One further finds that the DE decreases if the polymer grating changes from its reduced state to its oxidised state, and if the potential is scanned back, the DE is also reversed, with only little hysteresis (Fig.6.2-6(C)). This DE change with the potential is in good accordance with the change of the real part of the refractive index of PANI upon the potential change (c.f. Chapter 3).[67,68] In earlier work, Schanze and co-workers also demonstrated that the DE is more responsive to changes in the real part of the refractive index than to changes in absorptivity (i.e. imaginary part of the refractive index).[43a] This means that the DE change of PANI/PSS polymer grating as

a function of the applied potential was mainly caused by the change of the real part of the refractive index which was induced by the change of the applied potential (i.e. the change of the redox state of PANI/PSS).
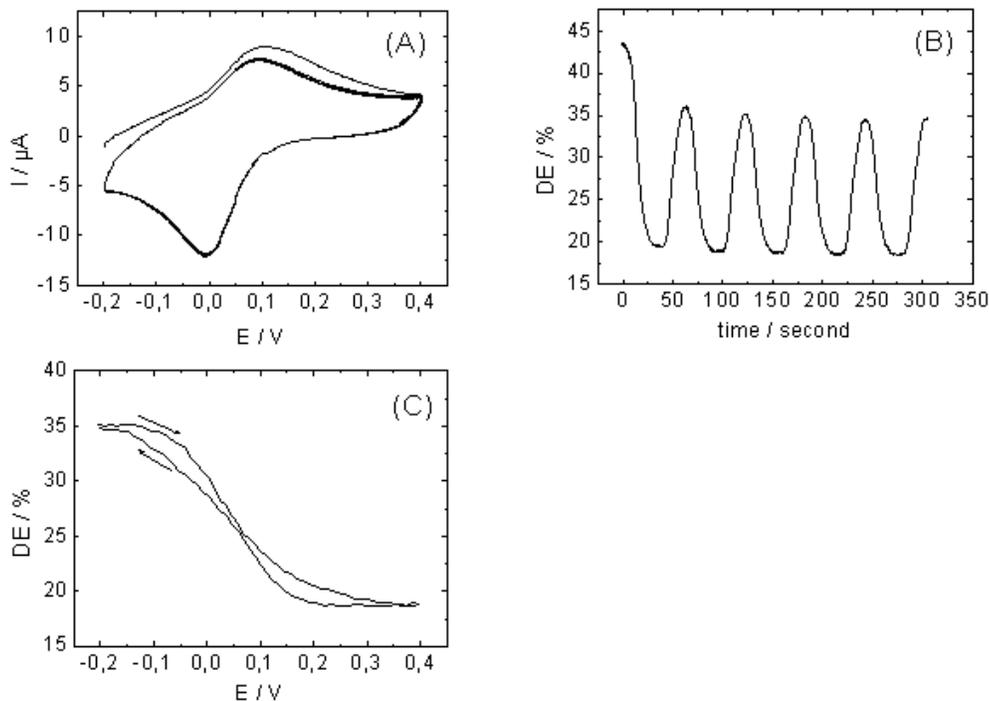
Fig.6.2-6 *Cyclic Voltammograms (A) and diffraction efficiency changes with the potential change (B and C) of a PANI/PSS polymer grating (Fig.6.2-3(A)-(C)) measured in 0.1M PBS buffer, pH7.2. CV scan rate 20mV/s.*

6.2.4.2 pH Modulation of the Diffraction Efficiency

It has been demonstrated previously that the redox behavior of PANI/polyelectrolytes depends strongly on its environmental pH (c.f. Chapter 4).[61-63] So the DE of PANI/PSS grating should also be modulated by a change of pH. Shown in Figure 6.2-7 (A) are the DE changes of the polymer grating with the potential change measured at different pH conditions. It is clear that the DE shows a different potential response in different pH solutions. In other words, the DE shows different pH response at different potentials (i.e. different redox states). At lower potentials (e.g. –0.15V), the DE shows a nicely linear relationship with pH in the range between pH 4 and pH 8 (Fig.6.2-7(B)). However, this linearity no longer exists at higher potentials above 0 V. This different DE dependence on pH at different potentials can be explained by the different redox behavior of PANI/PSS in different pH

environments, as shown in Figure 6.2-7(C). In strong acidic conditions, PANI/PSS show two separate redox processes. With the increase of pH, the two redox processes come closer and finally overlap to form only one broad redox peak at pH>5, at the same time the redox potentials move toward the negative direction with the increase of pH. Thus, in all pH conditions shown above, PANI/PSS is in its fully reduced state at a lower potential like –0.15V, so the DE shows a regular change with the pH at such potentials. However, at higher potential like +0.4V, PANI/PSS is only fully oxidised in higher pH solution; while in lower pH solution, PANI/PSS is only in its partially-oxidised state, thus at higher potentials a relative higher DE is observed in lower pH solutions than that in higher pH solutions.
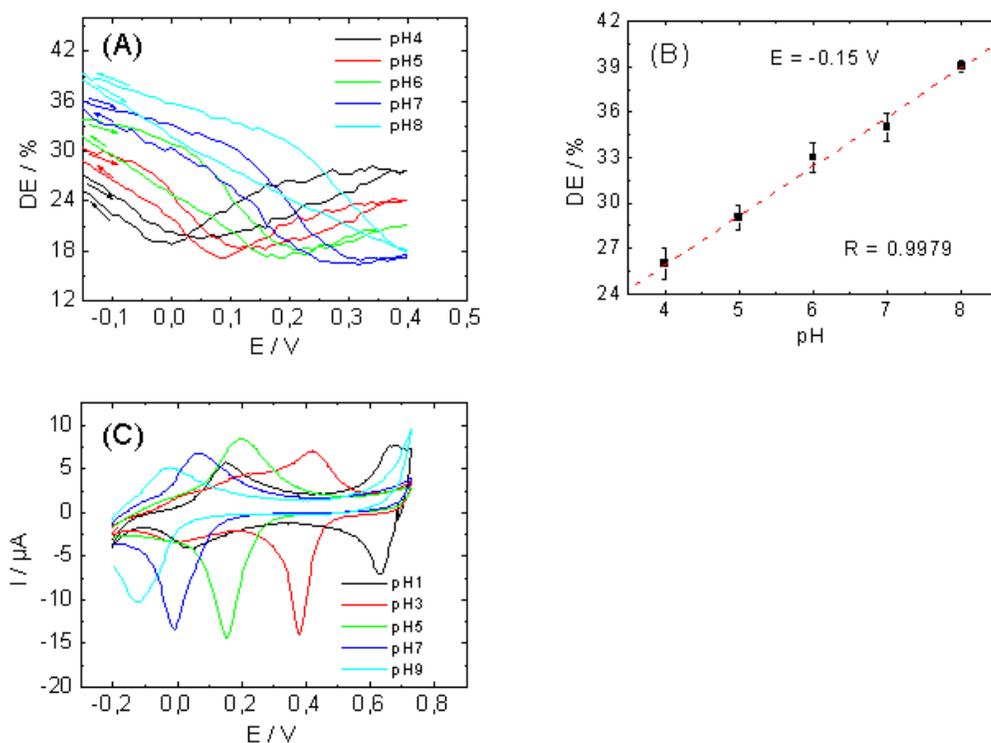
Fig.6.2-7 *(A) DE changes of the polymer grating with the potential in different pH buffer solutions. The arrows show the corresponding potential scan directions. (B) The linear relationship between the DE and pH in the range pH4~pH8 when the grating is kept at -0.15V where it is in its full reduced state in all cases (c.f. (C)). (C) CV curves of the polymer grating measured in buffer solutions with different pH. Buffer solutions: pH1, HCl solution; pH3~pH9, 0.1M citrate-phosphate buffer solution. CV scan rate was 20mV/s.*

6.2.4.3 Electrocatalytic Modulation of the Diffraction Efficiency

102

Because PANI/PSS gratings remain electroactive in neutral pH (vide supra), and previous results of unpatterned PANI/PSS composites show that it can electrocatalytize the oxidation of NADH, so PANI/PSS grating can also be used to monitor this electrocatalytic event by monitoring the DE change. Shown in Figure 6.2-8 is the DE change with the change of NADH concentration measured in 0.1M PBS buffer (pH7.2) at +0.4V for which the polymer grating is in its oxidised state. As
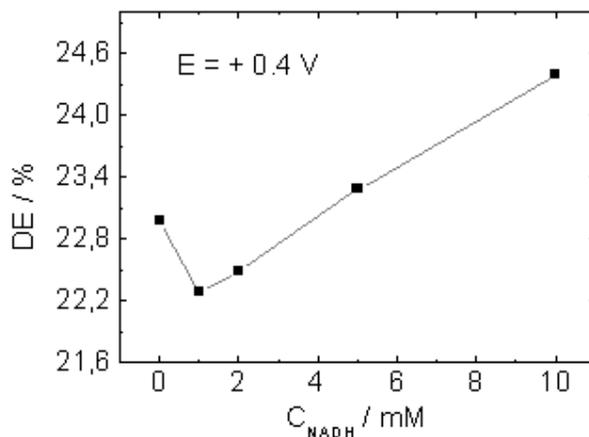
Fig.6.2-8 *Diffraction efficiency changes of a PANI/PSS grating measured in 0.1M PBS buffer (pH7.2) with different amount of NADH when the potential was fixed at +0.4V.*

can be seen, with the first addition of NADH, the DE decreases a little, which was caused by the refractive index increase of the surrounding dielectric due to the addition of NADH, thus the smaller refractive index contrast between the polymer grating and its surrounding dielectric. However, with further additions of NADH, the DE increases gradually with the increase of the amount of NADH, as a result of the electrocatalytic oxidation of NADH by the polymer grating. At the same time, part of the polymer grating was reduced, which results in an increase in the average refractive index of the polymer grating, thus the increased DE.

6.2.5 Conclusions

In this first part, we demonstrate that well-defined PANI composite polymer films can be successfully fabricated by both EP-MIMIC and μCP-LBL methods. Some of the

prepared patterned PANI films (especially those via the EP-MIMIC method) can be used as ideal optical diffraction gratings based on the ESPD mode. The DE of the grating can be tuned both by the potential change and by the environmental pH change. The DE change with pH strongly depends on the redox state of the polymer grating and it shows a linear relationship if the polymer grating is in its reduced state. Besides, because the obtained grating remains electroactive at neutral pH, it can also be used for the electrocatalytized oxidation of NADH, and the DE increases with the increase of NADH concentration, which points to the possibility of the present system for developing ESPD-based biosensors.

6.3 Template-induced Fabrication of PANI Inverse Opals by Electrochemical Method

6.3.1 Background

Recently, sacrificial template methods have been shown to be an effective approach for the fabrication of structured materials with unique properties that are difficult to produce by the afore mentioned patterning procedures.[69-74] The templates normally used include diblock copolymers,[75-77] anodic aluminium oxide,[78-80] organic or inorganic colloidal crystals,[81-83] and so on.[84-85] Among them, self-assembled colloidal crystals (opals) stand out to be ideal templates for creating three-dimensional (3D) highly ordered interconnected macroporous structures (the so-called "inverted opals" or "inverse opals"), which show potential applications ranging from photonic crystals to catalysts to bioreactors.[86-88] To date, numerous inverse opals, such as metals,[89] inorganic oxides,[81-83] polymers,[88a,88b,88e,90] etc., have been fabricated by using a variety of colloidal crystal templates.

The original interest for making conjugated polymer inverse opals arised from the motivation to prepare a photonic bandgap crystal with enhanced interaction with light, and to use it as a model system to investigate how the periodic structure of the crystal enhances the optoelectronic properties of the polymer and how the polymer enhances the properties of the photonic crystal, due to the ease of tunability of the refractive index of the conjugated polymer.[90a,90b] Recently, research interest also focused on their potential applications for biosensing purposes, by taking advantage of the highly ordered porous structure and the huge surface area they possessed.[88]

Until now, inverse opals based on different conjugated polymers, such as polypyrrole,[88b,90c,91a] polythiophene,[88a,91a] polyphenylenevinylene,[90a,90b] polyaniline,[91b] etc., have been prepared by polymerising the corresponding monomer in the interstitial voids of the colloidal crystal template, either chemically or electrochemically. Compared to the chemical synthesis, electrochemical polymerisation can control much easier the structure of the inverse opal (e.g. film thickness, size of interconnected pores, etc.) by either controlling the polymerisation time or the applied potential.[88,90,91]

Here, we use the electropolymerisation method to prepare PANI inverse opals by using polystyrene (PS) colloid assemblies as template. A PANI inverse opal was once fabricated by Caruso's group via the chemical polymerisation method. However, the quality of the obtained PANI inverse opal is very poor, due to the inherent drawbacks of the method used. By using electropolymerisation, we show that PANI inverse opals with much higher quality can be obtained. Furthermore, by controlling the polymerisation time, we can exactly control whether the topmost layer of the inverse opal is open or closed. Besides, efforts are also made towards making PANI composite inverse opal by electrocopolymerising aniline with different dopants, in order to explore their potential biosensing applications.

6.3.2 PS colloidal template

The PS colloidal templates were provided by Jianjun Wang in our group. Details on the preparation method can be found elsewhere.[92] Carboxylated PS particles (D = 839 nm) were used for the preparation of the template. By controlling proper conditions (e.g. solvent evaporation rate, substrate withdrawal rate, colloidal concentration, ect.), evaporation of the solvent leads to the formation of a well-ordered 2D or 3D PS colloidal assembly on the Au substrate. To increase the wettability of the Au substrate, the substrate was pre-functionised with a layer of hydrophilic thiol (normally MPS). Figure 6.3-1 shows one example of the prepared 3D PS colloidal arrays (PS opals). After the PS opaline film was dried, the PS spheres adhered well


Top View   **Side View**
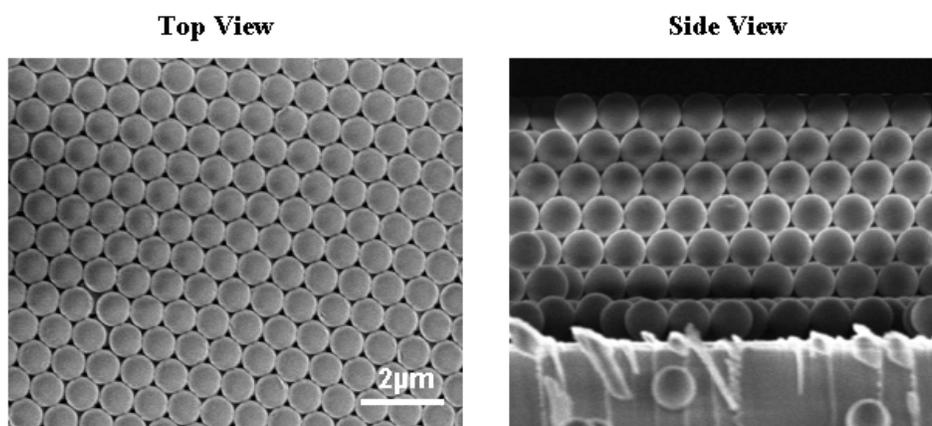
Fig.6.3-1 *Typical SEM images of a prepared 3D colloidal multilayer crystal.*

enough to each other and to the Au substrate without detaching or disintegrating, even by re-immersing them in solution. This good adhesion allowed us to use it as the template to prepare PANI inverse opals by the electropolymerisation, as shown below.

6.3.3 Preparation of PANI inverse opals

The fabrication procedure of the PANI inverse opals using the above prepared PS colloidal template by electropolymerisation is shown in Figure 6.3-2. The whole process was carried out in an electrochemical cell (c.f. Experimental Section 2.2.1). After infiltration of aniline solution (0.02 M aniline in 0.5 M H_2SO_4) into the interstices of the PS colloidal template, electropolymerisation was carried out by either a galvanostatic method or by cyclic voltammetry. After polymerisation, the resulting polymer film was thoroughly rinsed with 0.5 M H_2SO_4, then was exposed to a tetrahydrofuran (THF) solution for ~ 10 h to remove the PS template in order to obtain the well-structured PANI inverse opals.

Fill in aniline
electropolymerise

Removal of PS
by THF

PS colloid template
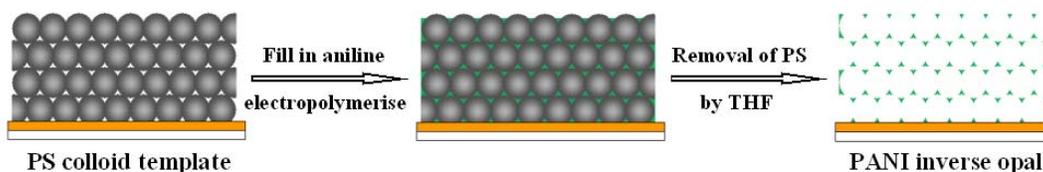
PANI inverse opal

Fig.6.3-2 *Schematic illustration of the procedure used for fabricating PANI inverse opals.*

The structures of the prepared PANI inverse opals were examined by scanning electron microscopy (SEM). Shown in Fig.6.3-3 are the SEM images of one sample of the PANI inverse opals fabricated by cyclic voltammetry at a scan rate of 20 mV/s for 10 cycles. It is clear that a well-ordered 3D network of PANI over a very large area (~ 0.7 cm^2, limited by the electrochemical cell) is obtained. This PANI opaline structure is believed to be held together by physical crosslinking and weak interactions like hydrogen bonding and van der Waals forces between PANI chains.[91b] From the enlarged image in (B), we can see that the pores are assembled in a hexagonal array and are connected to each other via similarly symmetrical smaller pores, indicating a truly 3D nature of the obtained structure. Compared with those prepared via chemical
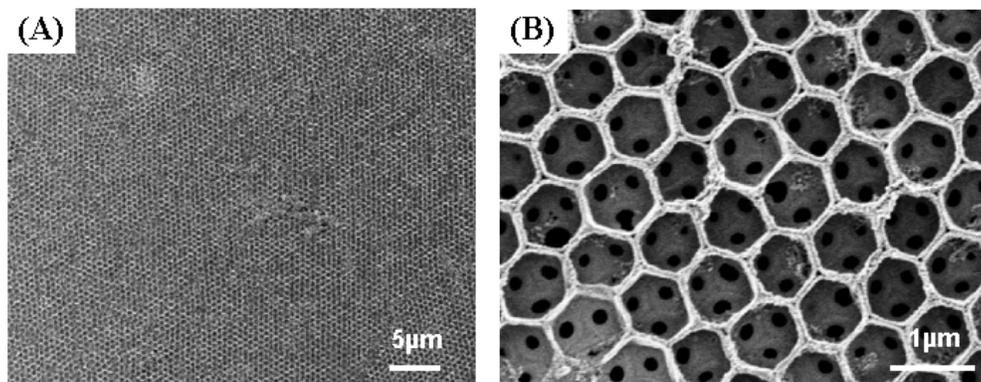
Fig.6.3-3 *SEM images of PANI inverse opals prepared via cyclic voltammetry method, at low (A) and higher (B) magnification scale.*

polymerisation method [91b], the quality of the PANI inverse opals we got by the electropolymerisation method was greatly enhanced. Furthermore, the shrinkage in our case (< 5%) is only one-third of that in the former case (~ 15%), retaining almost the original geometry of the used PS template. The improved quality in our case may arise from the controlled polymerisation process by using a slow potential scan rate, which allows the in-situ formed PANI chains to fill into the interstices of the PS template in a highly ordered way and form a much compacter structure. However, by chemical polymerisation method, the polymerisation rate is hard to control, which may result in the aggregation of the formed PANI chains and their package into a relatively loose and disordered structure. Actually, in our experiments, we found that the quality of the obtained PANI inverse opals decreased with the increase of the used potential scan rate. Too high a scan rate even leads to the collapse of the 3D structures.

We also prepared the PANI inverse opals by a galvanostatic method. This method allowed us to exactly control the structures of the obtained PANI opaline films. Figure 6.3-4 shows the voltage changes during the electropolymerisation process. There is a transition point (TP) in the curve, and the voltage increases very sharply after this point. A similar phenomenon was also found in the current changes seen during a potentiostatic preparation.[90c,93] This TP was ascribed to a rapid increase of the electrochemical reaction area once the growing surface of materials reached the template/bulk solution interface, and was confirmed by our experiments by stopping the polymerisation process at different stages as indicated by the arrows. SEM images
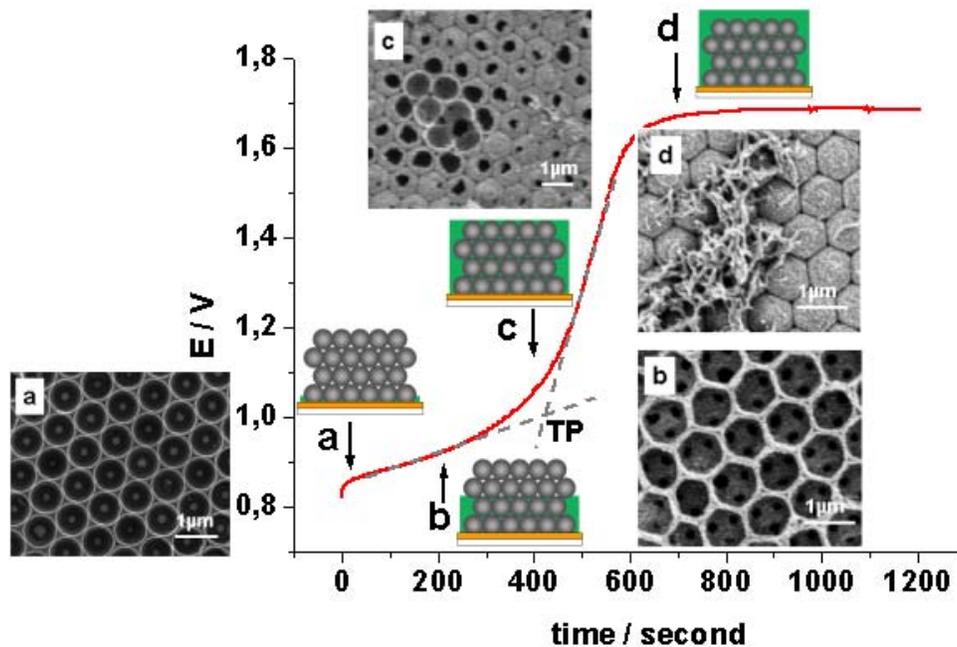
Fig.6.3-4 *Voltage changes during the electropolymerisation process for preparing PANI inverse opals by galvanostatic method at a current density of 0.05mA cm^{-2}. Inset sketches show the status quo of the formed PANI inside the PS template at each stopping point as indicated by the arrows. SEM images of the corresponding PANI inverse films obtained at these points are also shown.*

of the obtained PANI inverse opaline films at each stage are also shown in Figure 6.3-4. If the polymerisation process was stopped at a very early stage ((a), after 10s), a bowl-shaped PANI array was obtained. At this stage, the thickness of the formed PANI is thinner than that of a monolayer of PS particles (c.f. inset sketches for references). If the polymerisation process was stopped at a later stage ((b), after 200s, but before the TP), a totally opened 3D pore structure was obtained, with smaller channels connecting each pore to its neighbours. (c) corresponded to the termination of the polymerisation process near the TP. It is clear that at TP, some of the pores on the top layer began to close. If the polymerisation process continued further, then all the pores of the topmost layer were closed. Besides, dendritic-shaped PANI also formed on top of the closed pores ((d)). For practical purpose, an opened 3D structure like (b) is preferred, so care must be taken to stop the polymerisation process before the TP.

6.3.4 Preparation of PANI composite inverse opals

To explore their applications for biosensing purpose, we also tried to fabricate PANI composite inverse opals either by doping it with the negatively charged polyelectrolytes used before (c.f. Chapter 4), or by copolymerising aniline monomer with modified aniline with acidic groups like 2-aminobenzoic acid (2-ABA), in order to get an opaline film that remains electroactive at neutral pH environment. Shown in Figure 6.3-5 (A) and (B) are the SEM images of the prepared PANI composite inverse opaline films by copolymerisation aniline with either PAA or 2-ABA, respectively, using the same conditions as that for pure PANI case. It is clear that in both cases, the obtained structures collapsed to some extent, especially that of copolymer with 2-ABA. The main reason may be due to the poor mechanical properties of the used dopants or due to the phase separation during the polymerisation process.
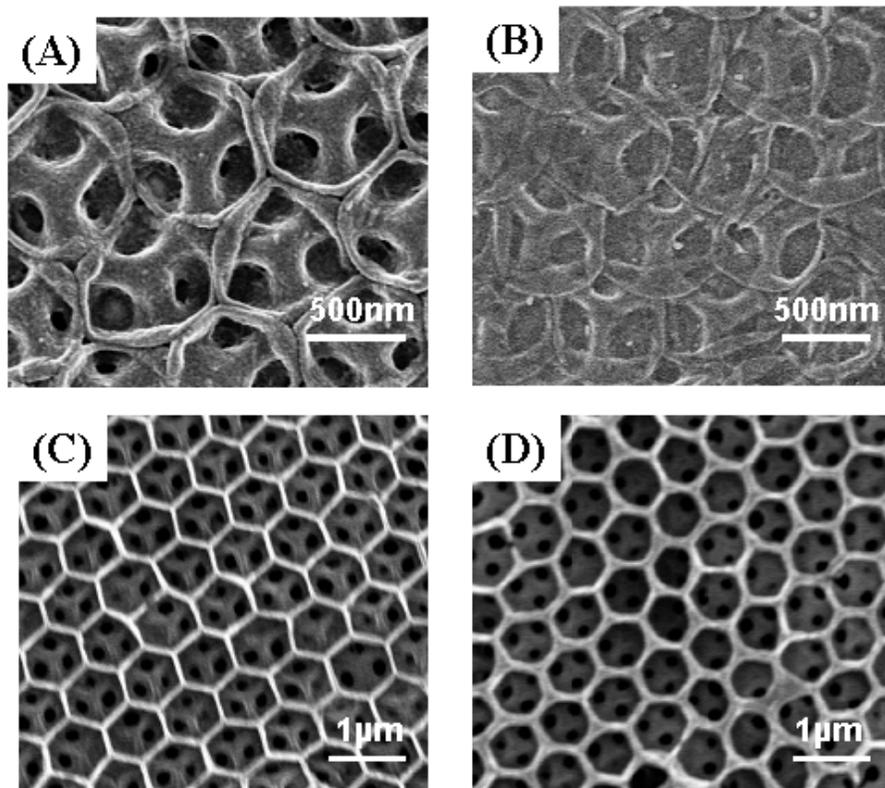
***Fig.6.3-5*** *SEM images of PANI composite inverse opaline films by copolymerising aniline with PAA (A), 2-ABA (B), or PSS (C) and (D). (A),(B), (C) were prepared via cyclic voltammetry method at a scan rate of 20 mV/s for 10 cycles, while (D) by galvanostatic method at a current density of 0.05mA for 10 min. The concentration of both PAA, PSS and 2-ABA is 0.02M based on the molecular weight of the corresponding monomers.*

However, if we use a dopant with a reported higher mechanical intensity, like PSS,[94] high-quality 3D structures can be obtained by either cyclic voltammetry or by the galvanostatic method, as shown in Figure 6.3-5 (C) and (D), respectively. Very nice interconnected hexagonal arrays were obtained in both cases, just like those of the pure PANI inverse opaline films. A most important finding is that, PANI/PSS inverse opaline films still retain a good redox activity in neutral pH after removal of the PS template by THF, as shown in Figure 6.3-6 (A). A broad redox peak is observed between –0.15V and +0.4V, with the redox potential at around +0.083V, similar to that found for the unpatterned PANI/PSS system (c.f. Chapter 4). Considering the huge surface area of the obtained PANI/PSS inverse opaline film and its capability of being redox-active at neutral pH conditions, the fabricated inverse opaline film should be a good candidate either as electrocatalyst (e.g. for the oxidation of NADH) or as a support for biomolecules, like enzymes or other proteins. Our preliminary results showed that the electrocatalytic ability of the PANI/PSS inverse opaline film toward the oxidation of NADH is more than one order of magnitude higher than that for unpatterned PANI/PSS film (Fig.6.3-6 (B)). By optimising the fabrication procedures used above and by selecting a more suitable system, the sensitivity of the PANI composite inverse opal film should be enhanced even more.
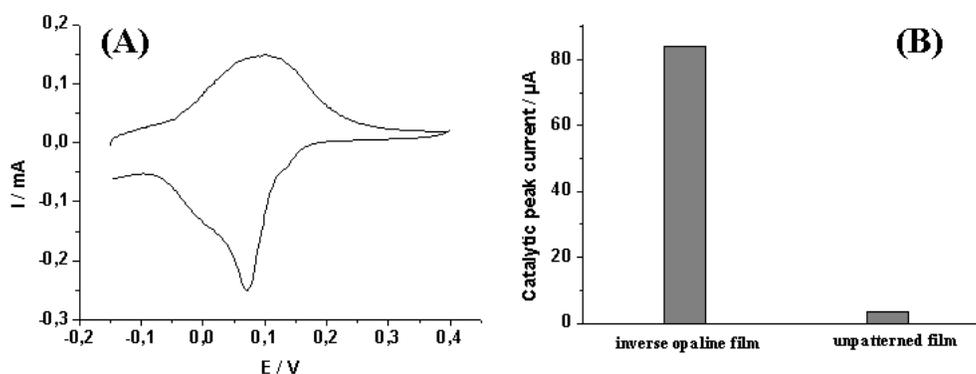
Fig.6.3-6 *(A) Cyclic voltammogram of a PANI/PSS inverse opaline film as shown in Fig.6.3-5 (C), measured in 0.1M PBS buffer, pH 7.1. (B) Comparison of the electrocatalytic ability of PANI/PSS inverse opaline film toward the oxidation of NADH and that of the unpatterned PANI/PSS film with the same film thickness. NADH concentration 10 mM. CV scan rate 5 mV/s.*

6.3.5 Conclusion

By using PS colloidal crystals as templates, 3D ordered arrays of PANI inverse opals were fabricated via electrochemical methods. Compared with those obtained by chemical synthesis, the inverse opaline film we obtained had a much higher quality. To explore their biosensing applications, we also tried for the first time to fabricate PANI composite inverse opals by doping the structure with different dopants, such as PAA, PSS or 2-ABA. It was found that the used dopants had an important effect on the structures of the obtained opaline films. By selecting suitable dopants, PANI composite inverse opals could be fabricated with a very high quality. Because the obtained PANI composite inverse opal films remain electroactive in neutral pH environment, and due to their huge surface area, they should be ideal candidates for biosensing applications, e.g., as electrocatalyst or bioreactors.

6.4 References

1. a) Y. Xia, J. A. Rogers, K. E. Paul, G. M. Whitesides, *Chem. Rev.* **1999**, *99*, 1823. b) M. Geissler, Y. Xia, *Adv. Mater.* **2004**, *16*, 1249.

2. a) W. M. Moreau, *Semiconductor Lithography: Principles and Materials*, Plenum, New York **1988**. b) *Handbook of Microlithography, Micromachining, and Microfabrication* (Ed: P. Rai-Choudhury), SPIE Optical Engineering Press, Bellingham, WA **1997**. c) *Microlithography-Science and Technology* (Eds: J. R. Sheats, B. W. Smith), Marcel Dekker, New York **1998**. d) M. J. Madou, *Fundamentals of Microfabrication: The Science of Miniaturization*, 2nd ed., CRC Press, Boca Raton, FL **2001**.

3. a) General reviews on photolithography: *Optical Lithography*, a special issue of *IBM J. Res. Dev.* **1997**, *1-2*, 3. b) *Resolution Enhancement Techniques in Optical Lithography* (Ed: A. K.-K. Wong), SPIE Optical Engineering Press, Bellingham, WA **2001**.

4. a) N. L. Abbott, J. P. Folkers, G. M. Whitesides, *Science* **1992**, *257*, 1380. b) N. L. Abbott, A. Kumar, G. M. Whitesides, *Chem. Mater.* **1994**, *6*, 596.

5. a) *Electron-Beam Technology in Microelectronic Fabrication* (Ed: G. R. Brewer), Academic Press, New York **1980**. b) R. G. Jones, P. C. M. Tate, *Adv. Mater. Opt. Electron.* **1994**, *4*, 139.

6. a) *Ion-Assisted Processing of Electronic Materials*, a special issue of *MRS Bull.* **1992**, *17***, June*, 23. b) D. Brambley, B. Martin, P. D. Prewett, *Adv. Mater. Opt. Electron.* **1994**, *4*, 55. c) S. Matsui, Y. Ochiai, *Nanotechnology* **1996**, *7*, 247.

7. H. Heinzelmann, D. W. Pohl, *Appl. Phys. A* **1994**, *59*, 89.

8. a) A.J. Bard, G. Denault, C. Lee, D. Mandler, D. O. Wipf, *Acc. Chem. Res.* **1990**, *23*, 357. b) *Scanning Electrochemical Microscopy* (Eds: A. J. Bard, M. V. Mirkin), Marcel Dekker, New York **2001**.

9. a) S. Wang, A. Taratorin, *Magnetic Information Storage Technology*, Academic Press, San Diego, CA **1999**. b) U. Hartmann, *Annu. Rev. Mater. Sci.* **1999**, *29*, 53. c) D. Weller, M. F. Doerner, *Annu. Rev. Mater. Sci.* **2000**, *30*, 611.

10. a) *Laser Microfabication-Thin Film Processes and Lithography* (Eds: D. J. Ehrlich, J. Y. Tsao), Academic Press, Boston, MA **1989** b) A. Miehr, R. A. Fischer, O. Lehmann, M. Stuke, *Adv. Mater. Opt. Electron.* **1996**, *6*, 27.

11. a) P. Calvert, *Chem. Mater.* **2001**, *13*, 3299. b) *Inkjet Printing of Functional Materials*, *MRS Bull.* **2003**, *28*, 802.

12. a) R. D. Piner, J. Zhu, F. Xu, S. H. Hong, C. A. Mirkin, *Science* **1999**, *283*, 661. b) D.S. Ginger, H. Zhang, C.A. Mirkin, *Angew. Chem. Int. Ed.* **2004**, *43*, 30.

13. a) E. E. Simanek, J. P. Mathias, C. T. Seto, D. Chin, M. Mammen, D. M. Gordon, G. M. Whitesides, *Acc. Chem. Res.* **1995**, *28*, 37. b) J.-M. Lehn, *Angew. Chem. Int. Ed. Engl.* **1988**, *27*, 89.

14. a) S. Park, J.-H. Lim, S.-W. Chung, C. A. Mirkin, *Science* **2004**, *303*, 348. b) H. Fan, K. Yang, D. M. Boye, T. Sigmon, K. J. Malloy, H. Xu, G. P. Lopez, C. J. Brinker, *Science* **2004**, *304*, 567.

15. a) N. Bowden, A. Terfort, J. Carbeck, G. M. Whitesides, *Science* **1997**, *276*, 233. b) T. L. Breen, J. Tien, S. R. J. Oliver, T. Hadzic, G. M. Whitesides, *Science* **1999**, *284*, 948. c) D. H. Gracias, J. Tien, T. L. Breen, C. Hsu, G. M. Whitesides, *Science* **2000**, *289*, 1170.

16. a) X.-D. Xiang, X. Sun, G. Briceño, Y. Lou, K.-A. Wang, H. Chang, W. G. Wallace-Freedman, S.-W. Chen, P. G. Schultz, *Science* **1995**, *268*, 1738. b) C. Stamm, F. Marty, A. Vaterlaus, V. Weich, S. Egger, U. Meier, U. Ramsperger, H. Fuhrmann, D. Pescia, *Science* **1998**, *282*, 449.

17. a) Y. Xia, G. M. Whitesides, *Angew. Chem., Int. Ed. Engl.* **1998**, *37*, 550. b) J. A. Rogers, K. E. Paul, R. J. Jackman, G. M. Whitesides, *Appl. Phys. Lett.* **1997**, *70*, 2658. c) Y. Xia, G. M. Whitesides, *Annu. Rev. Mater. Sci.* **1998**, *28*, 153.

18. a) J. A. Rogers, K. E. Paul, R. J. Jackman, G. M. Whitesides, *J. Vac. Sci. Technol. B* **1998**, *16*, 59. b) K. E. Paul, T. L. Breen, J. Aizenberg, G. M. Whitesides, *Appl. Phys. Lett.* **1998**, *73*, 2893. c) J. C. Love, K. E. Paul, G. M. Whitesides, *Adv. Mater.* **2001**, *13*, 604. d) J. Aizenberg, A. J. Black, G. M. Whitesides, *Nature* **1998**, *394*, 868. e) Y. C. Chang, L. L. Chang, L. Esaki, *Appl. Phys. Lett.* **1985**, *47*, 1324.

19. a) P. Hariharan, *Optical Holography: Principles, Techniques, and Applications*, 2nd ed., Cambridge University Press, New York **1996**. b) D. Kim, S. K. Tripathy, L. Li, J. Kumar, *Appl. Phys. Lett.* **1995**, *66*, 1166. c) M. Campbell, D. N. Sharp, M. T. Harrison, R. G. Denning, A. J. Turberfield, *Nature* **2000**, *404*, 53.

20. a) Y. Oppliger, P. Sixt, J. M. Stauffer, J. M. Mayor, P. Regnault, G. Voirin, *Microelectron. Eng.* **1994**, *23*, 449. b) W. Henke, W. Hoppe, H. J. Quenzer, P. Staudt-Fischbach, B. Wagner, *Microelectron. Eng.* **1995**, *27*, 267. c) W. Däschner,

P. Long, R. Stein, C. Wu, S. H. Lee, *J. Vac. Sci. Technol. B* **1996**, *14*, 3730. d) H. Wu, T. W. Odom, G. M. Whitesides, *Anal. Chem.* **2002**, *74*, 3267. e) C. Chen, D. Hirdes, A. Folch, *Proc. Natl. Acad. Sci. USA* **2003**, *100*, 1499. f) D. C. O'Shea, *Appl. Opt.* **1995**, *34*, 7518.

21. Y. Xia, E. Kim, X.-M. Zhao, J. A. Rogers, M. Prentiss, G. M. Whitesides, *Science* **1996**, *273*, 347.

22. a) X.-M. Zhao, Y. Xia, G. M. Whitesides, *Adv. Mater.* **1996**, *8*, 837. b) R. C. Bailey, K. J. Stevenson, J. T. Hupp, *Adv. Mater.* **2000**, *12*, 1930.

23. a) E. Kim, Y. Xia, X.-M. Zhao, G. M. Whitesides, *Adv. Mater.* **1997**, *9*, 651.

24. a) Y. Xia, E. Kim, G. M. Whitesides, *Chem. Mater.* **1996**, *8*, 1558. b) E. Kim, Y. Xia, G. M. Whitesides, *Nature* **1995**, *376*, 581. c) E. Kim, Y. Xia, G. M. Whitesides, *J. Am. Chem. Soc.* **1996**, *118*, 5722. d) W. S. Beh, I. T. Kim, D. Qin, Y. Xia, G. M. Whitesides, *Adv. Mater.* **1999**, *11*, 1038.

25. a) A. Kumar, G. M. Whitesides, *Appl. Phys. Lett.* **1993**, *63*, 2002. b) A. Kumar, H. A. Biebuyck, G. M. Whitesides, *Langmuir* **1994**, *10*, 1498. c) N. B. Larsen, H. Biebuyck, E. Delamarche, B. Michel, *J. Am. Chem. Soc.* **1997**, *119*, 3017. d) M. Geissler, H. Wolf, R. Stutz, E. Delamarche, U.-W. Grummt, B. Michel, A. Bietsch, *Langmuir* **2003**, *19*, 6301.

26. a) E. Delamarche, A. Bernard, H. Schmid, B. Michel, H. A. Biebuyck, *Science* **1997**, *276*, 779. b) E. Delamarche, A. Bernard, H. Schmid, A. Bietsch, B. Michel, H. Biebuyck, *J. Am. Chem. Soc.* **1998**, *120*, 500. c) P. J. A. Kenis, R. F. Ismagilov, G. M. Whitesides, *Science* **1999**, *285*, 83.

27. a) C. B. Gorman, H. A. Biebuyck, G. M. Whitesides, *Chem. Mater.* **1995**, *7*, 526. b) A. M. Massari, K. J. Stevenson, J. T. Hupp, *J. Electroanal. Chem.* **2001**, *500*, 185. c) R. A. P. Zangmeister, D. F. O'Brien, N. R. Armstrong, *Adv. Funct. Mater.* **2002**, *12*, 179.

28. a) S. L. Clark, M. F. Montague, P. T. Hammond, *Macromolecules*, **1997**, *30*, 7237. b) S. L. Clark, M. Montague, P. T. Hammond, *Supramolecular Science*, **1997**, *4*, 141. c) X. Jiang, P. T. Hammond, *Langumir*, **2000**, *16*, 8501.

29. S. A. MacDonald, C. G. Willson, J. M. Frechet, J. *Acc. Chem. Res.* **1994**, *27*, 151.

30. B. G. Healy, S. E. Foran, D. R. Walt, *Science* **1995**, *269*, 1078.

31. a) F. P. Zamborini, R. M. Crooks, *Langmuir* **1997**, *13*, 122. b) N. L. Jeon, I. S. Choi, G. M. Whitesides, N. Y. Kim, P. E. Laibinis, Y. Harada, K. R. Finnie, G. S. Girolami, R. G. Nuzzo, *Appl. Phys. Lett.* **1999**, *75*, 4201.

32. a) R. M. Crooks, A. J. Ricco, *Acc. Chem. Res.* **1998**, *31*, 219. b) M. Mrksich, G. M. Whitesides, *Trends Biotechnol.* **1995**, *12*, 228.

33. a) R. Singhvi, A. Kumar, G. P. Lopez, G. N. Stephanopoulos, D. I. C. Wang, G. M. Whitesides, D. E. Ingber, *Science* **1994**, *264*, 696. b) C. S. Chen, M. Mrksich, S. Huang, G. M. Whitesides, D. E. Ingber, *Biotechnol. Prog.* **1998**, *14*, 356.

34. P. Gosh, M. L. Amirpour, W. M. Lackowski, M. V. Pishko, R. M. Crooks, *Angew. Chem.*, *Int. Ed.* **1999**, *38*, 1592.

35. a) J. H. Burroughes, D. D. C. Bradley, A. R. Brown, R. N. Marks, K. Mackay, R. H. Friend, P. L. Burns, A. B. Holmes, *Nature (London)* **1990**, *347*, 539. b) D. Braun, A. Brown, E. Staring, E. W. Meijer, *Synth. Met.* **1994**, *65*, 85.

36. a) A. Dodadabalapour, L. Torsi, H. E. Katz, *Science* **1995**, *268*, 270. b) J. H. Burroughes, C. A. Jones, R. H. Friend, *Nature (London)* **1988**, *335*, 137.

37. a) R. H. Baugman, L. W. Shacklette, R. L. Elsenbaumer, E. J. Plichta, C. Becht, In *Molecular Electronics*; P. I. Lazarev, Ed.; Kluwer Academic Publishers: The Netherlands, **1991,** p 267. b) O. Inganas, Q. Pei, *Adv. Mater.* **1992**, *4*, 277.

38. M. C. Lonergan, E. J. Severin, B. J. Doleman, S. A. Beaber, R. H. Grubbs, N. S. Lewis, *Chem. Mater.* **1996**, *8*, 2298.

39. L. H. Chen, S. Jin, T. H. Tiefel, *Appl. Phys. Lett.* **1993**, *62*, 2440.

40. a) L. F. Rozsnyai, M. S. Wrighton, *J. Am. Chem. Soc.* **1994**, *116*, 5993. b) D. M. Collard, C. N. Sayre, *Synth. Met.* **1997**, *84*, 329. c) Z. Huang, P-C. Wang, A. G. MacDiarmid, Y. Xia, G. Whitesides, *Langmuir*, **1997**, *13*, 6480. d) Z. Huang, P-C. Wang, A. G. MacDiarmid, Y. Xia, G. Whitesides, *Synth. Met.* **1997**, *85*, 1375. e) T. Mäkelä, S. Pienimaa, S. Jussila, H. Isotalo, *Synth. Met.* **1999**, *101*, 705. f) Z. F. Li, E. Ruckenstein, *Macromolecules* **2002**, *35*, 9506. g) T. Cao, F. Wei, X. Jiao, J. Chen, W. Liao, X. Zhao, W. Cao, *Langmuir* **2003**, *19*, 8127.

41. J. Bargon, W. Behnck, T. Weidenbrück, T. Ueno, *Synth. Met.* **1991**, *41*, 1111.

42. a) M. S. A. Abdou, Z. W. Xie, A. M. Leung, S. Holdcroft, *Synth. Met.* **1992**, *52*, 159. b) L. Zhai, D. W. Laird, R. D. McCullough, *Langmuir* **2003**, *19*, 6492. c) B. Fabre, D. D. M. Wayner, *Langmuir* **2003**, *19*, 7145. d) J. A. Rogers, Z. Bao, A. Makhija, P. Braun, *Adv. Mater.* **1999**, *11*, 741. e) T. Granlund, T. Nyberg, L. S. Roman, M. Svensson, O. Inganäs, *Adv. Mater.* **2000**, *12*, 269.

43. a) K. S. Schanze, T. S. Bergstedt, B. T. Hauser, C. S. P. Cavalaheiro, *Langmuir* **2000**, *16*, 795-810. b). Z. Liang, K. Li, Q. Wang, *Langmuir* **2003**, *19*, 5555. c). Z. Liang, M. Rackaitis, K. Li, E. Manias, Q. Wang, *Chem. Mater.* **2003**, *15*, 2699.

44. a) J. B. Pendry, *J. Phys.: Condens. Mater.* **1996**, *8*, 1085. b) J. D. Joannopoulous, F. R. Villeneuve, S. Fan, *Nature*, **1997**, *386*, 143. c) V. Berger, *Curr. Opin. Solid State Mater. Sci.* **1999**, *4*, 209.

45. A. Kumar, G. M. Whitesides, *Science* **1994**, *263*, 60.

46. V. K. Gupta, N. L. Abbott, *Science* **1997**, *276*, 1533.

47. J. Zhang, C. R. Carlen, S. Palmer, M. B. Sponsler, *J. Am. Chem. Soc.* **1994**, *116*, 7055.

48. N. Kawatsuki, T. Hasegawa, H. Ono, T. Tamoto, *Adv. Mater.* **2003**, *15*, 991.

49. a) T. S. Bergstedt, B. T. Hauser, K. S. Schanze, *J. Am. Chem. Soc.* **1994**, *116*, 8380. b) B. T. Hauser, T. S. Bergstedt, K. S. Schanze, *J. Chem. Soc., Chem. Commun.* **1995**, 1945.

50. a) R. C. Bailey, J. T. Hupp, *J. Am. Chem. Soc.* **2002**, *124*, 6767. b) G. A. Mines, B.-C. Tzeng, K. J. Stevenson, J. Li, J. T. Hupp, *Angew. Chem. Int. Ed.* **2002**, *41*, 154. c) R. C. Bailey, J. T. Hupp, *Anal. Chem.*, **2003**, *75*, 2392.

51. Y. G. Tsay, C. I. Lin, J. Lee, E. K. Gustafson, R. Appelqvist, P. Magginetti, R. Norton, N. Teng, D. Charlton, *Clin. Chem.* **1991**, *37*, 1502.

52. F. Nakajima, Y. Hirakawa, T. Kaneta, T. Imasaka, *Anal. Chem.* **1999**, *71*, 2262.

53. P. M. St. John, R. Davis, N. Cady, J. Czajka, C. A. Batt, H. G. Craighead, *Anal. Chem.* **1998**, *70*, 1108.

54. F. Morhard, J. Pipper, R. Dahint, M. Grunze, *Sens. Actuators B* **2000**, *70*, 232.

55. a) J. B. Goh, R. W. Loo, R. A. McAloney, M. C. Goh, *Anal. Bioanal. Chem.* **2002**, *374*, 54. b) J. B. Goh, P. L. Tam, R. W. Loo, M. C. Goh, *Anal. Biochem.* **2003**, *313*, 262.

56. a) B. Rothenhäusler, W. Knoll, *Opt. Commun.* **1987**, *63*, 301. b) B. Rothenhäusler, W. Knoll, *Appl. Phys. Lett.* **1987**, *51*, 783. c) B. Fischer, B. Rothenhäusler, W. Knoll, *Thin Solid Films*, **1995**, *258*, 247.

57. a) F. Yu, S. J. Tian, D. Yao, W. Knoll, *Anal. Chem.* **2004**, *76*, 3530. b) F. Yu, D. Yao, W. Knoll, *Nucleic Acids Res.* **2004**, *32*, e75. c) F. Yu, W. Knoll, *Anal. Chem.* **2004**, *76*, 1971.

58. The diffraction efficiency (DE) here was defined as the ratio between the diffracted light intensity of the 1st order I_{d1} and that of the 0th order I_{d0}, i.e. DE = I_{d1}/I_{d0} (c.f. Fig.1 and references 50a and 50c).

59. A. F. Diaz, J. A. Logan, *J. Electroanal. Chem.*, **1980**, *111*, 111.

60. T. Ohsaka, Y. Ohnuki, N. Oyama, K. Katagiri, K. Kamisako, *J. Electroanal. Chem.* **1984**, *161*, 399.

61. A. A. Karyakin, A. K. Strakhova, A. K. Yatsimirsky, *J. Electroanal. Chem*. **1994**, *371*, 259.

62. a) P. N. Bartlett, P. R. Birkin, E. N. K. Wallace, *J. Chem. Soc., Faraday Trans.* **1997**, *93*, 1951. b) P. N. Bartlett, E. N. K. Wallace, *J. Electroanal. Chem.* **2000**, *486*, 23.

63. S. J. Tian, A. Baba, J. Y. Liu, Z. H. Wang, W. Knoll, M.-K. Park, R. Advincula, *Adv. Funct. Mater*. **2003**, *13*, 473.

64. a) S. J. Tian, J. Y. Liu, T. Zhu, W. Knoll, *Chem. Commun*. **2003**, *21*, 2738. b) S. J. Tian, J. Y. Liu, T. Zhu, W. Knoll, *Chem. Mater.* **2004**, *16*, 4103.

65. G. M. Whitesides, et al, "Soft lithography in biology and biochemistry", *Annual Review of Biomedical Engineering*, **2001,** *3*, 335.

66. A. Baba, M.-K. Park, R. C. Advincula, W. Knoll, *Langmuir* **2002**; *18*, 4648.

67. A. Baba, S. J. Tian, F. Stefani, C. J. Xia, Z. H. Wang, R. C. Advincula, D. Johannsmann, W. Knoll, *J. Electroanal. Chem*. **2004**, *562*, 95-103.

68. D. R. Kim, W. Cha, W.-K. Paik, *Synth. Metals* **1997**, *84*, 759-760.

69. B. Gates, Y. Yin, Y. Xia, *Chem. Mater.* **1999**, *11*, 2827.

70. a) P. Jiang, K. S. Hwang, D. W. Mittleman, J. F. Bertone, V. L. Colvin, *J. Am. Chem. Soc.* **1999**, *121*, 11630. b) K. M. Kulinowski, P. Jiang, H. Vaswani, V. L. Colvin, *Adv. Mater.* **2000**, *12*, 833.

71. H. Dai, E. W. Wang, Y. Z. Lu, S. S. Fan, C. M. Lieber, *Nature*, **1995**, *375*, 769.

72. Z. Pan, H. L. Lai, F. C. K. Au, X. Duan, et al. *Adv. Mater*. **2000**, *12*, 1186.

73. H. Yan, C. F. Blanfor, B. T. Holland, W. H. Smyrl, A. Stein, *Chem. Mater.* **2000**, *12*, 1134.

74. S. Rahman, H. Yang, *Nano Lett.* **2003**, *3*, 439.

75. M. Park, C. Harrison, P. M. Chaikin, R. A. Register, D. H. Adamson, *Science*, **1997**, *276*, 1401.

76. a) M. S. Morey, S. O'Brien, S. Schwarz, G. D. Stucky, *Chem. Mater.* **2000**, *12*, 898. b) W. Cheng, E. Baudrin, B. Dunn, J. I. Zink, *J. Mater. Chem.* **2001**, *11*, 92.

77. D. Grosso, C. Boissiere, B. Smarsly, T. Brezesinski, N. Pinna, P. A. Albouy, H. Amenitsch, M. Antonietti, C. Sanchez, *Nat. Mater.* **2004**, *3*, 787.

78. C. R. Martin, *Science* **1994**, *266*, 1961.

79. a) Z. H. Yuan, H. Huang, S. S. Fan, *Adv. Mater.* **2002**, *14*, 303. b) Z. H. Yuan, H. Huang, H. Y. Dang, J. E. Cao, B. H. Hu, S. S. Fan, *Appl. Phys. Lett.* **2001**, *78*, 3127.

80. S. Rahman, H. Yang, *Nano Lett.* **2003**, *3*, 439.

81. B. T. Holland, C. F. Blanford, A. Stein, *Science* **1998**, *281*, 538.

82. P. Jiang, J. F. Bertone, V. L. Colvin, *Scince* **2001**, *291*, 453.

83. M. A. Norell, P. Makovicky, J. M. Clark, *Nature* **1997**, *389*, 447.

84. H. Dai, E. W. Wong, Y. Z. Lu, S. Fan, C. M. Lieber, *Nature* **1995**, *375*, 769.

85. C. T. Kresge, M. E. Leonowicz, W. J. Roth, J. C. Vartuli, J. S. Beck, *Nature* **1992**, *359*, 710.

86. a) J. E. G. J. Wijnhoven, W. L. Vos, *Science*, **1998**, *281*, 802. P. V. Braun, P. Wiltziusm *Nature* **1999**, *402*, 603. c) N. T. Tetreault, H. Miguez, G. A. Ozin, *Adv. Mater.* **2004**, *16*, 1471.

87. a) P. lodahl, A. F. V. Driel, I. S. Nikolaev, A. Irman, K. Overgaag, D. Vanmaekelbergh, W. L. Vos, *Nature* **2004**, *430*, 654. b) P. Jiang, *Angew. Chem. Int. Ed.* **2004**, *43*, 5625.

88. a) T. Cassagneau, F. Caruso, *Adv. Mater.* **2002**, *14*, 1629. b) T. Cassagneau, F. Caruso, *Adv. Mater.* **2002**, *14*, 1837. c) Y. Wang, F. Caruso, *Chem. Commun.* **2004**, 1528. d) Y. Wang, F. Caruso, *Adv. Funct. Mater.* **2004**, *14*, 1012. e) W. Qian, Z. Gu, A. Fujishima, O. Sato, *Langmuir* **2002**, *18*, 4526.

89. a) O. D. Velev, P. M. Tessier, A. M. Lenhoff, E. W. Kaler, *Nature*, **1999**, *401*, 548. b) P. Jiang, J. Cizeron, J. F. Bertone, V. L. Colvin, *J. Am. Chem. Soc.* **1999**, *121*, 7957.

90. a) M. Deutsch, Y. A. Vlasov, D. J. Norris, *Adv. Mater.* **2000**, *12*, 1176. b) K. Yoshino, S. Tatsuhara, Y. Kawagishi, M. Ozaki, A. A. Zakhidov, Z. V. Vardeny, *Appl. Phys. Lett.* **1999**, *74*, 2590. c) T. Sumida, Y. Wada, T. Kitamura, S. Yanagida, *Chem. Commun.* **2000**, 1613. d) S. H. Park, Y. Xia, *Adv. Mater.* **1998**, *10*, 1045. f) S. A. Johnson, P. J. Oliver, T. E. Mallouk, *Science* **1999**, *283*, 963.

91. a) T. Cassagneau, F. Caruso, *Adv. Mater.* **2002**, *14*, 34. b) D. Wang, F. Caruso, *Adv. Mater.* **2001**, *13*, 350.

92. C.-A. Fustin, G. Glasser, H. W. Spiess, U. Jonas, *Adv. Mater.* **2003**, *15*, 1025.

93. C. Schönenberger, B. M. I. Van der Zande, L. G. J. Fokkink, M. Henny, C. Schmid, M. Krüger, A. Bachtold, R. Huber, H. Birk, U. Staufer, *J. Phys. Chem. B* **1997**, *101*, 5497.

94. A. Pud, N. Ogurtsov, A. Korzhenko, G. Shapoval, *Prog. Polym. Sci.* **2003**, *28*, 1701.

Chapter 7

Summary

In the present study, thin functional conducting polyaniline (PANI) films, either doped or undoped, patterned or unpatterned, were prepared by different approaches. The properties of the obtained PANI films were investigated in detail by a combination of electrochemistry with several other techniques, such as SPR, QCM, SPFS, diffraction, etc. The sensing applications (especially biosensing applications) of the prepared PANI films were explored.

Firstly, the pure PANI films were prepared by the electropolymerisation method and their doping/dedoping properties in acidic conditions were investigated in detail by a combination of electrochemistry with SPR and QCM. Dielectric constants of PANI at different oxidation states were obtained quantitatively. The results obtained here laid a good foundation for the following investigations of PANI films in neutral pH conditions.

Next, PANI multilayer films doped by a variety of materials were prepared by the layer-by-layer method in order to explore their biosensing applications, because of the loss of redox activity of pure PANI in neutral pH conditions. The dopants used include not only the traditionally used linear polyelectrolytes, but also, for the first tim, some other novel materials, like modified gold nanoparticles or modified carbon nanotubes. Our results showed that all the used dopants could form stable multilayer films with PANI. All the obtained PANI multilayer films showed good redox activity in a neutral pH environment, which makes them feasible for bioassays. We found that all the prepared PANI multilayer films can electrocatalyze the oxidation of NADH in neutral conditions at a low potential, although their catalytic efficiencies are different. Among them, PANI/carbon nanotube system showed the highest catalytic efficiency toward the oxidation of NADH, which makes it a good candidate as a NADH sensor. Besides, because some of the prepared PANI multilayer systems were end-terminated with –COOH groups (like PANI/Au nanoparticles system), which can be utilized to easily link biomolecules for biosensing applications. Here, we demonstrated, for the first time, to use the prepared PANI multilayer films for the DNA hybridisation

detection. The detection event was monitored either by direct electrochemical method, or by enzyme-amplified electrochemical method, or by surface plasmon enhanced fluorescence spectroscopic method. All the methods can effectively differentiate non-complementary DNA from the complementary ones, even at the single-base mismatch level.

It should also be noted that, our success in fabricating PANI multilayer films with modified Au nanoparticles or carbon nanotubes also offered another novel method for incorporating such novel materials into (conducting) polymers. Because of the unique electrochemical and optical properties of each component of the obtained PANI multilayer films, they should also find potential applications in many other fields such as microelectronics, or for electrochromic and photovoltaic devices.

Finally, patterned PANI films were fabricated by the combination of several patterning techniques, such as the combination of electrocopolymerization with micromolding in capillaries (EP-MIMIC), the combination of microcontact printing with the layer-by-layer technique (μCP-LBL), and the polystyrene (PS) template induced electropolymerisation method.

Using the obtained stripe-shaped PANI/PSS film, a redox-switchable polymer grating based on the surface-plasmon-enhanced mode was constructed and its application in the field of biosensing was explored. It was found that the diffraction efficiency (DE) of the grating was very sensitive to the applied potential (i.e. redox state of the film) as well as the pH environment of the dielectric medium. Moreover, the DE could also be effectively tuned by an electrocatalytic event, such as the electrocatalytic oxidation of NADH by the grating film.

By using PS colloidal crystal assemblies as templates, well-ordered 3D interconnected macroporous PANI arrays (PANI inverse opals) were fabricated via electropolymerisation method. The quality of the obtained inverse opals was much higher than those reported by chemical synthesis method. By electrochemical method, the structures of the prepared inverse opals can be easily controlled. To explore the possible biosensing applications of PANI inverse opals, efforts were also done toward the fabrication of PANI composite inverse opals. By selecting proper dopants, high quality inverse opals of PANI composites were fabricated for the first time. And the obtained opaline films remained redox-active in neutral pH conditions, pointing to their possible applications for electrobioassays.

Acknowledgements

I want to take this chance to thank all the people who had helped me during my stay here in MPIP over the past three years. Without their help, my Ph.D work would not have been accomplished so smoothly, and my life here would not have been so colourful.

First of all, I would like to thank Prof. Wolfgang Knoll, my supervisor, for giving me the nice opportunity to do my Ph.D in such a friendly international group. His insightful ideas and right-on-time suggestions had made my Ph.D research work going smoothly. Besides, I also want to thank him for his kind help in my personal life, especially those for my family.

I thank Prof. R. Zentel, who is willing to be my co-supervisor and help to revise my dissertation.

Akira, Fernando, Fang and Jing, thank you very much for introducing me to the wonderful surface-plasmon world when I first came here, and for many constructive discussions in my following work.

Thanks should also go to Prof. Rigoberto Advincula and Dr. Mi-Kyoung Park (University of Houston) for helping synthesising some of the used PANI samples; Dr. Tao Zhu and Dr. Krasimir Vasilev, who helped to synthesise the gold nanoparticles; Jianjun Wang, who provided me the polystyrene colloidal crystal templates; and Prof. Diethelm Johannsmann and Dr. Zhehui Wang (Technical University of Clausthal) for allowing us to use their QCM setup and helping interpret the QCM data.

I also want to thank Prof. Neal. R. Armstrong (University of Arizona) and Dr. Emmanuel Delamarche (IBM Zurich Research Laboratory) for their many encouraging suggestions on the patterning work and for providing some of the PDMS stamps.

Special thanks should go to my wife, Jianyun Liu, who did her postdoctor here also in Prof. Knoll's group, not only for her many enlightening ideas and valuable discussions on my research work, but also for her sacrificing much of her time to take care of my son and to do the housework after my son was born, which enabled me to concentrate on my study. Without her full support, my present research work would not have been possible.

The tasty Chinese food at our regular Chinese parties always satisfied my strong appetite and would make me always remember all the Chinese guys in our group.

Thank you, Jörn Lübben, Andreas Nicol, Gabi Herrmann, Walter Scholdei, and many others, for always helping me out of the problems arising from language issues.

What I should also mention is the active scientific and social activities within this group that I enjoyed a lot and from which I also benefited a lot, such as the winter school (highlighted by the skiing?), bicycle tour (field bicycles would be nice), regular group seminar (with cookies?), and frequent group and personal parties. I would say, the time I spent in the MPIP had been one of the most exciting periods in my life! I will always recall it!

Curriculum Vitae

Name: Shengjun Tian (S. J. Tian)

Gender: Male

Date of Birth: May 6th, 1971

Nationality: Chinese

EDUCATION AND WORKING EXPERIENCE

February, 2002—March, 2005

Ph.D in Material Science at Max-Planck Institute for Polymer Research, Mainz, Germany, under the supervision of Prof. Wolfgang Knoll.

July, 1997---January, 2002

Working as a lecturer at Chemistry Department, Henan Normal University, China.

September, 1994---June, 1997

Master in Physical Chemistry at Chemistry Department, Henan Normal University, China, under the supervision of Prof. Jinghua Li and Prof. Qingtang Cheng.

September, 1990---June, 1994

Bachelor in Chemistry at Chemistry Department, Henan Normal University, China.

PUBLICATIONS

(1) Jianyun Liu, Shengjun Tian, Peter Eigil Nielsen, Wolfgang Knoll. In Situ Hybridization of PNA/DNA Studied Label-free by Electrochemical Impedance Spectroscopy, *Chem. Commun.*, **2005**, in press. DOI: B419425J.

(2) Jianyun Liu, Shengjun Tian, Wolfgang Knoll. Properties of Polyaniline/Carbon nanotube mutilayer films in neutral solution and their application for stable low-potential detection of NADH, *Langmuir*, **2005**, in press. DOI: La0501233.

(3) Shengjun Tian, Neal R. Armstrong, Wolfgang Knoll. Electrochemically tunable surface-plasmon-enhanced diffraction gratings and their (bio-)sensing applications, *Langmuir*, **2005**, publish online, DOI: La0467741.

(4) Jianyun Liu, Shengjun Tian, Louis Tiefenauer, Peter Eigil Nielsen, Wolfgang Knoll. Simultaneously Amplified Electrochemical and Surface Plasmon Optical Detection of DNA Hybridization Based on Ferrocene-Streptavidin Conjugates, *Anal. Chem*., **2005**, publish online, DOI: ac048088c.

(5) <u>Shengjun Tian</u>, Jianyun Liu, Tao Zhu, and Wolfgang Knoll. Polyaniline/gold nanoparticle multilayer films: assembly, properties and biological applications, *Chem. Mater.*, **2004**, *164*, 103.

(6) Fang Yu, <u>Shengjun Tian</u>, Danfeng Yao and Wolfgang Knoll. Surface plasmon enhanced diffraction for label-free biosensing, *Anal. Chem.*, **2004,** *76,* 3530.

(7) Akira Baba, <u>Shengjun Tian</u>, Fernando Stefani, Chuanjun Xia, Zhehui Wang, Rigoberto C. Advincula, Diethelm Johannsmann and Wolfgang Knoll. Electropolymerization and doping/dedoping properties of polyaniline thin films as studied by electrochemical-surface plasmon spectroscopy and by the quartz crystal microbalance, *J. Electroanal. Chem*., **2004,** *562*, 95.

(8) <u>Shengjun Tian</u>, Jianyun Liu, Tao Zhu and Wolfgang Knoll. Polyaniline doped with modified gold nanoparticles and its electrochemical properties in neutral aqueous solution, *Chem. Commun.*, **2003**, 2738.

(9) <u>Shengjun Tian</u>**,** Akira Baba, Jianyun Liu, Zhehui Wang, Wolfgang Knoll. Electroactivity of Polyaniline Multilayer films in Neutral Solution and Their Electrocatalyzed Oxidation of ß-nicotinamide adenine dinucleotide, *Adv. Funct. Mater.*, **2003,** *13*, 473.

(10) <u>Shengjun Tian</u>, Jianyun Liu, T Zhu, Wolfgang Knoll. Polyaniline/gold nanoparticle films: assembly and electrochemical properties, *Eur. Cell. Mater.*, **2003,** *6, Suppl.1,* 79.

(11) Jianyun Liu, Danfeng Yao, <u>Shengjun Tian</u>, Wolfgang Knoll, Peter E. Nielsen. In situ hybridization kinetics of PNA/DNA by electrochemical impedance spectroscopy, *Eur. Cell. Mater.*, **2003,** *6, Suppl.1,* 112.

(12) Guoxi Xi, <u>Shengjun Tian</u>, Qingtang Cheng, Qingzhi Zhang. Studies on the thermal dissociation of sodium alginate, *Chemical World*, **2000**, *41*, 254.

(13) Xiuying Zhang, Xiangdong Lou, <u>Shengjun Tian.</u> Preparation of gas sensitive material LaNO3 by coordination-precipitation method, *Journal of Chinese Rare Earth Society*, **1999***, 17*, 74.

(14) <u>S. J. Tian</u>, G. X. Xi, Q. T. Cheng, X. D. Lou, J. H. Li. Mechanism and kinetics of thermal dissociation of inclusion complex of benzaldehyde with β – cyclodextrin, *J. Thermal Anal.*, **1998,** *53*, 825.

(15) G. E. Zhang, X. T. Li, <u>S. J. Tian</u>, J. H. Li, J.Y. Wang, X. D. Lou, Q. T. Cheng. Kinetic Studies on the thermal dissociation of β -cyclodextrin ethyl benzoate inclusion complexes, *J. Thermal Anal.*, **1998,** *54*, 947.

(16) Qingtang Cheng, Shengjun Tian, Guoxi Xi, Jinghua Li. β-cyclodextrin derivatives and their pharmaceutical applications, *Journal of Henan Normal University,* **1998***, 26(3)*, 47.

(17) Shengjun Tian, Qingtang Cheng, Guoxi Xi, Xiangdong, Lou, Jinghua Li. Preparation of inclusion complex of benzyl acetate with β-cyclodextrin and studies on its thermal dissociation, *Acta Phys-Chim. Sinica*, **1997,** *13*, 459.

(18) Shouzhi Yu, Xiaotao Li, Jinghua Li, Jingyun Wang, Shengjun Tian. Kinetic studies on the thermal dissociation of β -cyclodextrin cinnamyl alcohol inclusion complex, *J. Thermal Anal.*, **1997,** *49*, 1517.

(19) Jianji Wang, Kelei Zhuo, Shengjun Tian, Jinsuo Lu. Thermodynamic parameters of interaction between HCl and glucose in water, *Chemical World*, **1996,** *37*, 50.